Passivity-based analysis and control of AC microgrids

Integration, operation and control of energy storage systems

Universidad
Tecnológica
de Pereira

Oscar Danilo Montoya Giraldo

Passivity-based analysis and control of AC microgrids

Integration, operation and control of energy storage systems

Oscar Danilo Montoya Giraldo

This dissertation is submitted for the degree of
Ph.D in Engineering

Pereira, March 16, 2019
UNIVERSIDAD TECNOLÓGICA DE PEREIRA
Doctorate in Engineering

Passivity-based analysis and control of AC microgrids
Integration, operation and control of energy storage systems

Adviser: Alejandro Garcés Ruiz, Ph.D.
Universidad Tecnológica de Pereira
Pereira, Colombia

Co-adviser: Gerardo René Espinosa Pérez, Dr.
Universidad Nacional Autónoma de México
CDMX, México

Committee

Ph.D. Alexander Molina Cabrera, UTP. Pereira, Colombia.
Ph.D. Javier Rosero García, UNAL. Bogotá, Colombia.
Ph.D. Raymundo Enrique Torres Olguin, SINTEF. Trondheim, Norway.

Chair

Ph.D. Sandra Milena Pérez, UTP. Pereira, Colombia.

Pereira, March 16, 2019
Doctorado en Ingeniería con énfasis en Ingeniería Eléctrica
Universidad Tecnológica de Pereira
Cl. 27 # 10-02, Pereira, Risaralda
TEL: (+57)(6)3137122
www.utp.edu.co

Declaration

I hereby declare that this thesis entitled "Passivity-based analysis and control of AC microgrids" was carried out by me for the degree of Doctor in Engineering under the guidance and supervision of Alejandro Garcés Ruiz, PhD from the Universidad Tecnológica de Pereira and Gerardo René Espinosa Pérez from the Universidad Nacional Autónoma de México.

The contents of this document are original and have not been submitted in whole or in part for consideration for any other degree or qualification in this, or any other university. This thesis is my own work and contains nothing which is the outcome of work done in collaboration with others, except as specified in the text and Acknowledgments.

Oscar Danilo Montoya Giraldo

Acknowledgments

Thank you, God, for all your blessings to me and my family; for the strength you give me each day and for all the people around me who make life more meaningful. *Let your roots grow down into him, and let your lives be built on him. Then your faith will grow strong in the truth you were taught, and you will overflow with thankfulness.*

My first debt of thanks goes to my supervisor Alejandro Garcés, Ph.D, for his complete support, guidance and inspiration during these years of investigation. Alejandro was always available to deal with my questions, as insignificant as some of them were. Besides, he has given me many valuable ideas for investigation as well as his uninterested support to develop my own ideas. I especially thank him for forcing me to write in English; it was an invaluable lesson.

I would also like to thank my external advisor Dr Gerardo Espinosa Pérez, for allowing a short research visit at the Control Laboratory at the Engineering Faculty of the National Autonomous University of Mexico as well as for his complete support and successful advice for solving my doubts about control theory under the Hamiltonian paradigm.

Special thanks go to Walter Julián Gil and Luis Fernando Grisales for their friendship, also for the many discussions that we had about our personal lives, projects and dreams as well as our own doctoral projects; great ideas came from this.

I would also like to thank Dr Sofía Avila Becerril and my friend Isaac Ortega for sharing with me extended and productive discussions about control theory and friendly moments during my stay in Mexico City.

I want to thank my family for their love and support. Special thanks to my girlfriend and future wife Sara Bocanegra for understanding all the times that I sacrificed her invaluable company. She is my inspiration and fills my whole life with love and happiness: thanks for always being by my side.

I want to thank the Engineering Faculty at the Technological University of Bolivar for giving me enough time to finish this thesis successfully.

Finally, I would like to acknowledge the support of the Administrative Department of Science, Technology and Innovation of Colombia (COLCIENCIAS) through the National Scholarship Program under Grant 727-2015.

Abstract

Microgrids are essential subsystems of modern electric power systems. They allow providing electrical energy service for millions of people around the world by integrating multiple distributed energy resources and energy storage technologies at a small scale. This thesis studies these systems from the dynamical analysis and control point of view, to fulfill three main objectives: first, to model pulse-width-modulated voltage and current source converters for integrating distributed energy resources in ac microgrids (μGrids) with single-phase and three-phase topologies; second, to develop Hamiltonian models for representing the whole dynamics of ac μGrids via classical circuit theory, since this model exhibits interconnection and dissipation structures typical in Lagrangian and Hamiltonian modeling; third, to design passivity-based controllers for guaranteeing stable operation of the entire μGrids when these are operated under grid-connected or isolated modes. Hamiltonian modeling of power electronic converters based on voltage and current source technologies as well as Hamiltonian models of electrical μGrids facilitate the dynamical analysis under the passivity paradigm with stability and scalability criteria. The main contributions of this thesis are: integrating supercapacitors and superconducting coils in ac power grids through a unified control model; unified ac grid modeling via circuit theory and active and reactive power decoupling in power converters under grid-connected mode as well as voltage and frequency control for isolated μGrid configurations. Finally, simulation results corroborate the theoretical developments presented in this thesis.

List of abbreviations

This is a short list of the main abbreviations used in this thesis.

AC (ac)	:	Alternating current.
DC (dc)	:	Direct current.
DERs	:	Distributed energy resources.
IDA-PBC	:	Interconnection and damping assignment passivity-based control.
μGrids	:	Microgrids.
PLL	:	Phase-locked loop.
PI-PBC	:	Proportional-integral passivity-based control.
PWM-CSC	:	Pulse width modulated current source converter.
PWM-VSC	:	Pulse width modulated voltage source converter.
pH	:	port-Hamiltonian.
PV	:	Photovoltaic.
RMS (rms)	:	Root mean square.
SCES	:	Supercapacitor energy storage.
SMES	:	Superconducting magnetic energy storage.
SP-μGrid	:	Single-phase microgrid.
TP-μGrid	:	Three-phase microgrid.

Contents

Chapter 1

Introduction

This chapter presents the motivation for this thesis focusing on AC microgrids for providing electrical service to end-users via the integration and control of multiple distributed energy resources. The general concepts of Hamiltonian models and passivity-based control theory are sketched here. Additionally, the state-of-the-art as well as the objectives, contributions and publications derived from this thesis are presented.

1.1 Motivation

Recent advances in power electronics as well as the reduction in the cost in distributed generation and energy storage have added to the worldwide preoccupation about the greenhouse effects caused by power systems, have made possible the transformation of conventional passive power systems into active electrical networks with the integration of multiple distributed energy resources (DERs) [1–4]. Note that for integrating renewable energy resources in electrical grids, energy storage technologies are needed, since these devices allow reducing the energy fluctuations caused by variations in the weather (e.g., solar radiation and temperature in solar systems or wind speed, humidity and pressure in wind plants) or serving electrical users during periods of higher consumption and lower generation capabilities, i.e., demand response strategies [5–7]. The integration of DERs has greatly affected the electrical distribution system, much more so than the transmission system. Additionally, it has drawn attention in multiple areas, such as planning [8], operation [9] and control of power systems [10–12]; in the particular case of distribution systems, the planning studies are mainly focused on the improvement of the grid through optimization models related to economical dispatch and the reduction of power losses [7, 13, 14]; nevertheless, in the case of operation and control, the main challenges are oriented to guaranteeing the stable and reliable operation of the grid under variations in the load/generation [15, 16] or large

disturbances such as short-circuits and electromagnetic transients [10, 17, 18].

This investigation is oriented to the control of power electronic converters for the integration of DERs. The control is via linear and nonlinear control strategies guaranteeing dynamical stability in AC μGrids [19]. This area of research plays an important role in the current structure of distribution systems, due to the rapid penetration of renewable generation [20, 21] (mainly photovoltaic and wind) as well as the increasing penetration of energy storage devices [10, 22–24], which have produced multiple challenges in classical distribution systems, such as bidirectional power flow [25], dynamical energy compensation [24], harmonic distortion, and voltage and frequency oscillations [26, 27], which need to be analyzed from a dynamical point of view.

An additional interest of this thesis lies in the particular mathematical structure of the power electronic converters fed by a current or voltage source and the grid itself, which allows designing nonlinear control strategies that guarantee stability in the sense of Lyapunov [19]. This mathematical structure is widely known in the specialized literature as the Hamiltonian formulation, which makes evident the intrinsic relation between the energy stored in the electrical network with its dynamical representation [28–30]. Also, a Hamiltonian structure is the main component of passivity-based control theory to design robust and reliable controllers guaranteeing stability conditions [31,32]; besides, this control approach allows the scalability of the power system via the theory interconnected systems [33], which corresponds to an important advantage of the passivity-based control theory when compared with classical linear and nonlinear control approaches.

1.2 Problem statement

Modern electrical networks have changed from hydro-thermal systems with passive loads and a clear separation between generation, transmission and distribution, to active electrical networks with distributed energy resources (DERs) which include renewable generation [21], energy storage systems [34–36] and dynamic loads [4, 10, 37, 38]. These technologies can be integrated into the electric power system by using power electronic converters under the concept of microgrids (μGrids) [39–41], allowing improvements in voltage regulation, reducing power oscillations caused by renewable energy, performing frequency regulation, and supplying energy to the loads during service outages [4]. However, these improvements can be only achieved by using effective control strategies that consider the μGrid as a whole and not only as individual components [42, 43].

All μGrids have power electronic converters based on forced commutation (e.g., voltage/current source [44] [11, 42]) or line commutation technologies [45]. These allow advanced control strategies for operation in transient and steady state [10]. Several control strategies have been explored in the specialized literature, namely: fuzzy-logic [46, 47],

feedback linearization [11, 17, 44], model predictive [48] and passivity-based control [49–53]. Nevertheless, proportional-integral controls [10, 54] are the most used approaches.

These controls are used when the μGrid operates in grid-connected mode. However, they must be modified in island mode in order to support voltage profile and regulate electrical frequency by using a primary/secondary control [55] that, in turn, can be centralized or distributed [4]. The former is highly efficient but relies on the communication system [56] while the latter requires fewer communication channels, which entails fewer investment costs and allows scalability [57, 58].

Closed-loop stability must be guaranteed in the increasingly complex μGrids [15]. However, in many cases, the optimal tuning of a proportional-integral control in one device could affect negatively the stability of the grid. This is because the model of the system is oversimplified and the control is locally designed. In this context, we can pose the following research question:

How to control each component so that the stability of the entire μGrid is guaranteed under interconnected and islanded operation modes?

In order to answer this question it is necessary to use a generalized theory with the following characteristics: i) Applicable to different types of devices (e.g., renewable energy, batteries, and energy storage devices, among others), ii) Applicable to the nonlinear intrinsic models of the components, iii) Easily integrable with the model of the entire system, iv) Suitable to include the communication system, v) Guaranteed stability in different operative conditions, and vi) Scalable.

Passivity-based control can be an appropriate control strategy to fulfill all these control tasks [28]. However, research is required in order to apply this control paradigm to μGrids taking into account all the complexities inherent in power networks.

Note that in the specialized literature there exist a few references that propose the application of the passivation theory to operate AC μGrids, considering the natural passive model of the electrical system. Nevertheless, these approaches are mainly focused on single-phase microgrids (SP-μGrids) [15, 19] as shown in Section 1.4 where a detailed review of the state of the art is presented.

1.3 Background

1.3.1 Microgrids

Nowadays, the advance of power electronics for designing distributed generation and energy storage systems has been proceeding steadily [1, 4]. These distributed energy resources are typically connected in distribution systems [59, 60]. The interconnection of those devices at distribution levels has changed the concept of passive networks with unidirectional flows to

active networks with bidirectional flows, generating massive changes in distribution networks [1, 61, 62]. The main changes correspond to the redesign of protection schemes and control strategies to operate all distributed energy resources as an intelligent entity, in order to improve its static and dynamic performance. Figure 1.1 presents a schematic representation of the μGrid concept, which is defined by the U.S. Department of Energy as follows[1]

Definition 1 (Microgrid) *A microgrid is a group of interconnected loads and DERs with clearly defined electrical boundaries that acts as a single controllable entity with respect to the grid and can connect and disconnect from the grid to enable it to operate in both grid-connected or island modes.*

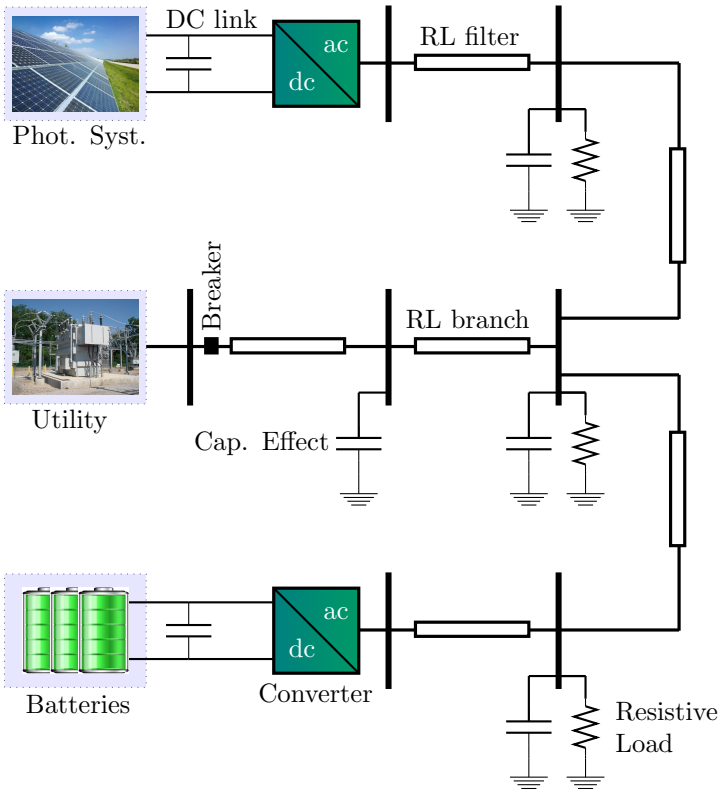

Figure 1.1: Possible configuration of a generic μGrid [63]

In addition, Table 1.1 presents a short list of successful μGrid experiences in the USA. Most of the information related to μGrid projects presented in Table 1.1 was taken from [64].

[1]This definition was taken from [4]

Based on these short successful experiences, it is possible to conclude that energy storage is a necessary complement to guarantee the reliability, quality and uninterruptable operation of any μGrid, i.e., energy storage devices give dynamical support to the μGrid and they are entrusted with guaranteeing its dynamical stability by supplying generation and demand variations [10, 65]. The next section shows the main applications of energy storage devices to electric power systems.

Table 1.1: Some successful μGrid real systems in the USA

Project lead and title	**Location**	**Technologies**	**References**
Chevron Energy Solutions – CERTS microgrid demonstration	Santa Rita Jail, CA	large-scale energy storage PV generation fuel cells	[66]
SDG&E – Beach Cities microgrid	Borrego Springs, CA	Storage system outage management system automated distribution control advanced metering infrastructure	[67]
University of Hawaii – Transmission congestion relief	Maui, HI	Intermittency management system wind turbines dynamic simulations modeling	[68]
University of Nevada Las Vegas – "Hybrid" Homes: dramatic residential demand reduction in the desert southwest	Las Vegas, NV	PV, advanced meters in-home dashboard automated demand response storage system	[64]
ATK Space Systems – powering a defense company with renewables	Promontory, UT	hydro-turbines compressed air storage solar thermal, wind turbines waste heat recovery system	[64]
City of Fort Collins – mixed distribution resources	Fort Collins, CO	PV, bio-fuel CHP thermal storage, fuel cell microturbines, PHEV Demand response	[64]
Illinois Institute of Technology – the perfect power prototype	Chicago, IL	advanced meters intelligent system controller gas fired generators demand response controller uninterruptable power supply energy storage	[64]
Allegheny Power – WV super circuit demonstrating the reliability benefits of dynamic feeder reconfiguration	Morgantown, WV	biodiesel combustion engine microturbine, PV energy storage advanced wireless communications dynamic feeder reconfiguration	[69]
Con Ed – interoperability of DR resources	New York, NY	PHEVs, fuel cell combustion engines intelligent islanding dynamic reconfiguration fault isolation	[64]

1.3.2 Energy storage devices

Energy storage technologies have emerged as promising low-cost alternatives to improve the dynamical performance of power systems [70, 71]. These devices allow compensating for the power and frequency oscillations in electrical networks which are produced by the intermittence of the primary energy resources in renewable generation applications [72, 73], large disturbances caused by variations in the circuit topology or short-circuit events [10, 11, 15].

Multiple energy storage devices have been developed based on different design technologies. The most prominent and widely used are based on chemical, mechanical and electrical technologies [65]. In chemical technologies, the batteries correspond to the first energy storage devices commonly employed for power systems and industrial applications, the most attractive devices being Ion-Lithium, Nickel-Metal and Lead-Acid alloys [36,74]. In the case of mechanical technologies, the most common energy storage devices are fly-wheels, compressed-air and pumped-hydro systems; and their main applications are related with transient stability and economic dispatch in power systems [10, 70, 75]. Finally, electrical energy storage is an emerging technology that uses electrical and magnetic fields to store energy, e.g., supercapacitors and ultracapacitors [76] as well as superconducting magnetic energy storage have been recently developed [77]. The main applications of these technologies are in distribution systems for compensating for the fluctuations produced by renewable energies and frequency regulation in isolated operation [72, 78].

For μGrid applications, energy storage based on chemical and electrical technologies are preferred. Batteries are typically for power support and energy compensation over long periods [79, 80], while electrical energy storage devices are used for their high power density and fast response to transient phenomena and high variation in renewable generation applications [72, 78].

1.3.3 Hamiltonian Systems

Passivity-based control is a mathematically well-founded control theory based on the Lagrangian and Hamiltonian formulations [28, 81]. In particular, in power systems, the port-Hamiltonian (pH) structure has advantages over Lagrangian models, since dynamical models related to circuits and power electronic converters have a natural Hamiltonian structure [19]. The main advantage of representing power systems and μGrids with Hamiltonian models lies in the strong relation between energy storage, dissipation and interconnection structures with physical electrical phenomena such as inductive, capacitive and resistive effects in transmission and distribution lines, power electronic converters and generation systems [15].

This thesis uses the pH formulation to represent the interaction between DERs and

μGrids through the dynamical modeling of power electronic converters by using an averaging modeling of dynamical systems [29, 82]. The main idea of using Hamiltonian formulations for modeling and controlling power systems lies in the possibility of exploiting the natural open-loop Hamiltonian model of the network for designing nonlinear controllers under Lyapunov's stability paradigm while preserving their interconnection properties [19, 28, 31].

1.4 Related work

This section presents a brief literature review in the context of designing passivity based controllers for DERs and μGrids. The analysis is mainly concentrated on superconducting coils, supercapacitors, batteries, and photovoltaic and wind generation systems. Additionally, there is presented a general approximation to analyze AC μGrids via the passivation theory approach.

Table 1.2 presents the most popular control strategies for energy storage devices. Only three energy storage technologies are considered: superconducting coils, batteries, and supercapacitors. These are precisely the components in the scope of the thesis.

Table 1.2: Summary of investigations related to energy storage devices

Energy storage technology	Control approach	Type of converter	References
Superconducting coils	Passivity-based control	PWM-CSC	[83]
	Linear matrix inequalities	PWM-CSC	[84]
	Feedback linearization	PWM-CSC and VSC	[11, 44]
	Passivity-based control	VSC with DC/DC Chopper	[85]
	Model predictive control	VSC with DC/DC Chopper	[86]
	Proportional-integral control	VSC with DC/DC Chopper	[87]
Supercapacitors	Passivity-based control	DC/DC	[88]
	Model predictive control	VSC with DC/DC	[89]
	Fuzzy logic control	VSC with DC/DC	[90]
Batteries	Adaptive Passivity-based control	Bidirectional Boost converter	[91]
	Model predictive control	DC/DC	[92, 93]
	Fuzzy-sliding mode control	DC/DC	[94]

Note that [83] presents a PBC approach for controlling a superconducting coil connected directly to a robust grid with a PWM-CSC for managing the current flowing through the superconducting coil as well as managing the active power interchange between the SMES system and the electrical network so as to compensate for the power fluctuations in renewable generation sources, such as wind or solar photovoltaic. In addition, in [84], the same problem is analyzed by using a matrix inequalities approach. The authors of [11] propose the use of PWM-CSC for stabilizing power systems with rotatory machines during electromagnetic transients caused by short-circuit events. For this purpose, they

used a decoupling control method based on a feedback control method. In [44] proposed a superconducting coil integrated with the power system via a VSC in cascade ith a DC-DC chopper for compensating for voltage fluctuations in sensitive loads. A feedback strategy is employed to control those converters. In [85] a passivity-based control approach based on the energy shaping strategy is employed for integrating superconducting coils into microgrids in order to compensate for the power oscillations introduced by renewable generation. in addition, [86] proposes a model predictive control approach for reducing the power losses caused by eddy currents in transformers, by integrating superconducting coils with VSCs in cascade with DC-DC choppers. Authors of [87] propose a conventional proportional integral control for smoothing the power from photovoltaic plants using VSCs with DC-DC choppers for integrating the SMES system into the grid. In the case of the integration of supercapacitors, authors of [88] propose the use of this energy storage system for enlarging the useful life of a fuel cell. They presented a PBC approach applied to DC-DC converters for the control of the supercapacitor and fuel cell. In [89] is proposed a model predictive controller for integrating supercapacitors with a connection cascade between a VSC and a DC-DC converter for load frequency control applications. Authors of [90] present a fuzzy control approach for supercapacitor integration in elevator applications for smoothing speed variations during elevator movements. In the case of battery integration, in [91] apply an adaptive PBC approach to hybrid battery/photoivoltaic systems for smoothing power oscillations as well as providing constant voltage at load terminals using DC-DC converters. [92] propose a model predictive control approach for smoothing the power output of diesel plants for marine applications via DC-DC converters. Authors of [93] use the same control approach for electric vehicle applications.

Although passivity-based control has been proposed for controlling energy storage devices, those articles focus only on analyzing one specific device, without taking into account the rest of the electrical network, which does not bring about the possibility of extending the stability properties to the whole of the electrical network.

Table 1.3 shows some papers that explore different control techniques to integrate wind and photovoltaic generators in power μGrids. Note that passivity-based control theory appears recurrently in the review of the state-of-the-art.

Note that [29] and [95, 96] propose PBC approaches for optimally tracking the power from wind energy by controlling induction machines through back-to-back voltage source converters in isolated and grid connected applications. In [97], instantaneous active and reactive power theory is presented for controlling double-fed induction generators in wind generation applications for interconnection to unbalanced three-phase microgrids. In [98] is proposed an adaptive fuzzy controller for wind turbines in applications to the voltage regulation of TP-μGrids. In [20] a model predictive control approach for permanent-magnet synchronous machines in wind generation is presented. Authors of [42]

Table 1.3: Summary of investigations related to photovoltaic and wind generation

Generation technology	**Control approach**	**Type of grid**	**References**
Wind generators	Passivity-based control	SP-μGrids and TP-μGrids	[29, 95, 96]
	Instantaneous power theory	TP-μGrids	[97]
	Adaptive fuzzy logic control	TP-μGrids	[98]
	Model predictive control	TP-μGrids	[20]
	Adaptive control	TP-μGrids	[42]
	Control by consensus	TP-μGrids	[99]
	Backstepping control	TP-μGrids	[100]
Photovoltaic generators	Passivity-based P control	TP-μGrids	[101]
	Model predictive control	TP-μGrids	[102]
	Instantaneous power theory	TP-μGrids	[103]

propose an interconnection of permanent-magnet synchronous machine with a combination of diode-bridge in conjunction with a PWM-CSC for wind generation considering an adaptive control strategy. In [99] is presented a consensus control for voltage and frequency control of virtual synchronous generators in isolated TP-μGrid applications. In [100] is proposed a backstepping control approach for voltage source converters connected in back-to-back form for managing induction machines in wind generation systems. In the case of photovoltaic applications, in [101] is proposed a proportional PBC control approach for controlling voltage source inverters in solar generation integration to three-phase networks. In [102] a combination of photovoltaic and wind plants for water desalination applications is presented by employing a supervisor predictive controller. In [103] a classical PI control is used for maximum power point tracking in solar systems based on voltage-power control or active-reactive power control, depending on the amount of energy available in the solar system and the requirements of the three-phase grid.

After a detailed review of the literature, there were found only two approximations that analyze the whole microgrid as a complete entity. The first one, [19], explores the structural properties of μGrids via passivation theory; nevertheless, it focuses particularly on a single-phase μGrid with linear and nonlinear components without considering details about the converters. The second one, [104], studies the operating conditions that allow an inverter-based μGrids with meshed topologies to remain stable. However, they reduce the dynamics of the grid to conventional power flow equations, assuming that the line parameters are independent of the frequency. Additionally, it is important to mention that there are some papers that analyze stability in DC microgrids [26, 105–108]

Based on this review of the existing state-of-the-art, it is clear that there are no approaches that analyze three-phase μGrids considering simultaneously distributed generators and energy storage devices via passivation theory. This lack is used in this thesis as an opportunity

for investigation. Passivity theory is chosen as the tool of analysis of electrical networks due to the fact that most of the elements analyzed in this investigation can be modeled by using pH formulations [15, 19].

1.5 Objectives

1.5.1 General

To design passivity-based controllers for power electronic converters for integrating distributed energy resources (DERs) in AC μGrids.

1.5.2 Specifics

1. To study different mathematical models that represent the full dynamical behavior of power electronic converters.

2. To analyze the structural properties of the dynamical models obtained using different reference frames.

3. To propose linear and nonlinear controllers using passivity-based control theory to integrate and operate the DERs in μGrids.

4. To develop general dynamical models that allow operating the μGrids considering single-phase and three-phase representations and taking into account different operating scenarios.

5. To develop passivity-based controllers for non-autonomous systems via the dynamics of the error with proportional-integral actions.

1.6 Scope

This thesis focuses on the port-Hamiltonian modeling of μGrids, including distributed energy resources such as distributed generation and energy storage devices. Nevertheless, to analyze all the aspects associated with this topic is not realistic or achievable in just one doctoral thesis. Hence, this research is limited, as follows.

1. Integration of renewable generation (wind or solar) based on current source modeling at the DC sides of the power electronic converters. This means that the dynamics of the primary resource is not considered in the model. This assumption is valid for the

time window considered and allows a general methodology that would otherwise be very dependent on the control of the DC side.

2. Integration of energy storage devices based on chemical and electrical technologies, i.e., batteries, supercapacitors and superconducting magnetic energy storage.

3. Control active and reactive power of power electronic converters based on pulse width modulated voltage and current technologies.

4. Alternating-current microgrids operating under master–slave mode with three-phase and single-phase configurations.

The general approach of this thesis is that of a theoretical investigation from the point of view of dynamical analysis considering passivity-based control as a nonlinear robust and mathematically well-founded control theory. The validation of the proposed controllers for interfacing DERs with distribution networks has been carried out with MATLAB/SIMULINK software. The experimental validation of the proposed passivity-based approaches is left for future research.

1.7 Contributions

The main contributions of this thesis are:

- The development of a general passivity-based Hamiltonian formulation for power electronic converters based on voltage and current source technologies that allows integrating multiple DERs in single-phase and three-phase μGrids.

- The application of the passivity-based control theory for operating single-phase and three-phase power electronic converters in μGrids for supporting active and reactive power independently, i.e., four-quadrant operation, and also the possibility of controlling the voltage and frequency for isolated microgrid applications.

- The possibility of analyzing dynamical models for power electronic converters preserving their Hamiltonian mathematical structure under different reference frames (time-varying and time-invariant reference frames) as well as designing passivity-based controllers that guarantee stable operation in the sense of Lyapunov.

- The definition of the desired operating point (trajectory) for the control requirements in the power electronic converters by measuring the voltage and current variables, which allows avoiding the off-line solution of the conventional power flow equations and allows

preserving the stable operation of the grid independent of variations in the the load or topology.

- The analysis and inclusion of electrical energy storage systems based on superconducting coils and supercapacitors for dynamic energy compensation in μGrids with three-phase and single-phase topologies.

1.8 List of publications

Next, the lists of journal and conference publications as well as the undergraduate thesis are presented.

1.8.1 Journal papers derived from this thesis

1. **O. D. Montoya**, and W. Gil-González, "Active and reactive power conditioning using SMES devices with PMW-CSC: A feedback nonlinear control approach," *Ain Shams Engineering Journal*, early access, **2019**, pp. 1-10. `https://www.sciencedirect.com/science/article/pii/S209044791930005X?via%3Dihub`. **SJR 2017 Q1**

2. **O. D. Montoya**, W. Gil-González, and A. Garces, "Control for EESS in ThreePhase Microgrids Under TimeDomain Reference Frame via PBC Theory," *IEEE Transactions on Circuits and Systems II: Express Briefs*, early access, **2019**, pp. 1-5. `https://ieeexplore.ieee.org/document/8618425`. **SJR 2017 Q1**

3. **O. D. Montoya**, and W. Gil-González, "Time-Domain Analysis for Current Control in Single-Phase Distribution Networks Using SMES Devices with PWM-CSCs," *Electric Power Components and Systems*, **2019**, pp. 1-10. `https://doi.org/10.1080/15325008.2018.1531325`. **SJR 2017 Q2**

4. **O. D. Montoya**, G. Espinosa-Pérez, and F. M. Serra, "Distributed Energy Resources Integration in AC Grids: a Family of Passivity-Based Controllers," *Revista Iberoamericana de Automática e Informática Industrial*, **2018**. `https://polipapers.upv.es/index.php/RIAI/article/view/10666/10679`. **SJR 2017 Q3**

5. **O. D. Montoya**, A. Garces, S. Avila-Becerril, G. Espinosa-Pérez, and F. M. Serra, "Stability Analysis of Single-Phase Low-Voltage AC Microgrids with Constant Power Terminals," *IEEE Transactions on Circuits and Systems II: Express Briefs*, early access, **2018**, pp. 1-5. `https://ieeexplore.ieee.org/document/8509162`. **SJR 2017 Q1**

6. **O. D. Montoya**, A. Garcés, and G. Espinosa-Pérez, "Indirect IDA-PBC for Active and Reactive Power Support in Distribution Networks Using SMES Systems with PWM-CSC," *Journal of Energy Storage*, vol. 17, **2018**, pp. 261-271. https://doi.org/10.1016/j.est.2018.03.004. **SJR 2017 Q1**

7. S. Avila-Becerril, G. Espinosa-Pérez, **O. D. Montoya** and A. Garcés, "Control of a Detailed Model of Microgrids from a Hamiltonian Approach," *IFAC-PapersOnLine*, vol. 51, no. 3, **2018**, pp. 187-192. https://doi.org/10.1016/j.ifacol.2018.06.051. **SJR 2017 Q3**

8. W. Gil-González, and **O. D. Montoya**, "Passivity-based PI control of a SMES system to support power in electrical grids: A bilinear approach," *Journal of Energy Storage*, vol. 18, **2018**, pp. 459-466. https://doi.org/10.1016/j.est.2018.05.020. **SJR 2017 Q1**

9. **O. D. Montoya**, W. Gil-González, and F. M. Serra, "PBC Approach for SMES Devices in Electric Distribution Networks," *IEEE Transactions on Circuits and Systems II: Express Briefs*, early access, **2018**, pp. 1-5. https://ieeexplore.ieee.org/document/8290947/. **SJR 2017 Q1**

10. **O. D. Montoya**, A. Garcés, and F. M. Serra, "DERs integration in microgrids using VSCs via proportional feedback linearization control: Supercapacitors and distributed generators," *Journal of Energy Storage*, vol. 16, **2018**, pp. 250-258. https://doi.org/10.1016/j.est.2018.01.014. **SJR 2017 Q1**

11. **O. D. Montoya**, A. Garcés, G. and Espinosa-Pérez, "A generalized passivity-based control approach for power compensation in distribution systems using electrical energy storage systems," *Journal of Energy Storage*, vol. 16, **2018**, pp. 259-268. https://doi.org/10.1016/j.est.2018.01.018. **SJR 2017 Q1**

1.8.2 Additional journal papers

1. **O. D. Montoya**, "On Linear Analysis of the Power Flow Equations for DC and AC Grids with CPLs," *IEEE Transactions on Circuits and Systems II: Express Briefs*, early access, **2019**, pp. 1-5. https://ieeexplore.ieee.org/document/8620316. **SJR 2017 Q1**

2. **O. D. Montoya**, V. M. Garrido, W. Gil-González and L. F. Grisales-Noreña, "Power Flow Analysis in DC Grids: Two Alternative Numerical Methods," *IEEE Transactions on Circuits and Systems II: Express Briefs*, early access, **2019**, pp. 1-5. https://ieeexplore.ieee.org/document/8606244. **SJR 2017 Q1**

3. **O. D. Montoya**, W. Gil-González and A. Garces, "Sequential quadratic programming models for solving the OPF problem in DC grids," *Electric Power Systems Research*, vol. 169, April **2019**, pp. 18-23. https://doi.org/10.1016/j.epsr.2018.12.008. **SJR 2017 Q1**

4. **O. D. Montoya**, W. Gil-González and A. Garces, "Economic dispatch of energy storage systems in DC microgrids employing a semidefinite programming model," *Journal of Energy Storage*, vol. 21, Feb. **2019**, pp. 1-8. https://doi.org/10.1016/j.est.2018.10.025. **SJR 2017 Q1**

5. **O. D. Montoya**, A. Garces and C. A. Castro, "Optimal Conductor Size Selection in Radial Distribution Networks Using a MINLP Formulation," *IEEE Latin America Transactions*, vol. 16, no. 8, **2018**, pp. 2213-2220. http://www.ewh.ieee.org/reg/9/etrans/ieee/issues/vol16/vol16issue08Aug.2018/19MONTOYA.htm. **SJR 2017 Q2**

6. **O. D. Montoya**, "Numerical Approximation of the Maximum Power Consumption in DC-MGs with CPLs via an SDP Model," *IEEE Transactions on Circuits and Systems II: Express Briefs*, early access, **2018**, pp. 1-5. https://ieeexplore.ieee.org/document/8443095. **SJR 2017 Q1**

7. **O. D. Montoya**, W. Gil-González and A. Garces, "Optimal Power Flow on DC Microgrids: A Quadratic Convex Approximation," *IEEE Transactions on Circuits and Systems II: Express Briefs*, early access, **2018**, pp. 1-5. https://ieeexplore-ieee-org.ezproxy.utp.edu.co/document/8469013. **SJR 2017 Q1**

8. **O. D. Montoya**, A. Grajales and A. Garces and C. A. Castro, "Distribution Systems Operation Considering Energy Storage Devices and Distributed Generation," *IEEE Latin America Transactions*, vol. 15, no. 5, **2017**, pp. 890-900. https://ieeexplore.ieee.org/document/7910203/. **SJR 2017 Q2**

9. L. F. Grisales, **O. D. Montoya**, A. Grajales, R. A. Hincapie and M. Granada, "Optimal Planning and Operation of Distribution Systems Considering Distributed Energy Resources and Automatic Reclosers," *IEEE Latin America Transactions*, vol. 16, no. 1, **2018**, pp. 126-134. https://ieeexplore.ieee.org/document/8291464. **SJR 2017 Q2**

10. L. F. Grisales, A. Grajales, **O. D. Montoya**, R. A. Hincapie, M. Granada, and C. A. Castro, "Optimal location, sizing and operation of energy storage in distribution systems using multi-objective approach," *IEEE Latin America Transactions*, vol. 15,

no. 6, **2017**, pp. 1084-1090. https://ieeexplore.ieee.org/document/7932696. **SJR 2017 Q2**

11. **O. D. Montoya**, L. F. Grisales-Noreña, D. González-Montoya, C. A. Ramos-Paja and A. Garces, "Linear power flow formulation for low-voltage DC power grids," *Electric Power Systems Research*, vol. 163, Part A **2018**, pp. 375-381. https://doi.org/10.1016/j.epsr.2018.07.003. **SJR 2017 Q1**

12. W. Gil-González, and **O. D. Montoya** and A. Garcés, "Control of a SMES for mitigating subsynchronous oscillations in power systems: A PBC-PI approach," *Journal of Energy Storage*, vol. 20, **2018**, pp. 163-172. https://www.sciencedirect.com/science/article/pii/S2352152X18303852. **SJR 2017 Q1**

13. **O. D. Montoya**, L. F. Grisales, and V. M. Garrido, "Optimal Location and Sizing of Capacitors in Radial Distribution Networks Using an Exact MINLP Model for Operating Costs Minimization," *WSEAS Transactions on Business and Economics*, vol. 17, **2017**, pp. 244-252. http://www.wseas.org/multimedia/journals/economics/2017/a545916-558.php. **SJR 2017 Q3**

1.8.3 Conference papers

1. Walter Gil-González, **O. D. Montoya**, A. Garcés, F. M. Serra, and G. Magaldi, "Output Voltage Regulation For DCDC Buck Converters: a PassivityBased PI Design," in *2019 IEEE 10th Latin American Symposium on Circuits & Systems (LASCAS)*, Armenia, Quindío, Colombia, Feb. 2018. **2019**.

2. **O. D. Montoya**, V. M. Garrido, W. Gil-González, A. Garces, and L. F. Grisales-Noreña, "Controller Design for VSCs in Distributed Generation Applications: An IDA-PBC Approach," in *2018 IEEE International Autumn Meeting on Power, Electronics and Computing (ROPEC 2018)*, Ixtapa, Mexico, Nov. 2018, **2018**.

3. **O. D. Montoya**, V. M. Garrido, W. Gil-González, E. Holguín, and A. Garces, " An Exact Feedback Linearization Control of a SMES System to Support Power in Electrical Grids," in *IEEE 2018 9th Power, Instrumentation and Measurement Meeting (EPIM 2018)*, Salto, Uru., Nov. 2018, **2018**.

4. **O. D. Montoya**, J. E. Campillo, W. Gil-González, and A. Garces, "Integration of PV Arrays in DC Power Grids via Unidirectional Boost Converters: a PBC Approach," in *IEEE 2018 9th Power, Instrumentation and Measurement Meeting (EPIM 2018)*, Salto, Uru., Nov. 2018, **2018**.

5. S. Avila-Becerril, **O. D. Montoya**, G. Espinosa-Pérez, and A. Garcés, "Decentralized Passivity-Based Control for Microgrids," *Latin American Conference on Automatic Control 2018 (CLCA 2018)*, Quito, Ecuador, Oct. 2018, **2018**.

6. **O. D. Montoya**, W. Gil-González, and A. Garcés, "SCES Integration in Power Grids: A PBC Approach under abc, $\alpha\beta 0$ and dq0 Reference Frames," in *2018 IEEE PES Transmission and Distribution Conference and Exhibition Latin America (T&D LA 2018)*, Lima, Perú, Sept. 2018, **2018**, pp. 1-5. `https://ieeexplore.ieee.org/document/8511707`

7. M. Bravo, A. Garcés, O. D. Montoya and C. R. Baier, "Nonlinear Analysis for the Three-Phase PLL: A New Look for a Classical Problem," in *2018 IEEE 19th Workshop on Control and Modeling for Power Electronics (COMPEL), Padua, Italy*, **2018**, pp. 1-6. `https://ieeexplore-ieee-org.ezproxy.utp.edu.co/document/8460081`

8. I. Ortega-Velázquez, G. Espinosa-Pérez, **O. D. Montoya**, A. Garcés, and L. F. Grisales, "Current Control Mode in PV Systems Integrated with DC-DC Converters for MPPT: An IDA-PBC Approach," in *2018 IEEE Green Technologies Conference (GreenTech)*, Austin, TX, **2018**, pp. 1-6. `https://ieeexplore.ieee.org/document/8373593/`

9. **O. D. Montoya**, W. Gil-González, A. Escobar-Mejía, A. Garcés, and L. F. Grisales, "Nonlinear Control for Battery Energy Storage Systems in Power Grids," in *2018 IEEE Green Technologies Conference (GreenTech)*, Austin, TX, **2018**, pp. 65-70. `https://ieeexplore.ieee.org/document/8373604/`

10. **O. D. Montoya**, A. Garcés, I. Ortega-Velázquez and G. Espinosa-Pérez, "Passivity Based Control for Battery Charging/Discharging Applications by Using a Buck-Boost DC-DC Converter," in *2018 IEEE Green Technologies Conference (GreenTech)*, Austin, TX, **2018**, pp. 89-94. `https://ieeexplore.ieee.org/document/8373608/`

11. **O. D. Montoya**, A. Garcés, F. M. Serra, and G. Magaldi, "Apparent Power Control in Single-Phase Grids Using SCES Devices: An IDA-PBC Approach," in *2018 IEEE 9th Latin American Symposium on Circuits & Systems (LASCAS)*, Puerto Vallarta, Jal., Mexico **2018**, pp. 1-4. `https://ieeexplore.ieee.org/abstract/document/8399963/`

12. F. Salazar-Caceres, M. Bueno-Lopez, **O. D. Montoya** and A. Garcés, "LQR control for superconducting magnetic energy storage on distribution networks using feedback linearization," in *2017 IEEE 3rd Colombian Conference on Automatic Control (CCAC)*,

Cartagena, Colombia, **2017**, pp. 1-6. https://ieeexplore.ieee.org/document/8276480/

13. **O. D. Montoya**, W. Gil-González, A. Garcés and G. Espinosa-Pérez, "IDA Passivity Based Control for Superconducting Magnetic Energy Storage with PWM-CSC," in *2017 Ninth Annual IEEE Green Technologies Conference (GreenTech)*, Denver, CO, **2017**, pp. 89-95. https://ieeexplore.ieee.org/document/7923943/

14. W. Gil-González, **O. D. Montoya**, A. Garcés and A. Escobar-Mejía, "Supervisory LMI-Based State-Feedback Control for Current Source Power Conditioning of SMES," in *2017 Ninth Annual IEEE Green Technologies Conference (GreenTech)*, Denver, CO, **2017**, pp. 145-150. https://ieeexplore.ieee.org/document/7923951/

1.8.4 Undergraduate theses

1. **J. J. Arias-Posso**, "*Reconfiguración óptima de redes de distribución empleando un Algoritmo Metaheurístico Híbrido: una Combinación entre los algoritmos genéticos y las hormigas león*," Ingeniería Eléctrica, Universidad Tecnológica de Pereira, Pereira, Colombia, Junio, **2018**, Páginas 45. http://repositorio.utp.edu.co/dspace/handle/11059/9400

2. **D. Valencia-González**, "*Control no lineal de potencia aparente basado en pasividad de un convertidor monofásico aplicado a la generación distribuida*," Ingeniería Eléctrica, Universidad Tecnológica de Pereira, Pereira, Colombia, Abril, **2018**, Páginas 48. http://repositorio.utp.edu.co/dspace/handle/11059/8983

3. **B. A. Bolaños-Bastidas**, "*Control no lineal de un supercapacitor para control de potencia activa y reactiva en microrredes*," Ingeniería Eléctrica, Universidad Tecnológica de Pereira, Pereira, Colombia, Marzo, **2018**, Páginas 65. http://repositorio.utp.edu.co/dspace/handle/11059/8924

4. **N. A. Ramírez-Beltrán**, "*Control de potencia activa y reactiva empelando un convertidor por fuente de tensin para aplicaciones de generacin distribuida*," Ingeniería Eléctrica, Universidad Tecnológica de Pereira, Pereira, Colombia, Junio, **2017**, Páginas 55. http://repositorio.utp.edu.co/dspace/handle/11059/8003

5. **L. A. Cortes-Fuertes**, "*Operación eficiente de almacenadores de energía en micro-redes*," Ingeniería Eléctrica, Universidad Tecnológica de Pereira, Pereira, Colombia, Noviembre, **2016**, Páginas 67. http://repositorio.utp.edu.co/dspace/handle/11059/7410

1.9 Document outline

The remainder of this thesis is organized as follows.

Chapter 2 presents the general theory related to Hamiltonian dynamical modeling applied to bilinear systems as well as the theoretical derivation of passivity-based proportional-integral control and interconnection and damping assignment approaches. The dynamics of the error theory is introduced for solving the tracking trajectories problem, transforming this problem into an equivalent regulation problem.

Chapter 3 presents the mathematical modeling associated with power electronic converters based on voltage and current source technologies by applying the averaging modeling theory. The integration of supercapacitors, superconducting coils, batteries and renewable generation is also analyzed there, from the point of view of converter technology and control requirements.

Chapter 4 presents the mathematical structure of the whole electrical network considering single-phase and three-phase structures. Additionally, this chapter discusses concepts of islanding and grid-connecting operation modes for AC microgrids, focusing on the control objectives.

Chapter 5 presents the simulation results obtained from the application of passivity-based controllers for integrating DERs in SP-μGrids and TP-μGrids. The application of supercapacitors and superconducting coils for energy compensation, batteries for isolated applications with renewable energy resources and multiple combination of DERs are also analyzed.

Chapter 6 presents the conclusions and outlines future research needs.

1.10 Summary of the chapter

This chapter presented the conceptualization of this thesis by analyzing the main components of AC μGrids. First, the motivation for carrying out this investigation was presented by highlighting the transition from passive to active μGrids due to the rapid advances in power electronic devices in terms of efficiency, cost reduction, and energy density, among others. Second, a comprehensive review of the state-of-the-art was presented for supporting the research question addressed in the problem statement section, which is about the possibility of proposing a general PBC approach for integrating multiple DERs in AC μGrids. Finally, the objectives of this thesis as well as its scope were also presented here to make their verification easier in the following chapters. Lists of publications derived directly from this work were also presented.

Chapter 2

Preliminaries about Hamiltonian systems and passivity control design

This chapter presents the concept of a Hamiltonian system, focusing on dynamical systems with port-Hamiltonian structure. In addition, nonlinear control analysis and designing based on interconnection and damping assignment as well as passivity-based proportional-integral control for general bilinear systems are presented and analyzed.

2.1 Passive and dissipative systems

The concept of dissipation can be intuitively understood as a general phenomenon of energy loss[1], which corresponds to an intrinsic property of any physical system. This idea was initially introduced for analyzing electrical machines [109] and widely exploited in the field of control theory [110, 111]. From the point of view of power systems, energy dissipation is mainly produced by the resistive effects in conductors and mechanical friction in rotatory machines [33]. From an analytical standpoint, the notion of dissipativity can be studied by introducing two main concepts related to a nonlinear dynamical system with the general structure presented in Fig. 2.1 [30]:

- The *supply rate* is a real-valued function that measures the energy flowing through the dynamical system. It is defined by $w\left(u, y\right)$, where u represents the control inputs and y the desired outputs.
- The amount of energy stored in the system is quantified by a *storage function* $\mathcal{V}\left(x\right)$.

[1]Note that the concept of energy loss is presented in the context of the transformation of energy into heat, mainly caused by dissipation in real processes, e.g., resistive effects in electrical circuits or friction in mechanical systems, among others.

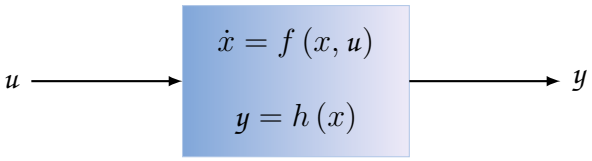

Figure 2.1: Generic representation of a nonlinear dynamical system

The dissipativity can be defined if the supply rate is such that for all admissible $u(t)$ and $x(0)$, this function fulfills

$$\int_0^t \left| w\left(u(\tau), y(\tau)\right)\right| d\tau \leq +\infty,\ t \in \mathbb{R}^+; \tag{2.1}$$

where w is assumed to be integrable independently of the input and initial conditions. The concept of admissibility is related to the existence of a bounded solution for the set of differential equations that defines the dynamical behavior of the physical system under analysis [112].

The relation between the supply rate w and the energy storage function $\mathcal{V}$ is well-established by the dissipation inequality, which means that along the time trajectories of a dissipative system the increase in the stored energy is not greater than the supply rate [113]. This relation is mathematically formulated as follows.

Definition 2 (Dissipative system) *A dynamical system is said to be dissipative if there exists an energy storage function $\mathcal{V}(x)$ such the following dissipation inequality holds.*

$$\mathcal{V}(x(t)) \leq \mathcal{V}(x(0)) + \int_0^t \left| w\left(u(\tau), y(\tau)\right)\right| d\tau; \tag{2.2}$$

along every possible trajectory followed by the dynamical system starting at $x(0)$, for all $x(0)$ and $t \geq 0$.

Note that the concept of *storage function* no longer has to be attached to a physical interpretation of energy [113]. Although this perspective was dominant at the time when this theory was introduced, the concept of storage function has acquired a much more general meaning with the latest developments in the field [19, 28].

Now, the concept of passive system is introduced [30, 33]

Definition 3 (Passive system) *A dissipative dynamical system is said to be passive with the supply rate $w\left(u, y\right) = u^T y$ and storage function $\mathcal{V}(x)$ if $\mathcal{V}(0) = 0$ for all $t \geq 0$ and*

$$\mathcal{V}(x(t)) \leq \mathcal{V}(x(0)) + \int_0^t u(\tau)^T y(\tau) d\tau; \tag{2.3}$$

A dynamical system is said to be *strictly passive* if the following definition is fulfilled

Definition 4 (Strictly passive system) *A dynamical system is a strictly passive system if it is passive and there exists a positive definite function $\mathcal{S}(x)$ for all $t \geq 0$ and*

$$\mathcal{V}\left(x\left(t\right)\right) = \mathcal{V}\left(x\left(0\right)\right) + \int_0^t u(\tau)^T y(\tau) d\tau - \int_0^t \mathcal{S}\left(x(\tau)\right) d\tau; \tag{2.4}$$

If the equality holds in (2.4) and $\mathcal{S}\left(x(t)\right) \equiv 0$, the dynamical system is said to be lossless [114]. For practical purposes, in the specialized literature, the function $\mathcal{S}\left(x\right)$ is referred to as a dissipative function. It can be positive semidefinite and some authors use it to define systems as *weak passive systems*. The concept of passivity is particularly important for the analysis of ac microgrids, since power electronic converters as well as the electrical network itself exhibit this property in their dynamical models [31, 72, 113].

2.2 Stability in the sense of Lyapunov

Lyapunov theory is a well known methodology to characterize the dynamical behavior of dynamical systems around equilibrium points or trajectories. For the sake of completeness, this theory is briefly presented in this section. Most of these results were taken from [30, 33, 114].

Consider a general nonlinear autonomous dynamical system:

$$\dot{x}\left(t\right) = f\left(x\left(t\right)\right), \quad x\left(0\right) = x_0, \quad t \in \mathcal{I}_{x_0} \tag{2.5}$$

where $x(t) \in \mathcal{D} \subseteq \mathbb{R}^n$, $t \in \mathcal{I}_{x_0}$ represents the state vector, $\mathcal{D}$ is an open set with $0 \in \mathcal{D}$, $f : \mathcal{D} \to \mathbb{R}^n$ is continuous on $\mathcal{D}$, and $\mathcal{I}_{x_0} = [0, \tau_{x_0})$, $0 \leq \tau_{x_0} \leq \infty$.

For every initial condition $x(0) \in \mathcal{D}$ and every $\tau_{x_0} > 0$, the dynamical system (2.5) possesses a unique solution $x : [0, \tau_{x_0}) \to \mathcal{D}$ on the interval $[0, \tau_{x_0})$. Unless otherwise stated, it is assumed that $f(0) = 0$ and $f(\cdot)$ is Lipschitz continuous on $\mathcal{D}$. The following definition introduces several types of stability corresponding to the zero solution $x(t) = 0$ of (2.5) for $\mathcal{I}_{x_0} = [0, \tau_{x_0})$.

Definition 5 (Characterization of stability)

i. The zero solution $x(t) \equiv 0$ to (2.5) is Lyapunov stable if, for all $\epsilon > 0$, there exists $\delta = \delta(\epsilon) > 0$ such that if $\|x(0)\| < \delta$, then $\|x(t)\| < \delta$, $t \geq 0$.

ii. The zero solution $x(t) \equiv 0$ to (2.5) is (locally) asymptotically stable if it is Lyapunov stable and there exists $\delta > 0$ such that if $\|x(0)\| < \delta$, then $\lim_{t\to\infty} x\left(t\right) = 0$.

iii. The zero solution $x(t) \equiv 0$ to (2.5) is globally asymptotically stable if it is Lyapunov stable and for all $x(0) \in \mathbb{R}^n$, $\lim_{t\to\infty} x(t) = 0$.

iv. The zero solution $x(t) \equiv 0$ to (2.5) is unstable if it is not Lyapunov stable.

Theorem 1 (Lyapunov's Theorem) *Consider the nonlinear dynamical system (2.5) and assume that there exists a continuously differentiable function $\mathcal{V} : \mathcal{D} \to \mathbb{R}$ such that*

$$\mathcal{V}(0) = 0, \tag{2.6}$$

$$\mathcal{V}(x) > 0, \quad x \in \mathcal{D}, \quad x \neq 0, \tag{2.7}$$

$$\nabla\mathcal{V}(x)^T f(x) \leq 0, \quad x \in \mathcal{D}. \tag{2.8}$$

Then the zero solution $x(t) \equiv 0$ to (2.5) is Lyapunov stable. If, in addition,

$$\nabla\mathcal{V}(x)^T f(x) < 0, \quad x \in \mathcal{D}, \quad x \neq 0, \tag{2.9}$$

then the zero solution $x(t) \equiv 0$ to (2.5) is asymptotically stable.

For a complete proof of Lyapunov's theorem, see [30].

2.3 Port-Hamiltonian systems

The general structure of a port-Hamiltonian (pH) system takes the following form [19,28,49].

$$\begin{aligned} \dot{x} &= [\mathcal{J}(x,u) - \mathcal{R}(x)]\nabla\mathcal{H}(x) + \mathcal{G}(x)u \\ y &= \mathcal{G}^T(x)\nabla\mathcal{H}(x) \end{aligned} \tag{2.10}$$

Here, $x \in \mathbb{R}^n$ are the state variables, $\mathcal{J}(x,u) \in \mathbb{R}^{n\times n}$ is an skew-symmetric interconnection matrix, $\mathcal{R}(x) = \mathcal{R}^T(x) \in \mathbb{R}^{n\times n}$ is a positive semidefinite symmetric dissipation matrix, $\nabla\mathcal{H}(x) \in \mathbb{R}^n$ is the gradient of the Hamilton function ($\mathcal{H}(x) \in \mathbb{R}^{0,+}$), $\mathcal{G}(x) \in \mathbb{R}^{n\times p}$ is the input matrix, and $y \in \mathbb{R}^p$ and $u \in \mathbb{R}^p$ are called the port variables: their inner product corresponds to the *supply rate* w [113].

It is straightforward to demonstrate that the pH system defined in (2.10) is passive and dissipative. Additionally, Lyapunov's stability theory allows demonstrating passivity in case the input u is equal to zero [112], as presented below.

$$\begin{aligned} \dot{\mathcal{H}}(x) &= \nabla\mathcal{H}(x)^T\dot{x} \\ \dot{\mathcal{H}}(x) &= \nabla\mathcal{H}(x)^T[\mathcal{J}(x,u) - \mathcal{R}(x)]\nabla\mathcal{H}(x) + \nabla H(x)^T\mathcal{G}(x)u \end{aligned} \tag{2.11}$$

Now, if some terms in (2.11) are rearranged and combined to (2.10), then the following result is reached.

$$\dot{\mathcal{H}}(x) = -\nabla\mathcal{H}(x)^T\mathcal{R}(x)\nabla\mathcal{H}(x) + y^T u \tag{2.12}$$

Here, $y^T u$ is, as it was previously, the *supply rate*. Note that if the dissipation matrix $\mathcal{R}(\cdot) \succeq 0$ is positive semidefinite, then the expression (2.12) may be reduced to

$$\dot{\mathcal{H}}(x) \leq y^T u \tag{2.13}$$

Note that (2.11) is a passive system since the change in the total energy stored is less than or equal to w, $\forall t \geq 0$ [112], as presented in Definition 3.

It is important to point out that in electrical systems, from power systems to μGrids, the open-loop dynamical system has an intrinsic Hamiltonian structure [29], which implies that passivity-based control based on Hamiltonian formulations is an adequate control approach for analyzing these systems [72,78]. In the next section, the general concepts of the application of passivity-based control theory to Hamiltonian systems will be presented.

2.4 Passivity-based control

Different passivity-based control approaches have been developed based on energy modification via damping injection and interconnection modification [28]. Two approaches stand out: interconnection and damping assignment (IDA-PBC) [31], and proportional-integral (PI-PBC) [29, 115]. Both techniques employ the same energy shaping principle. The possible applications of these techniques depend on the nature of the dynamical system under study, e.g., IDA-PBC is ideal for nonlinear systems with an affine structure, while PI-PBC is applicable mainly to bilinear systems. Nevertheless, both can be applied for controlling power electronic converters based on voltage or current source technologies [49, 78].

2.4.1 Bilinear systems

Electrical power systems, especially μGrids, allow a bilinear mathematical model due to the insertion of distributed energy resources via power electronic converters [77]. Here, the main interest is in a particular type of bilinear systems, called pH-bilinear systems. A pH-bilinear system can be defined as follows.

Definition 6 (pH-bilinear system) *A pH-bilinear system is a nonlinear dynamical system such that there are products between the state variables and control inputs with the following structure*

$$\mathcal{D}\dot{x} = [\mathcal{J}(u) - \mathcal{R}]x + \varphi(t); \tag{2.14}$$

where $\mathcal{D} \in \mathbb{R}^{n\times n}$ is a positive definite diagonal matrix, commonly known as the inertia matrix, $\mathcal{J}(u)$, $\mathcal{R}$, x and u fulfill the definition given for (2.10), while $\varphi(t) \in \mathbb{R}^n$ is a vector that contains all external inputs. These inputs can be either time-dependent or time-independent.

Note that the physical existence of a pH-bilinear system implies that the control inputs u and the external inputs $\varphi(t)$ are bounded for $t > 0$ [115]. Based on this, the existence of an admissible behavior for the state variables can be defined as follows

Definition 7 (Admissible trajectory [115]) *The dynamical behavior $x^\star$ corresponds to an admissible trajectory of (2.14) if it is bounded, differentiable and*

$$\mathcal{D}\dot{x}^\star = \left[\mathcal{J}\left(u^\star\right) - \mathcal{R}\right] x^\star + \varphi(t)\,; \tag{2.15}$$

for some bounded and well-defined $u^\star$.

Recall that the bilinear system (2.14) is nonlinear and non-autonomous [29]. Hence, $x^\star$ corresponds to a trajectory, not an operating point. Nevertheless, the tracking trajectory problem for Hamiltonian systems has not been solved yet. For this reason, a transformation to a regulation problem is commonly used for solving the control tasks via the dynamics of the error [113], as is required for applying the PI-PBC approach [77].

To reformulate the tracking trajectories problem into a regulation problem [29], the following variables can be defined:

$$\begin{aligned} \tilde{x} &= x - x^\star, \\ \tilde{u} &= u - u^\star, \end{aligned} \tag{2.16}$$

where $\tilde{x}$ and $\tilde{u}$ represents the error of the state variables and the control variables, respectively. In addition, $x^\star$ represents the desired trajectories (defined by the control designer and the particular dynamics of the system under study), and $u^\star$ defines the desired control inputs, which can be obtained by solving (2.15).

If (2.16) is substituted in (2.14) and combined with (2.15), the dynamics of the error is mathematically defined as

$$\mathcal{D}\dot{\tilde{x}} = \left[\mathcal{J}\left(u\right) - \mathcal{R}\right] \tilde{x} + \mathcal{J}\left(\tilde{u}\right) x^\star; \tag{2.17}$$

Note that (2.17) corresponds to a pH-bilinear system as a function of the error variables, which implies that the stability properties of this system can be imposed via Lyapunov's stability theory in order to define its desired dynamical performance.

2.4.2 IDA-PBC

Interconnection and damping assignment passivity-based control [116,117] tries to modify the dynamical behavior of a Hamiltonian system by moving the current behavior to the desired behavior by changing its energy flow [28, 49]. In general terms, the desired Hamiltonian model can be defined as follows:

$$\mathcal{D}\dot{\tilde{x}} = \left[\mathcal{J}_d\left(u\right) - \mathcal{R}_d\right]\tilde{x}; \tag{2.18}$$

where $\mathcal{J}_d\left(u\right)$ is the desired interconnection matrix, which is typically selected as the open-loop interconnection matrix, i.e., $\mathcal{J}_d\left(u\right) = \mathcal{J}\left(u\right)$, to simplify the control input as presented in [31]. Additionally, $\mathcal{R}_d$ corresponds to the desired damping matrix, which is conventionally selected to be a diagonal positive definite matrix [49].

To find the general structure of the IDA-PBC as applied to pH-bilinear systems, the set of equations (2.18) can be compared to (2.17), and by making some straightforward manipulations, this allows obtaining the following expression.

$$\mathcal{J}\left(\tilde{u}\right)x^{\star} = \left[\mathcal{R} - \mathcal{R}_d\right]\tilde{x}; \tag{2.19}$$

Solving the set of equations (2.19) gives the general expression for $\tilde{u}$. It is worth noting that if the desired control inputs $u^{\star}$ obtained from (2.15) are combined with (2.19), the classical IDA-PBC approach presented in [28, 49] is easily reached.

To prove stability with the IDA-PBC approach applied to a bilinear system, the Hamiltonian function is selected as the Lyapunov candidate function:

$$\mathcal{V}(\tilde{x}) = \mathcal{H}_d(\tilde{x}) = \frac{1}{2}\tilde{x}^T\mathcal{D}\tilde{x}. \tag{2.20}$$

Note that (2.20) corresponds to a quadratic positive definite function, which fulfill the first two Lyapunov stability conditions [33, 114], i.e., $\mathcal{V}(0) = 0,\ \tilde{x} = 0$ and $\mathcal{V}(0) > 0,\ \tilde{x} \neq 0$, respectively.

Taking the temporal derivative of $\mathcal{V}(\tilde{x})$, substituting into (2.18) and making some algebraic manipulations, one obtains

$$\dot{\mathcal{V}}(\tilde{x}) = \tilde{x}^T\mathcal{D}\dot{\tilde{x}} = -\tilde{x}^T\mathcal{R}_d\tilde{x}; \tag{2.21}$$

From (2.21), the following conclusions about stability of the dynamics of the error can be made:

- if $\mathcal{R}_d$ is positive semidefinite, then (2.18) is stable in the sense of Lypaunov.
- if $\mathcal{R}_d$ is positive definite, then (2.18) is asymptotically stable in the sense of Lypaunov.
- if $\mathcal{R}_d$ is positive definite, then the exponential stability of (2.18) in the sense of Lypaunov can be guaranteed for $\beta \leq \lambda_{\min}(\mathcal{D}^{-1}\mathcal{R}_d)$, where $\dot{\mathcal{V}}(\tilde{x}) \leq -\beta\mathcal{V}(\tilde{x})$.

2.4.3 PI-PBC control

Proportional-integral passivity-based control is a nonlinear control for non-affine systems that guarantees asymptotic stability in the sense of Lyapunov [77]. This approach was originally proposed by [29] for general bilinear systems. To define the general control law employed by PI-PBC control approach, the candidate Lyapunov function (2.20) and its corresponding time derivative function are applied to (2.17), which produces

$$\dot{\mathcal{V}}(\tilde{x}) = -\tilde{x}^T \mathcal{R} \tilde{x} + \tilde{x}^T \mathcal{J}\left(\tilde{u}\right) x^\star; \tag{2.22}$$

Observe that by using the bilinear properties in (2.17), one obtains

$$\mathcal{J}\left(\tilde{u}\right) x^\star = \sum_{i=1}^{p} \tilde{u}_i \mathcal{J}_i x^\star; \tag{2.23}$$

Now, substituting (2.23) into (2.22) and remembering that $\mathcal{R}$ is positive semidefinite, the following expression can be obtained.

$$\dot{\mathcal{V}}(\tilde{x}) \leq \sum_{i=1}^{p} \tilde{u}_i \tilde{x}^T \mathcal{J}_i x^\star; \tag{2.24}$$

If the i^{th} component of the output function y is defined as $y_i = \tilde{x}^T \mathcal{J}_i x^\star$, then (2.24) takes the form

$$\dot{\mathcal{V}}(\tilde{x}) \leq y^T \tilde{u}; \tag{2.25}$$

which corresponds to the definition 3 for a passive system with *supply rate* w.

To design a control input under the proportional-integral concept, the following control structure is employed [115].

$$\begin{aligned} u &= -\mathcal{K}_p y + \mathcal{K}_i z; \\ \dot{z} &= -y; \end{aligned} \tag{2.26}$$

where $\mathcal{K}_p$ is a symmetric positive definite matrix that contains all proportional gains, $\mathcal{K}_i$ is a positive definite symmetric matrix that contains all integral gains, and z is an auxiliary variable associated to the integral component of the PI-PBC design, as reported by [29].

The stability analysis of the proposed control law applied to the dynamics of the error can be carried out with an extended candidate Lypunov function, $\mathcal{W}(\tilde{x}, z)$, defined as follows [15, 77]

$$\mathcal{W}(\tilde{x}, z) = \mathcal{V}(\tilde{x}) + \frac{1}{2} z^T \mathcal{K}_i z; \tag{2.27}$$

Taking the temporal derivative of (2.27), and combining (2.22) with (2.18) and rearranging some terms, one obtains

$$\begin{aligned}\dot{\mathcal{W}}(\tilde{x}, z) &= \dot{\mathcal{V}}(\tilde{x}) - z^T \mathcal{K}_i y; \\ &= -\tilde{x}^T \mathcal{R} \tilde{x} - y^T \mathcal{K}_p y \\ &\leq -\lambda_{\min}\{\mathcal{K}_p\} \left|\left|y\right|\right|^2 - \left|\left|\mathcal{R}^{1/2}\tilde{x}\right|\right|^2\end{aligned} \tag{2.28}$$

which is the same expression studied in [115] to guarantee asymptotic stability for the dynamics of the error approach. This result implies that the PI-PBC approach can be used for bilinear systems such as (2.17 in terms of the concepts of Lyapunov stability, guaranteeing stability convergence, as below.

$$\lim_{t\to\infty} ||x(t) - x^\star(t)|| = 0; \tag{2.29}$$

Finally, Equation (2.29) shows that the desired operating point or trajectory can be achieved by applying PI-PBC to a bilinear system.

The two main approaches based on passivity-based control theory, employing interconnection and damping assignment or employing the action of a proportional-integral control, were presented in this chapter for analyzing non-affine dynamical systems in terms of the Lyapunov stability criteria, based on Hamiltonian formulations [77, 117]. These mathematical structures will play a significant role when the bilinear behavior of power electronic converters for the integration of distributed energy resources will be studied in Chapter 3.

2.5 Summary of the chapter

This chapter explored the mathematical foundations of the design of passivity-based controls for bilinear pH-bilinear systems. The most important characteristics of passive and dissipative systems were presented by focusing on their strong relation to energy storage functions and physical systems.

Lyapunov's stability concepts were used as the fundamental basis for designing controllers for pH-bilinear systems. Nevertheless, only concepts about practical and asymptotical stability were discussed, since the passivity-based theory analyzed here for bilinear systems allows guaranteeing these kinds of stability when power electronic converters are analyzed.

A theoretical derivation of passivity-based controllers based on classical interconnection and damping assignment as well as on proportional-integral actions were discussed by considering the dynamics of the error, so as to transform tracking trajectory problems into regulation problems.

Chapter 3

Power electronic converters: Hamiltonian modeling and control

Power electronic converters allow integrating multiple distributed energy resources into power systems, by controlling the active and reactive power independently. Two power electronic converter technologies are studied in this thesis: the pulse-width-modulated voltage source converter and the pulse-width-modulated current source converter. These are the most common technologies in practical applications for three-phase microgrids. The Hamiltonian formulation for single-phase and three-phase converter configurations are also explored from the circuits theory point of view. In addition, the mathematical modeling of the synchronous reference frame phase locked loop, the three-phase and single-phase converters are studied.

3.1 Power electronic converters in μGrids

Power electronic converters are essential devices for the integration, management, and operation of renewable energy resources and energy storage systems in electrical power grids [4]. These devices also allow interfacing alternating-current to direct-current power grids from low-voltage to high-voltage applications and vice versa [118]. Fig. 3.1 presents the classical interconnection of multiple distributed energy resources into a μGrids via power electronic converters [63].

The power electronic converters in this thesis for control and stability purposes are represented via averaged models [82], by simplifying discontinuous commutation states to modulation index equivalents [31]. Additionally, the power converters of interest are pulse-width-modulated current source converters (PWM-CSC) [73] or pulse-width-modulated voltage source converters (PWM-VSC) [31].

Note that pulse-width commutated power electronic converters (i.e., PWM-VSC and

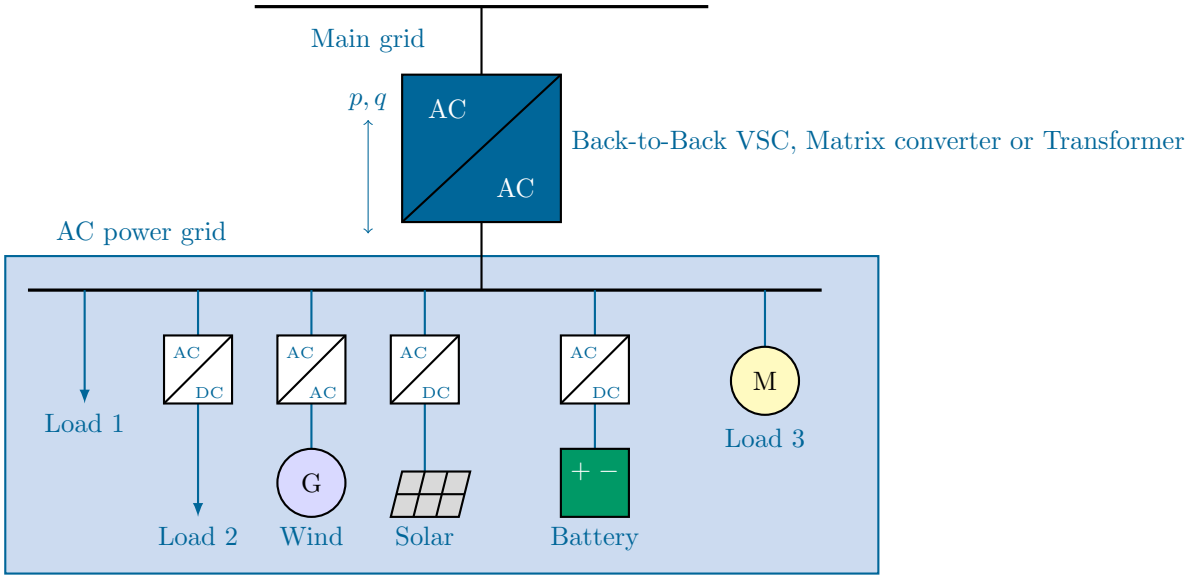

Figure 3.1: Typical interconnection of distributed energy resources in AC power grids [63]

PWM-CSC) can be designed for single-phase as well as three-phase configurations with minimal changes in their principles. For this reason, single-phase configurations will be analyzed before the three-phase schemes. Additionally, it is important to point out that in this thesis, PWM-VSC will be employed to integrated supercapacitors and renewable generation whereas PWM-CSC will help to integrate superconducting coils.

3.2 Internal connection of power electronic converters

Voltage and current source converters are typically constituted by arrays of switches with IGBT or MOSFET technologies [119], which are operated (opened or closed) via pulse-width or space-vector modulation methods. Fig. 3.2 depicts the internal connection of these single-phase and three-phase converters.

Observe that PWM-VSC are made up by arrays of IGBTs with two or three legs, where in the DC side a DC voltage source is required, as shown in Figs. 3.2(a) and 3.2(b). This implies that the two IGBTs of the same leg can not conduct at the same instant; this is in order to avoid short-circuits at the DC link.

In the case of PWM-CSCs, they are composed by the series connection of IGBTs and power diodes which are distributed in pairs for each leg, as presented in Figs. 3.2(c) and 3.2(d). The function of each power diode is to prevent inversions of the DC current. These converters maintain a path for the DC current, which means that one upper and one down

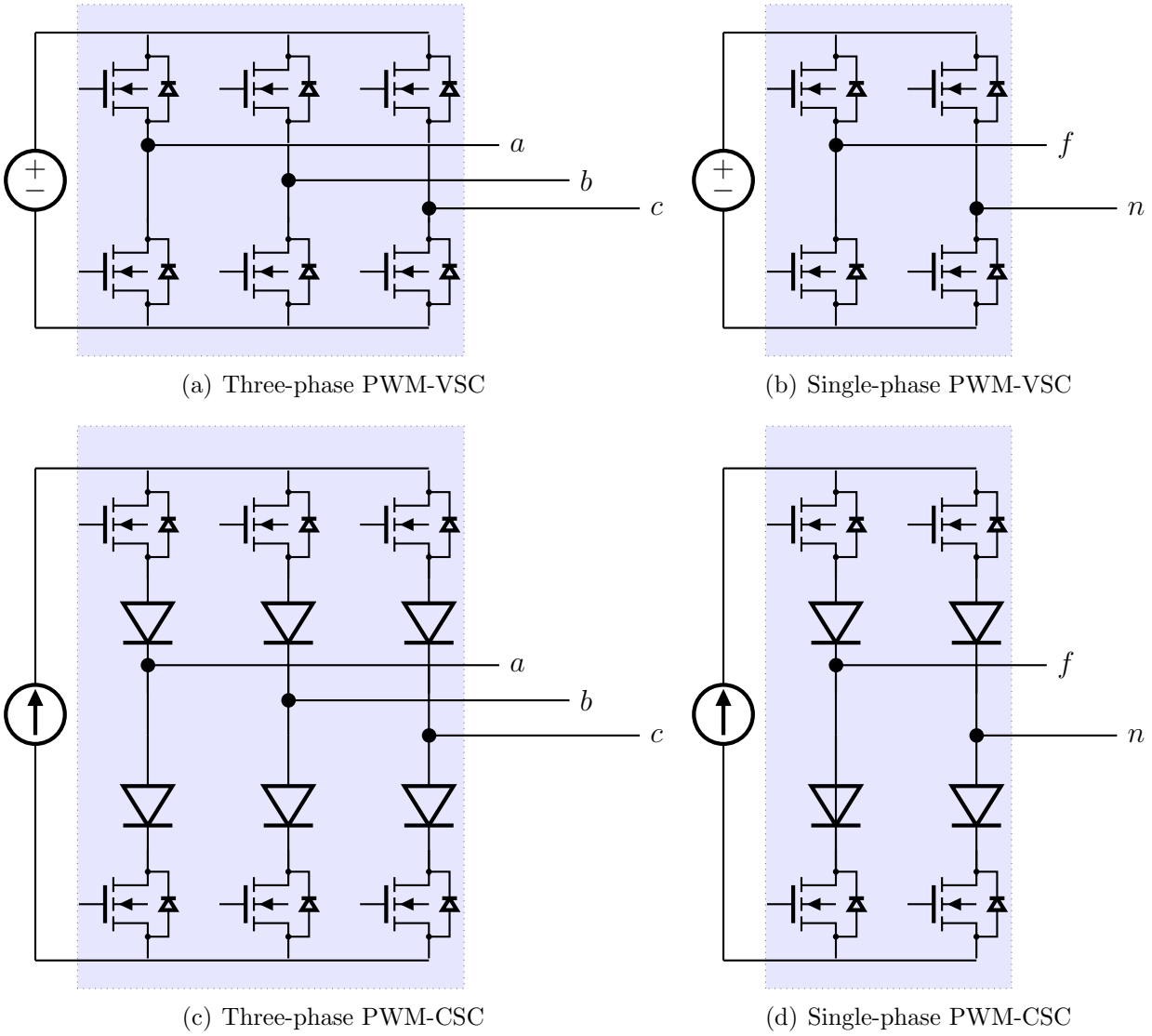

(a) Three-phase PWM-VSC

(b) Single-phase PWM-VSC

(c) Three-phase PWM-CSC

(d) Single-phase PWM-CSC

Figure 3.2: Internal switch connection and diodes for making three-phase and single-phase power electronic converters based on voltage and current source technologies

IGBT must be conducting all times to avoid open circuits at the DC link. The details of the modulation of the topology of each of these converters can be found in [120]. This thesis uses averaging modeling to analyze these converters.

3.3 Single-phase converters

The PWM-VSC is more suitable for interconnecting solar photovoltaic and wind power as well as supercapacitors, whereas the PWM-CSC is more suitable for integrating superconducting coils. The former requires an electrolytic capacitor in the DC side for controlling the DC voltage, as depicted in Fig. 3.3(a), while the latter can control the DC current directly, as can be seen in Fig. 3.3(b) [11, 76].

From Fig. 3.3 there can be seen the main differences between the PWM-VSC and PWM-CSC lines in the shunt capacitive filter C_f located in the AC side of the converter as well as the elements interconnected in their DC sides. In the case of PWM-VSC, a parallel combination between a capacitive element C_{sc} and a DC current source i_s is made [31, 63], whereas in the PWM-CSC, a superconducting coil L_{sc} is directly interconnected in the DC side of the converter [72, 78].

Note that both converters employ in their AC sides a series inductive-resistive filter ($R_f - L_f$). In addition, in the case of PWM-VSC, if renewable energy resources or batteries are non-existent, then this implies that $i_s = 0$, and the capacitance in its DC side may become

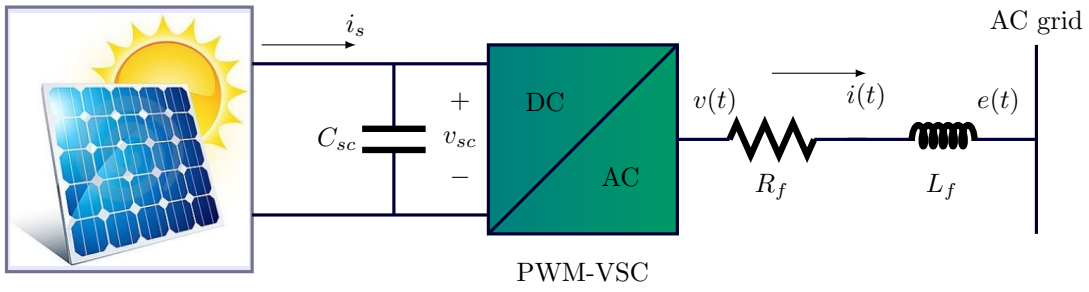

(a) Single-phase PWM-VSC

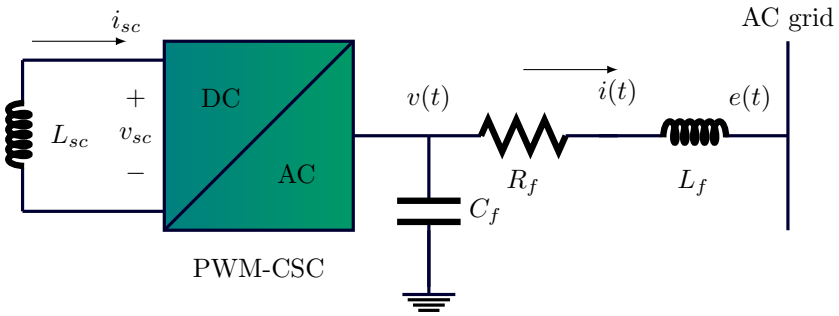

(b) Single-phase PWM-VSC

Figure 3.3: Interconnection of DERs in single-phase μGrids via PWM-VSCs and PWM-CSCs

a supercapacitor energy storage system [63].

For the mathematical interpretation, $e(t)$ is the voltage in the AC grid, while $v(t)$ is the AC voltage output in each converter and $i(t)$ is the AC current flowing to the series filter. In the DC side, v_{sc} is the DC voltage at each converter, while i_{sc} is the current through the superconducting coil, and t is the time.

3.3.1 Dynamical modeling

Equations (3.1) and (3.2) present the averaged models[1] of single-phase converters for the integration of DERs in single-phase μGrids [19, 31, 63, 72].

Dynamical model for the PWM-VSC

$$\begin{aligned} L_f \tfrac{d}{dt} i(t) &= -R_f i(t) + m(t) v_{sc}(t) - e(t); \\ C_{sc} \tfrac{d}{dt} v_{sc}(t) &= i_s(t) - m(t) i(t); \end{aligned} \tag{3.1}$$

Dynamical model for the PWM-CSC

$$\begin{aligned} L_f \tfrac{d}{dt} i(t) &= -R_f i(t) + v(t) - e(t); \\ C_f \tfrac{d}{dt} v(t) &= m(t) i_{sc}(t) - i(t); \\ L_{sc} \tfrac{d}{dt} i_{sc}(t) &= -m(t) v(t); \end{aligned} \tag{3.2}$$

Note that both dynamical systems have a similar mathematical structure. The variable t will be suppressed from here on, for simplicity and brevity in the mathematical modeling. On the other hand, it is straightforward that both dynamical models take the form defined by (2.13) for bilinear non-affine non-autonomous dynamical systems if $m(t)$ is considered as the control input. Additionally, observe that both models are under-actuated since there is only a control input and more than one differential equation for each dynamical model. The matrices and vectors that allow writing (3.1) and (3.2) as (2.14) are presented in Table 3.1.

3.3.2 Selection of the references

The operation of power electronic converters requires not only their dynamical modeling: it is also necessary to know what is the desired dynamical performance to achieve the control objectives by integrating these devices into AC μGrids. The main idea of the integration of multiple DERs is the possibility of interchanging active and reactive power between the

[1]Note that averaged models allow designing controllers in the continuous-time domain, by simplifying discrete states as continuous states, which facilitates stability proofs.

Dynamical model for PWM-VSC
$\mathcal{D} = diag\begin{pmatrix} L_f \\ C_{sc} \end{pmatrix}, \quad \mathcal{J} = \begin{pmatrix} 0 & m \\ -m & 0 \end{pmatrix}, \quad u = m$
$\mathcal{R} = diag\begin{pmatrix} R_f \\ 0 \end{pmatrix}, \quad x = \begin{pmatrix} i \\ v_{sc} \end{pmatrix}, \quad \varphi = \begin{pmatrix} -e \\ i_s \end{pmatrix}$
Dynamical model for PWM-CSC
$\mathcal{D} = diag\begin{pmatrix} L_f \\ C_f \\ L_{sc} \end{pmatrix}, \quad \mathcal{J} = \begin{pmatrix} 0 & 1 & 0 \\ -1 & 0 & m \\ 0 & -m & 0 \end{pmatrix}, \quad u = m$
$\mathcal{R} = diag\begin{pmatrix} R_f \\ 0 \\ 0 \end{pmatrix}, \quad x = \begin{pmatrix} i \\ v \\ i_{sc} \end{pmatrix}, \quad \varphi = \begin{pmatrix} -e \\ 0 \\ 0 \end{pmatrix}$

Table 3.1: Hamiltonian representation of each single-phase power electronic converter technology

converter and the main grid. Henc, the variable of interest in terms of control is the filter current i (see Fig. 3.2) since this current allows managing the total power to the AC grid. Next, the general procedure to control the active and reactive power for a single-phase power electronic converter is presented.

To achieve the control objectives by integrating DERs in AC μGrids, the selection of the reference for the filter current is given in detail later in this chapter. A sinusoidal behavior for the voltage profile provided by the main grid e is supposed, which implies that the filter current i exhibits the same dynamical performance of this voltage, as presented below.

$$e = \sqrt{2}V_{rms}\cos(\omega t) \quad \text{V}; \tag{3.3}$$

$$i = \sqrt{2}I_{rms}\cos(\omega t - \theta) \quad \text{A}; \tag{3.4}$$

Here, I_{rms} and V_{rms} denote the root mean square vales of the current and voltage, respectively.

Note that by employing a phasorial representation of the sinusoidal signals, the voltage and current defined by (3.3) and (3.4) can be expressed as

$$\mathbf{E} = V_{rms}\angle 0 \quad \text{V}; \tag{3.5}$$

$$\mathbf{I} = I_{rms}\angle -\theta, \quad \text{A}; \tag{3.6}$$

Remembering that the complex power is defined by $\mathbf{S} = \mathbf{E}\mathbf{I}^*$, then

$$\mathbf{S} = V_{rms}I_{rms}\angle\theta, \quad \text{VA}; \tag{3.7}$$

Now, if the complex power (apparent power) is defined as a function of the desired behaviors of the active and reactive power, i.e., $P_{ac}^{\star}$ and $Q_{ac}^{\star}$, then (3.7) can be rewritten as

$$P_{ac}^{\star} = V_{rms} I_{rms} \cos(\theta), \quad \text{W}; \tag{3.8}$$

$$Q_{ac}^{\star} = V_{rms} I_{rms} \sin(\theta), \quad \text{VAr}; \tag{3.9}$$

On the other hand, the current defined by (3.4) can be reformulated as

$$i = \sqrt{2} I_{rms} \left(\cos(\omega t)\cos(\theta) + \sin(\omega t)\sin(\theta)\right) \quad \text{A}; \tag{3.10}$$

Note that by recurring to (3.8) and (3.9), the reference for the filter current i given in (3.10) as a function of the desired active and reactive power is

$$i = \frac{\sqrt{2}}{V_{rms}} \left(P_{ac}^{\star}\cos(\omega t) + Q_{ac}^{\star}\sin(\omega t)\right) \quad \text{A}; \tag{3.11}$$

Observe that (3.11) depends on the time-varying sinusoidal functions ($\sin(\omega t)$ and $\cos(\omega t)$), respectively. This implies that these signals need to be estimated as functions of the voltage input e. For this reason, the following quadrature signal generator is employed [76, 121].

Define the quadrature signal of the voltage profile delivered by the grid as

$$e_{\parallel} = \frac{e}{\sqrt{2} V_{rms}} = \cos(\omega t); \tag{3.12}$$

Now, suppose that there is a dynamical system that allows generating a perpendicular signal of $e_{\parallel}(t)$, which is defined by

$$\begin{bmatrix} \dot{z}_1 \\ \dot{z}_2 \end{bmatrix} = \begin{pmatrix} -k_s & \omega \\ -\omega & 0 \end{pmatrix} \begin{bmatrix} z_1 \\ z_2 \end{bmatrix} + \begin{bmatrix} k_s \\ 0 \end{bmatrix} e_{\parallel}(t); \tag{3.13}$$

where k_s defines the convergence rate of the state variables z_1 and z_2 to their reference values, with k_s a positive constant. Additionally, it is important to point out that (3.13 is a passive Hamiltonian system, since it fulfills Definition 3. From [76, 121], the general solution of this dynamical system is

$$\begin{bmatrix} e_{\parallel} \\ e_{\perp} \end{bmatrix} = \begin{pmatrix} 1 & 0 \\ 0 & \alpha \end{pmatrix} \begin{bmatrix} z_1 \\ z_2 \end{bmatrix}; \tag{3.14}$$

where $e_\perp$ is perpendicular to $e_\parallel$ and α helps to define if it is leading or lagging, i.e., $\alpha = +1$ if $e_\perp$ lags $e_\parallel$ but $\alpha = -1$ if $e_\perp$ leads $e_\parallel$. For the case of interest in this thesis (see Eq. (3.6)), $\alpha = +1$ is selected, which allows defining the reference signal of the filter current to be

$$i^\star = \frac{\sqrt{2}}{V_{rms}} \left(P^\star_{ac} z_1 + Q^\star_{ac} z_2\right) \quad \text{A}; \tag{3.15}$$

Finally, the selection of the desired active and reactive power behaviors depends exclusively on the control designer as well as the grid requirements as function of the availability of renewable generation or storing capabilities [63].

3.4 Three-phase power electronic converters

Three-phase PWM-VSCs and PWM-CSCs have the same functionality as single-phase configurations. Nevertheless, they can be interconnected with three-phase balanced and unbalanced distribution networks by including additional forced-commuted switches, as presented in Fig. 3.2 [11]. For simplicity, three-phase variables can be added to Fig. 3.3, which allows developing the dynamical models presented in the next subsection.

The main difference between single-phase and three-phase converter configurations is that single-phase models are non-autonomous, while three-phase models can be modeled in terms of either autonomous or non-autonomous reference frames. Next, the three-reference frames for a three-phase power electronic converter will be presented.

3.4.1 Dynamical modeling in the *abc* reference frame

This reference frame corresponds to the conventional time-varying working reference frame for TP-μGrids. The dynamical models of PWM-VSC as well as PWM-CSC are obtained by applying Kirchhoff's first law to any node with at least one capacitance, and Kirchhoff's second law to any closed-loop trajectory with at least one inductance [78]. These dynamical models are presented below.

Dynamical model for the PWM-VSC in *abc* reference frame

$$\begin{aligned} L_f \tfrac{d}{dt} i_{abc} &= -R_f i_{abc} + m_{abc} v_{sc} - e_{abc}; \\ C_{sc} \tfrac{d}{dt} v_{sc} &= i_s - m^T_{abc} i_{abc}; \end{aligned} \tag{3.16}$$

where the subscript *abc* represents a group of three variables, e.g., $i_{abc} = [i_a \; i_b \; i_c]^T$.

Dynamical model for the PWM-CSC in abc reference frame

$$\begin{aligned} L_f \tfrac{d}{dt} i_{abc} &= -R_f i_{abc} + v_{abc} - e_{abc}; \\ C_f \tfrac{d}{dt} v_{abc} &= m_{abc} i_{sc} - i_{abc}; \\ L_{sc} \tfrac{d}{dt} i_{sc} &= -m_{abc}^T v_{abc}; \end{aligned} \tag{3.17}$$

Note that the three-phase model of the PWM-VSC corresponds to a fourth-order dynamical model with three control inputs m_{abc}. The dynamical model of the PWM-CSC corresponds to a seventh-order dynamical model with the same number of control inputs as the PWM-VSC. This evidences the under-actuated nature of these dynamical models. By comparison with (2.14), the inertia, damping and interconnection matrices will be easily obtained as well as the structure of the state variables, control, and external inputs, respectively.

3.4.2 Dynamical modeling in the $\alpha\beta 0$ reference frame

This reference frame allows turning three-phase variables y_{abc} into the variables $y_{\alpha\beta 0}$. This transformation is known in the specialized literature as Clarke's transformation [122]. It can be formulated as follows.

$$y_{\alpha\beta 0} = T y_{abc} \Rightarrow \begin{pmatrix} y_\alpha \\ y_\beta \\ y_0 \end{pmatrix} = k \begin{pmatrix} 2 & -1 & -1 \\ 0 & \sqrt{3} & -\sqrt{3} \\ 1 & 1 & 1 \end{pmatrix} \begin{pmatrix} y_a \\ y_b \\ y_c \end{pmatrix}; \tag{3.18}$$

Here, k is a positive constant associated to the possibility of obtaining a transformation invariant in power or invariant in signal magnitudes between both reference frames.

Note that if the three-phase variables have a sinusoidal behavior, then the zero component of the $\alpha\beta 0$ takes a zero value:

$$\begin{pmatrix} y_a \\ y_b \\ y_c \end{pmatrix} = \sqrt{2} Y_{rms} \begin{pmatrix} \cos(\theta) \\ \cos\left(\theta - \frac{2}{3}\pi\right) \\ \cos\left(\theta + \frac{2}{3}\pi\right) \end{pmatrix}, \quad \begin{pmatrix} y_\alpha \\ y_\beta \\ y_0 \end{pmatrix} = \sqrt{2} Y_{rms} \begin{pmatrix} \cos(\theta) \\ \sin(\theta) \\ 0 \end{pmatrix}; \tag{3.19}$$

If Clarke's transformation is applied to the dynamical models of the PWM-VSC and PWM-CSC, then the following dynamical models are obtained in the $\alpha\beta$ reference frame.

Dynamical model for the PWM-VSC in $\alpha\beta$ reference frame

$$\begin{aligned} L_f \tfrac{d}{dt} i_{\alpha\beta} &= -R_f i_{\alpha\beta} + m_{\alpha\beta} v_{sc} - e_{\alpha\beta}; \\ C_{sc} \tfrac{d}{dt} v_{sc} &= i_s - m_{\alpha\beta}^T i_{\alpha\beta}; \end{aligned} \tag{3.20}$$

where the subscript $\alpha\beta$ represents a group of two variables, e.g., $i_{\alpha\beta} = [i_\alpha \; i_\beta]^T$.

Dynamical model for the PWM-CSC in $\alpha\beta$ reference frame

$$\begin{aligned} L_f \tfrac{d}{dt} i_{\alpha\beta} &= -R_f i_{\alpha\beta} + v_{\alpha\beta} - e_{\alpha\beta}; \\ C_f \tfrac{d}{dt} v_{\alpha\beta} &= m_{\alpha\beta} i_{sc} - i_{\alpha\beta}; \\ L_{sc} \tfrac{d}{dt} i_{sc} &= -m_{\alpha\beta}^T v_{\alpha\beta}; \end{aligned} \tag{3.21}$$

Observe that when Clarke's transformation was applied, the PWM-VSC model was reduced to a third-order dynamical model with two control inputs, whereas the PWM-CSC models was reduced to a fifth-order model with the same number of control inputs.

3.4.3 Dynamical modeling in the $dq0$ reference frame

This transforms three-phase variables y_{abc} into three DC variables y_{dq0}. This transformation is known as Park's transformation [11, 49] and can be formulated as

$$y_{dq0} = W y_{abc}$$

$$\begin{pmatrix} y_d \\ y_q \\ y_0 \end{pmatrix} = k \begin{pmatrix} \cos\left(\hat{\theta}\right) & \cos\left(\hat{\theta} - \frac{2}{3}\pi\right) & \cos\left(\hat{\theta} + \frac{2}{3}\pi\right) \\ -\sin\left(\hat{\theta}\right) & -sin\left(\hat{\theta} - \frac{2}{3}\pi\right) & -sin\left(\hat{\theta} + \frac{2}{3}\pi\right) \\ \frac{\sqrt{2}}{2} & \frac{\sqrt{2}}{2} & \frac{\sqrt{2}}{2} \end{pmatrix} \begin{pmatrix} y_a \\ y_b \\ y_c \end{pmatrix} \tag{3.22}$$

where k fulfills the same function as it did for Clarke's transformation. Additionally, $\hat{\theta}$ is to the relative angular position of the rotating $dq0$ reference frame, which is estimated as a function of the angular speed by

$$\hat{\theta} = \int_{t_0}^{t} (\hat{\omega}\tau)\, d\tau + \hat{\theta}_0; \tag{3.23}$$

where $\hat{\omega}$ is calculated by employing phase-looked-loop (PLL) techniques, as will be presented in the next section [123, 124]. Note that if $\hat{\omega}$ is equal to the angular frequency of the three-phase signals (3.19), then $\hat{\theta} = \theta$, which implies that the $dq0$ reference frame turns the non-autonomous time-varying dynamical systems (3.1) and (3.2) into the autonomous dynamical system [49, 73].

If Park's transformation is applied to the dynamical models for the PWM-VSC and PWM-CSC given in (3.1) and (3.2), then, suppressing the zero component in the $dq0$ reference

frame (the three-phase AC system without neutral access), the following dynamical models in Park's reference frame are obtained.

Dynamical model for the PWM-VSC in dq reference frame

$$\begin{aligned} L_f \tfrac{d}{dt} i_{dq} &= -(R_f + L_f \Omega) i_{dq} + m_{dq} v_{sc} - e_{dq}; \\ C_{sc} \tfrac{d}{dt} v_{sc} &= i_s - m_{dq}^T(t) i_{dq}; \end{aligned} \tag{3.24}$$

where the subscript dq represents a group of two variables, e.g., $i_{dq} = [i_d \; i_q]^T$, and

$$\Omega = \begin{pmatrix} 0 & \hat{\omega} \\ -\hat{\omega} & 0 \end{pmatrix}$$

is defined as a skew-symmetric matrix, which entails by definition that their components are contained inside of the interconnection matrix $\mathcal{J}$ in the Hamiltonian formulation.

Dynamical model for the PWM-CSC in dq reference frame

$$\begin{aligned} L_f \tfrac{d}{dt} i_{dq} &= -(R_f + L_f \Omega) i_{dq} + v_{dq} - e_{dq}; \\ C_f \tfrac{d}{dt} v_{dq} &= m_{dq} i_{sc} - C_f \Omega v_{dq} - i_{dq}; \\ L_{sc} \tfrac{d}{dt} i_{sc} &= -m_{dq}^T v_{dq}; \end{aligned} \tag{3.25}$$

Observe that the total number of equations associated to Clarke's and Park's reference frames remains constant, i.e., four for the PWM-VSC model and five for the PWM-CSC model.

Note that all the dynamical models for the three-phase PWM-CSCs and PWM-VSCs analyzed in above sections satisfy the definition of a pH-bilinear structure as in Definition 6. These pH-bilinear structures are obtained by comparison between the abc, $\alpha\beta 0$ and $dq0$ models (see Eqs. (3.16)–(3.17), (3.20)–(3.21) and (3.24)–(3.25), respectively) and the bilinear standard model defined by (2.14).

3.5 Three-phase PLL

Here the phase-locked loop system for a three-phase system is only discussed for the purpose of providing information about its passivity-based structure and its dynamical behavior for balanced and unbalanced grid conditions. Its rigorous stability analysis is beyond the scope of this thesis.

A PLL is a key component for μGrids since it allows measuring the frequency of the grid and transforming three-phase sinusoidal signals with constant angular speed into three

constant signals by employing a proportional-integral estimator with the schematic structure presented in Fig. 3.4 [123].

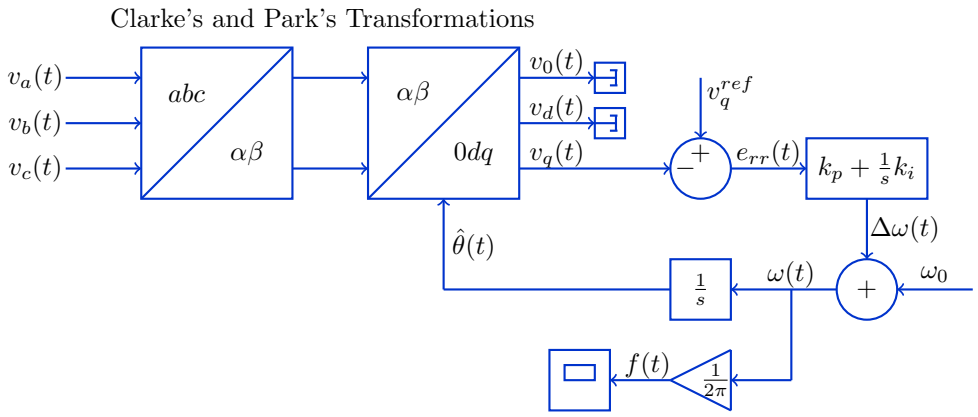

Figure 3.4: Proportional-integral conception of a three-phase PLL estimator

The conventional synchronous reference-frame PLL consists of a phase detector, a loop filter, and a voltage-controlled oscillator, as depicted in Fig. 3.4. Its objective is to estimate the frequency of the grid $\hat{\omega}$ and an angle $\hat{\theta}$ that defines a rotating reference frame dq which, for the sake of simplicity, is attached to the d axis. The dynamical model of this PLL can be reduced to an ordinary differential equation in the plane θ, γ as follows:

$$\begin{aligned} \dot{\hat{\theta}} &= -k_p(v_\alpha(t)\sin(\hat{\theta}) + v_\beta(t)\cos(\hat{\theta})) + k_i\gamma + \omega_0 \\ \dot{\gamma} &= -v_\alpha(t)\sin(\hat{\theta}) - v_\beta(t)\cos(\hat{\theta}) \end{aligned} \tag{3.26}$$

where $\hat{\theta}$ is the estimated angle, γ is the state variable associated to the integral action of the filter, and $v_\alpha(t), v_\beta(t)$ are obtained from the power-invariant Clarke's transformation given by

$$\begin{aligned} v_\alpha(t) &= \sqrt{\tfrac{2}{3}}\left(v_a(t) - \tfrac{v_b(t)}{2} - \tfrac{v_c(t)}{2}\right) \\ v_\beta(t) &= \sqrt{\tfrac{2}{3}}\left(-\tfrac{\sqrt{3}v_b(t)}{2} + \tfrac{\sqrt{3}v_c(t)}{2}\right) \end{aligned} \tag{3.27}$$

where k_p is a proportional gain, and k_i is an integral gain such that $\{k_i, k_p\} \in \mathbb{R}^+$. Note this is a non-autonomous dynamical system, since the voltages $v_a(t), v_b(t), v_c(t)$ depend explicitly on time. Note that this representation was obtained by applying an invariant power transformation.

Lemma 1 (pH representation) *Let us define state variables $z_1 = \hat{\theta}, z_2 = \gamma$. Then the synchronous reference frame PLL can be represented as the following Hamiltonian system*

$$\dot{z} = (\mathcal{J} - \mathcal{R}) \frac{\partial \mathcal{H}(t,z)}{\partial z} \tag{3.28}$$

with

$$\mathcal{J} = \begin{pmatrix} 0 & 1 \\ -1 & 0 \end{pmatrix} \quad \mathcal{R} = k_p \begin{pmatrix} 1 & 0 \\ 0 & 0 \end{pmatrix} \tag{3.29}$$

$$\mathcal{H}(t,z) = \int_0^{z_1} v_q(t,\theta')d\theta' + \frac{k_i}{2} z_2^2 + \omega_0 z_2; \tag{3.30}$$

$$v_q(t,\theta) = v_\alpha(t)\sin(\theta) + v_\beta(t)\cos(\theta); \tag{3.31}$$

Remark 1 *Considering the interconnection and damping matrix defined by (3.29), the storage function shown in (3.30) and the time-varying function presented in (3.31), and making some calculations and substitutions in (3.28), the proof can be completed. Note that $\mathcal{H}$ depends on the time.*

3.5.1 Operation under balanced conditions

Consider the voltage signals of a balanced three-phase grid with sequence *abc*:

$$\begin{aligned} v_a(t) &= \sqrt{2} V_{rms} \cos(\omega t) \\ v_b(t) &= \sqrt{2} V_{rms} \cos\left(\omega t - \frac{2\pi}{3}\right) \\ v_c(t) &= \sqrt{2} V_{rms} \cos\left(\omega t + \frac{2\pi}{3}\right) \end{aligned} \tag{3.32}$$

where V_{rms} is the root mean square of the voltage signal in positive sequence per phase of the three-phase power system. Substituting (3.31) in (3.27) and after some straightforward calculations, the following expression is obtained:

$$v_q(t,\theta) = \sqrt{3} V_{rms} \sin(\theta - \omega t) \tag{3.33}$$

where v_q is the voltage output in the quadrature axis in Park's reference frame. For other versions of the $0\alpha\beta$ transformation, the constant $\sqrt{3}V_p$ will be different. However, the form of the function remains the same. Usually, the voltage is normalized and therefore it is possible to assume that $V_{rms} = 1$ in per-unit representation.

3.5.2 Constant frequency

Consider first the case of an infinite bus in which the voltage and frequency of the grid is constant.

Lemma 2 (Autonomous transformation) *The synchronous reference-frame PLL given by (3.28) can be transformed into an autonomous system for a balanced grid with constant frequency by the following affine transformation.*

$$\begin{pmatrix} x_1 \\ x_2 \end{pmatrix} = \begin{pmatrix} z_1 \\ z_2 \end{pmatrix} - \begin{pmatrix} \omega t \\ (\omega - \omega_0)/k_i \end{pmatrix} \tag{3.34}$$

This transformation preserves the Hamiltonian structure of the system, that is,

$$\dot{x} = (\mathcal{J} - \mathcal{R})\frac{\partial \mathcal{H}}{\partial x} \tag{3.35}$$

Proof 1 *Let us define a constant $\alpha = \sqrt{3}$ and note that under balanced conditions, (3.33) becomes $v_q = \alpha \sin(x_1)$. Therefore the Hamiltonian becomes*

$$\mathcal{H} = 2\alpha \sin^2\left(\frac{x_1}{2}\right) + \frac{k_i}{2}x_2^2 \tag{3.36}$$

which is time independent. In addition, $\partial\mathcal{H}/\partial x = \partial\mathcal{H}/\partial z$. The rest of the proof is a consequence of substituting (3.34) in (3.28).

□

For the sake of clarity, the PLL model can be rewritten explicitly as

$$\dot{x}_1 = -k_p\alpha \sin(x_1) + k_i x_2; \tag{3.37}$$

$$\dot{x}_2 = -\alpha \sin(x_1); \tag{3.38}$$

Now we will study the stability properties of this model.

Theorem 2 (Periodic equilibrium points) *The autonomous dynamical system given by (3.37) and (3.38) has equilibrium points at $x^\star = (n\pi, 0)$. These equilibria are a sink for $n = 2m$ and a saddle node for $n = 2m + 1$, where m is an integer.*

Proof 2 *Consider the Jacobian matrix $J_m = Df(x_0)$*

$$J_m = \begin{pmatrix} -k_p\alpha\cos(x_1) & k_i \\ -\alpha\cos(x_1) & 0 \end{pmatrix}; \tag{3.39}$$

its determinant $det(J_m)$ and trace $Tr(J_m)$ evaluated at zero are given by

$$|J_m| = k_i\alpha$$
$$Tr(J_m) = -k_p\alpha$$

Since $|J_m| > 0$ and $Tr(J_m) < 0$ for $(2m, 0)$, it is possible to conclude that this equilibrium is stable. In the same way, since $|J_m| < 0$ for $(2m + 1, 0)$, we can conclude it is a saddle node.

□

Remark 2 *This equilibrium point is hyperbolic, hence we can invoke the Hartman–Grobman theorem [114] in order to extend this result to non-linear dynamical systems.*

Lemma 3 (Dissipative pH system) *The autonomous dynamical system given by (3.37) and (3.38) is a dissipative Hamiltonian system as presented in Definition 3. In addition, the Hamiltonian has a minimum at $x^* = (2m\pi, 0)$ with $m \in \mathbb{Z}$.*

Remark 3 *The proof of this lemma can be made by substituting $\mathcal{H}, \mathcal{J}, \mathcal{R}$ in (3.28) and evaluating the Hessian of $\mathcal{H}$ which is given by (3.36).*

From Theorem 2, it is clear that the equilibrium points appear in multiples of 2π. Without loss of generality we can study the equilibrium at (0,0). Applying this theorem to the PLL model we obtain the following result.

Theorem 3 (Stability properties) *The dissipative Hamiltonian system given by (3.37) and (3.38) has an isolated minimum at $(0, 0)$. Therefore, it is asymptotically stable. In addition, a lower bound of the attraction region is given by*

$$\Omega = \left\{ (x_1, x_2) \in \mathbb{R}^2 : \sin^2\left(\frac{x_1}{2}\right) + \frac{k_i}{4\alpha}x_2^2 < 1 \right\}$$

Proof 3 *The proof of the first part of this proposition is obtained by directly invoking Lemma 3 and Lyapunov's stability Theorem 1 [30]. The attraction region is obtained by solving the optimization problem*

$$h_m = \inf\left\{ \mathcal{H}(x_1, x_2) : \ \dot{\mathcal{H}}(x_1, x_2) = 0, x \neq 0 \right\}; \tag{3.40}$$

which gives $x_1 = \pm\pi$, $x_2 = 0$ and $h_m = 2\alpha$. Therefore, h_m is a sub-level set of $\mathcal{H}$ and an estimate of the attraction region is given by $\mathcal{H} < h_m$.

□

Fig. 3.5 shows the attraction region Ω for $k_i = \alpha$. This plot illustrates the conditions for the convergence of the PLL under ideal conditions (e.g., constant frequency).

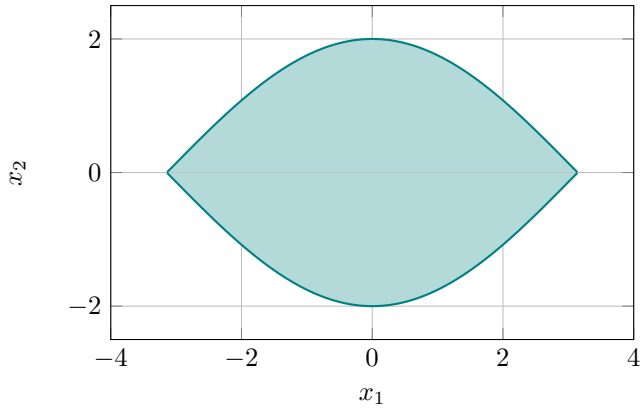

Figure 3.5: Lower bound of the attraction region for $k_i = \alpha$

3.5.3 Unbalanced conditions

Consider now the case in which the grid is under small unbalanced conditions and the fact that v_α, v_β are given by

$$v_\alpha = \sqrt{3}V_p \cos(\omega t) + \epsilon\sqrt{3}V_p \sin(\omega t)$$
$$v_\beta = -\sqrt{3}V_p \sin(\omega t)$$

where $0 < \epsilon << 1$ is an small imbalance on the grid which produces a negative sequence. Therefore, the dynamical system can be represented as

$$\dot{x} = (\mathcal{J} - \mathcal{R}) \left(\frac{\partial \mathcal{H}}{\partial x} \right) + \epsilon g(t, x, \epsilon) \tag{3.41}$$

with

$$g(t, x, \epsilon) = \alpha \sin(\omega t) \sin(x_1 + \omega t) \begin{pmatrix} -k_p \\ -1 \end{pmatrix} \tag{3.42}$$

Lemma 4 (Periodic solutions) *There exist positive constants δ and k such that $\forall|\epsilon| < \delta$, the PLL has a unique 2T-periodic solution $\tilde{x}$ such that $\|\tilde{x}(t)\| \leq k\epsilon$ and this solution is exponentially stable.*

Proof 4 *Note that (3.41) is just the autonomous system (3.37) with a continuous 2T-periodic perturbation. Since the autonomous system is exponentially stable at (0,0) then the perturbed system is also 2T-periodic and exponentially stable [114].*

□

As a direct consequence of Lemma 4, any unbalanced condition will produce oscillations of the estimated frequency and angle.

3.5.4 Operation of the PLL during a transient in the grid

Consider the case in which the grid has a balanced transient, for example a three-phase short-circuit that modifies the frequency of the grid. The primary control acts on the synchronous generators and/or voltage source converters, resulting in a new stable operating point. However, this transient can affect the performance of the PLL. In this case, the frequency of the grid is given by $\omega + \Delta\omega(t)$ where $\|\Delta\omega(t)\| \leq \epsilon$. The voltage can also change, but we can scale by dividing by its magnitude (recall the transient is balanced). Define a set of variables $x_1 = \theta - \omega(t)t$ and $x_2 = \gamma + (\omega_0 - \omega(t))/k_i$. For the sake of simplicity, in the following the time dependence of $\Delta\omega$ is omitted.

Lemma 5 (Transient Hamiltonian representation) *For balanced transient operation, the synchronous reference-frame PLL can be represented as*

$$\dot{x} = (\mathcal{J} - \mathcal{R})\frac{\partial \mathcal{H}}{\partial x} + u(t)$$

with $\mathcal{H}, \mathcal{R}, \mathcal{J}$ as in Lemmas 1 and 2, and

$$u(t) = \begin{pmatrix} \dot{\omega}t \\ \dot{\omega}/k_i \end{pmatrix}$$

Note that the estimated frequency of the grid can be obtained from x_1. However, the PLL could lose its ability to estimate, due to this transient. Therefore it is important to determine the exact conditions under which the PLL maintains its ability to estimate the frequency after a transient.

3.5.5 Single-phase PLL

In single-phase μGrids for controlling active and reactive power independently or supporting the voltage and frequency in isolated networks, it is required to measure the grid frequency. This measurement is made in these grids via Single-phase PLLs [125]. Multiple topologies have been proposed to address this problem, via an orthogonal signal generator, as presented in Fig. 3.6 [126].

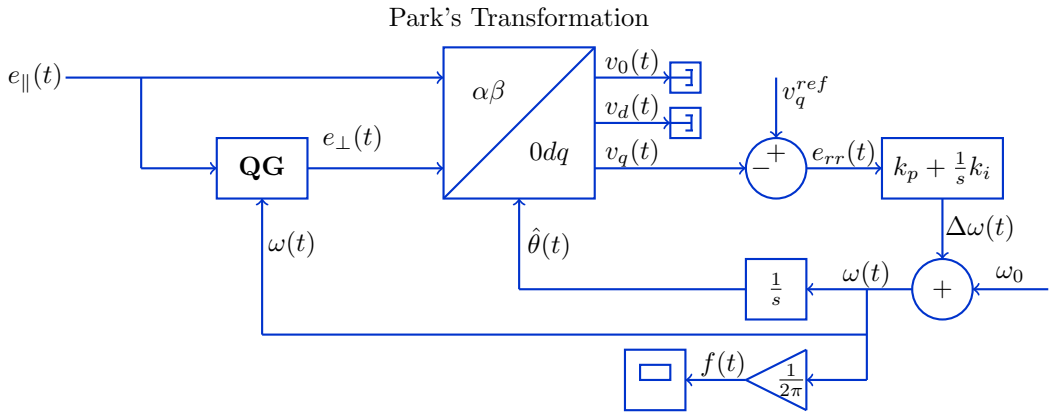

Figure 3.6: Proportional-integral conception of a single-phase PLL estimator

Note that the single-phase PLL structure is similar to the three-phase PLL, since it uses Park's transformation in conjunction with a PI estimator. Notwithstanding, a quadrature generator (**QG** in Fig. 3.6) allows transforming $e_{\parallel}$ into an orthogonal signal $e_{\perp}$ by measuring its instantaneous frequency, in order to generate the needed inputs for Park's transformation. In this thesis, the single-phase PLL structure for controlling single-phase converters is employed; furthermore, its analysis is beyond the scope of this thesis.

3.6 Summary of the chapter

This chapter presented the general characteristics of the power electronic converters based on voltage and current source technologies for μGrid applications. A general topology for those converters was presented in terms of the composition of their switches, which are operated via pulse-width-modulation strategies.

These converters for single-phase and three-phase μGrids were dynamically modeled through an averaged representation with continuous functions, which allows finding a natural pH-bilinear structure for proposing passivity-based controllers. The single-phase converters needed a non-autonomous dynamical model, while the three-phase converters could use either autonomous or non-autonomous dynamical models, depending on the reference frame employed, i.e., time-domain (abc), Clarke's ($\alpha\beta 0$) and Park's ($dq0$) reference frames, respectively.

Lastly, the structures of single-phase and three-phase PLLs were studied in order to highlight their importance for control purposes in AC μGrids. Nevertheless, note that only the three-phase model was exhaustively analyzed in comparison to the single-phase case, since those systems did not correspond to the main focus of study in this thesis.

Chapter 4

Hamiltonian modeling of AC μGrids

This chapter studies the general characteristics of AC μGrids focusing on their mathematical modeling in different modes of operation. Single-phase and three-phase representations are studied and mathematically formulated as Hamiltonian systems controlled by ports. Additionally, constant-power terminals are integrated via power electronic converters based on voltage source technologies.

4.1 Operating modes of AC μGrids

Microgrids can be operated in two main modes: grid-connected [127] and isolated [128]. Fig. 4.1 presents both concepts applied to generic AC μGrid configurations by considering the two possible operative states of the main breaker. Suppose the main breaker is governed by a binary variable δ. Then, if δ takes the lower state ($\delta = 0$), the main breaker is closed and the μGrid operates in grid-connected mode. Otherwise, if δ takes the upper state ($\delta = 0$), the main breaker is opened and the μGrid operates in isolated mode. The next definitions present both concepts clearly.

Definition 8 (Grid-connected operating mode) *A μGrid is operating in grid-connected mode if there exists an interconnection between the μGrid and the AC power grid ($\delta = 0$) and the voltage and frequency are totally controlled by the grid, which behaves as an infinite bar. This implies that all DERs contained in the μGrid operate in active/reactive power control mode. This operating condition is also known as a master–slave scheme [129].*

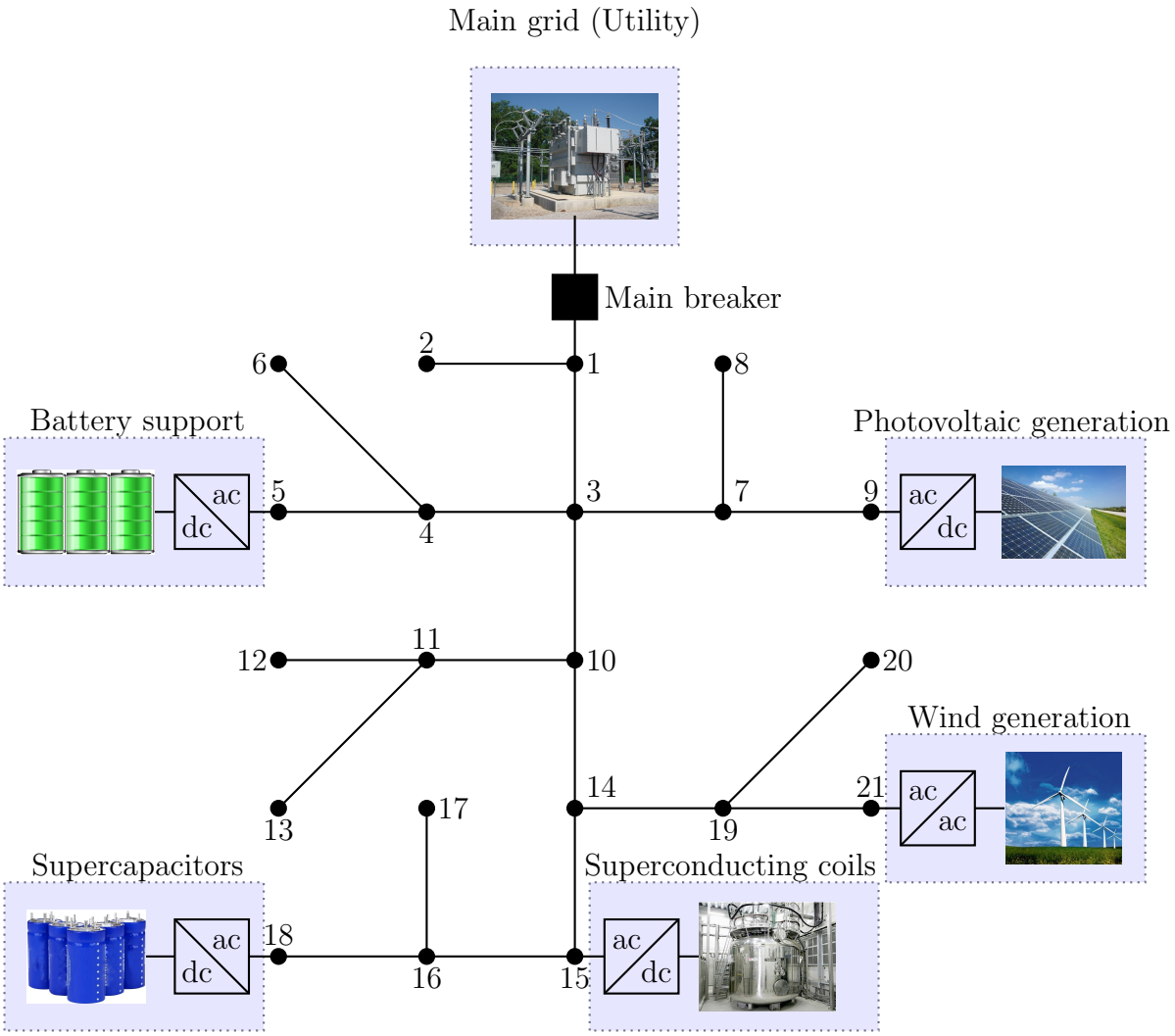

Figure 4.1: Interconnection of multiple DERs in AC μGrids for operation in grid or isolated operating modes

Definition 9 (Isolated operating mode) *A μGrid is operating in isolated mode if the interconnection to the AC grid is interrupted ($\delta = 1$) or does not exist, and all DERs work cooperatively to support the voltage and frequency in the grid by maintaining the energy balance in the whole μGrid.*

Observe that in isolated operating mode, the μGrid may be operated via a master–slave strategy if there exists a robust energy storage system (see the battery support in Fig. 4.1)

that works as a slack node, i.e., controlling the voltage and frequency regulation, which implies that the remaining group of DERs will continue working under the slave philosophy.

In this thesis, the main interest is to analyze the passivity-based properties of AC μGrids. The master–slave strategy is considered for developing the complete dynamical model of the network. This implies that there will always exist an ideal source that allows supporting the voltage and frequency in the μGrid. This source may be the main grid or a large-battery energy storage system integrated through a voltage source converter.

4.2 Modeling of passive components in AC μGrids

The dynamical modeling of electrical distribution networks can be obtained by applying circuit laws in conjunction with graph theory [19]. The inductive and capacitive effects of the distribution lines as well as the shunt capacitive filters are employed to formulate its dynamical behavior. Constant power consumption or generation are typically integrated in the grid via power electronic converters for managing their consumption/generation via control actions [63]. The next subsections will give in detail the dynamical modeling of single-phase μGrids as well as their extension to the three-phase case.

4.2.1 Single-phase dynamical model

4.2.1.1 General considerations

Consider a generic single-phase μGrid with linear and nonlinear loads, which operates in grid-connected mode as depicted in Fig. 4.1. In addition, the following assumptions for the single-phase microgrid (SP-μGrid) are made:

Assumption 1 *The electrical connections between the different nodes in the SP-μGrid are modeled by a connected graph with n external ports. Each port has variables (v_k, i_k), $k = 1, \ldots, n-1$.*

Assumption 2 *There is a master–slave control. This implies that the SP-μGrid operates in grid-connected mode and that the grid provides the voltage profile and the fundamental frequency for the entire SP-μGrid.*

Assumption 3 *Each node has at least one electrical element connected directly to ground (electrical reference). This element corresponds to the capacitive effect between each branch (line) and the physical (electrical) ground.*

Assumption 4 *The constant-power pq terminals are modeled as single-phase voltage source converters. Each pq terminal corresponds to a constant power load or to a distributed energy resource (energy storage or distributed generator technology).*

4.2.1.2 Dynamical model of a generic node

Assume the existence of *pq* terminals for the $n-1$ nodes different from the master node, as presented in Fig. 4.2(a). Then, by applying Kirchhoff's first law,

$$f_k = g_k v_k + C_k \frac{d}{dt} v_k + i_k; \quad k = 2, 3, \ldots, n \tag{4.1}$$

where f_k is the current generated by the distributed energy resource or consumed by a nonlinear load connected at node k, which in matrix form can be rewritten as

$$f_l = \mathcal{G}_l v_l + \mathcal{C}_l \frac{d}{dt} v_l + i_l, \tag{4.2}$$

where $f_l = col(f_k) \in \mathbb{R}^{n-1}$, $\mathcal{C}_l, \mathcal{G}_l \in \mathbb{R}^{n-1 \times n-1}$ diagonal matrices with positive elements C_k and g_k, respectively. Note that $\mathcal{G}$ contains the conductive effects associated with the constant resistive loads interconnected to each node and must be a positive semidefinite matrix, while $\mathcal{C}_l$ must be a positive definite matrix to guarantee the existence of the voltage dynamics at each node. Additionally, observe that i_l, f_l and v_l are vectors that contain all nodal variables except for the master node, where the subscript zero is employed to refer to its variables.

4.2.1.3 Dynamical model of a generic branch

Suppose that there are b electrical lines in the SP-μGrid, represented by the internal edges of the graph, with variables (v_j, i_j), $j = 1, \ldots, b$. The lines can be modeled employing a classical Π model as depicted in Fig. 4.2(b), where L_j and R_j represent the series inductance and resistance parameters of the electrical conductor, and C_j is the capacitive effect between the conductor and the electrical reference.

By applying Kirchhoff's laws in one line one obtains that

$$v_m - v_n = v_j = L_j \frac{d}{dt} i_j + R_j i_j, \tag{4.3}$$

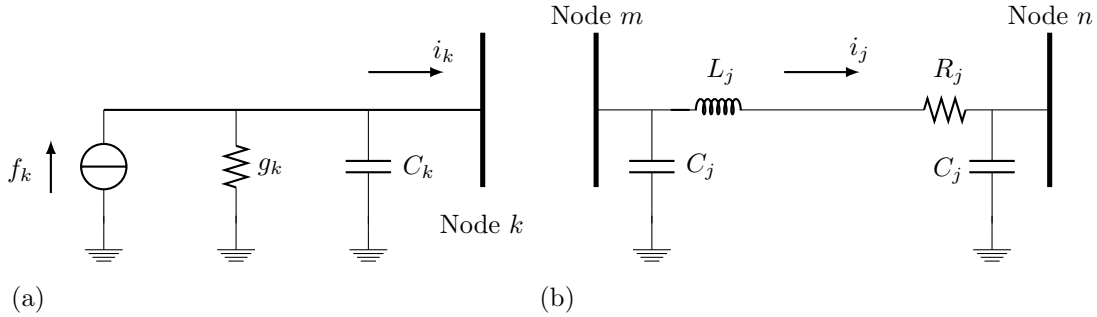

Figure 4.2: π model of the j^{th} electrical branch connected between m and n nodes

with v_m and v_n the voltages in both ends of the line (nodes m and n), which implies that v_j corresponds to the voltage drop in the j^{th} line, and i_j to the current flowing through this line. This expression can be generalized for all branches in matrix form as

$$v_{\mathcal{E}} = \mathcal{L}_{\mathcal{E}} \frac{d}{dt} i_{\mathcal{E}} + \mathcal{R}_{\mathcal{E}} i_{\mathcal{E}}, \tag{4.4}$$

where $v_{\mathcal{E}} = col(v_j) \in \mathbb{R}^b$, $i_{\mathcal{E}} = col(i_j) \in \mathbb{R}^b$, while $\mathcal{L}_{\mathcal{E}} = diag\{L_j\} \in \mathbb{R}^{b\times b}$ and $\mathcal{R}_{\mathcal{E}} = diag\{R_j\} \in \mathbb{R}^{b\times b}$ contain the inductive $L_j > 0$ and resistive $R_j > 0$ effects, respectively.

Note that the capacitive effects of each branch C_j will be considered in the dynamics of the electrical nodes.

4.2.1.4 Line–Node relationship

The line–node relationship is given by the Incidence matrix $\mathcal{A} \in \mathbb{R}^{b\times n}$ with entries equal to ± 1 depending on the incidence and the chosen current flow. Let the vector of nodal voltages be $v_{\mathcal{N}} = col(v_k) \in \mathbb{R}^n$, then

$$i_{\mathcal{N}} = \mathcal{A}^T i_{\mathcal{E}} \ , \ v_{\mathcal{E}} = \mathcal{A} v_{\mathcal{N}}. \tag{4.5}$$

Due to the existence of a master node, the vector of nodal voltages and currents can be split into

$$v_{\mathcal{N}} = \begin{bmatrix} v_0 \\ v_l \end{bmatrix}, \ \ i_{\mathcal{N}} = \begin{bmatrix} i_0 \\ i_l \end{bmatrix} \tag{4.6}$$

with $v_0 \in \mathbb{R}$ and $i_0 \in \mathbb{R}$ the master voltage and current respectively, while $v_l, i_l \in \mathbb{R}^{n-1}$ are the rest of the nodal voltage and currents. Under these conditions, Eq. (4.5) can also be rewritten as

$$v_{\mathcal{E}} = \begin{bmatrix} A_0 & A_l \end{bmatrix} \begin{bmatrix} v_0 \\ v_l \end{bmatrix} = \mathcal{A}_0 v_0 + \mathcal{A}_l v_l \tag{4.7a}$$

$$\begin{bmatrix} i_0 \\ i_l \end{bmatrix} = \begin{bmatrix} \mathcal{A}_0^T \\ \mathcal{A}_l^T \end{bmatrix} i_{\mathcal{E}} \ \ \Rightarrow \ \ i_l = \mathcal{A}_l^T i_{\mathcal{E}} \tag{4.7b}$$

with $A_0 \in \mathbb{R}^{b\times 1}$ the first column of A and $A_l \in \mathbb{R}^{b\times(n-1)}$. Equation (4.7)b also implies that $i_0 = A_0^T i_{\mathcal{E}}$, which is always satisfied since the master node is ideal.

4.2.1.5 Complete dynamical model

The dynamical model of the SP-μGrid is represented by the set of equations (4.4) and (4.2) in the line–node relation (4.7) as

$$\mathcal{L}_{\mathcal{E}}\frac{d}{dt}i_{\mathcal{E}} = -\mathcal{R}_{\mathcal{E}}i_{\mathcal{E}} + \mathcal{A}_l v_l + \mathcal{A}_0 v_0 \tag{4.8a}$$

$$\mathcal{C}_l\frac{d}{dt}v_l = -\mathcal{G}_l v_l - \mathcal{A}_l^T i_{\mathcal{E}} + f_l \tag{4.8b}$$

s.t.

$$i_0 = \mathcal{A}_0^T i_{\mathcal{E}} \tag{4.8c}$$

It is important to note that the dynamical model of the SP-μGrid (4.8) corresponds to a port-controlled Hamiltonian system with an external input

$$\mathcal{D}\dot{x} = [\mathcal{J} - \mathcal{R}]\nabla\mathcal{H}(x) + \Gamma \tag{4.9}$$

where $\mathcal{D} = diag\{\mathcal{L}_{\mathcal{E}}, \mathcal{C}_l\} \in \mathbb{R}^{(b+n-1)\times(b+n-1)}$, $\mathcal{D} = \mathcal{D}^T > 0$, the dissipation matrix $\mathcal{R} = diag\{\mathcal{R}_{\mathcal{E}}, \mathcal{G}_l\} \in \mathbb{R}^{(b+n-1)\times(b+n-1)}$, $\mathcal{R} = \mathcal{R}^T > 0$, the state $x = \begin{bmatrix} i_{\mathcal{E}}^T & v_l^T \end{bmatrix}^T \in \mathbb{R}^{b+n-1}$, the matrices

$$\Gamma = \begin{bmatrix} \mathcal{A}_0 v_0 \\ f_l \end{bmatrix} \in \mathbb{R}^{b+n-1}, \quad \mathcal{J} = \begin{bmatrix} 0 & \mathcal{A}_l \\ -\mathcal{A}_l^T & 0 \end{bmatrix} = -\mathcal{J}^T \tag{4.10}$$

and the quadratic function

$$\mathcal{H}(x) = \frac{1}{2}x^T x, \quad \nabla\mathcal{H}(x) = \left[\frac{\partial}{\partial x}\mathcal{H}(x)\right]^T = x \tag{4.11}$$

4.2.1.6 Integration of constant pq terminals via VSCs

The integration of any constant power pq terminal that models a nonlinear load interconnected to the SP-μGrid is made via a voltage source converter technology, as was presented in Fig. 3.2, which clearly exhibited a Hamiltonian representation as defined in the set of equations (3.1) with parameters presented in Table 3.1.

4.2.1.7 Stability analysis

We now study the dynamic behavior of a general SP-μGrid considering external sources Γ. In this context, the admissible trajectories $x^\star(t)$ are the set of state trajectories that the system can follow. These trajectories fulfill

$$\mathcal{D}\dot{x}^\star = [\mathcal{J} - \mathcal{R}]\nabla\mathcal{H}(x^\star) + \Gamma^\star \tag{4.12}$$

where

$$\Gamma^\star = \begin{bmatrix} \mathcal{A}_0 v_0 \\ f_l^\star \end{bmatrix}, \text{ and } \mathcal{H}(x^\star) = \frac{1}{2} x^{\star T} x^\star$$

Define the classical tracking error as $\tilde{x} = x - x^\star$. Then the dynamic behavior for the tracking error can be written as

$$\mathcal{D}\dot{\tilde{x}} = [\mathcal{J} - \mathcal{R}] \nabla \mathcal{H}(\tilde{x}) + \tilde{\Gamma} \tag{4.13}$$

In the next proposition, conditions for $\tilde{x} \to 0$ are given.

Proposition 1 *Assume that $v_0(t)$ and $f_l(t)$ are time-varying and that their steady state behaviors are well defined. Then, $\tilde{x}(t)$ of the system (4.13) is ultimately bounded. Moreover, if it is assumed that $f_l^\star(t) = f_l(t)$ is imposed by the constant power load controllers, which means $\tilde{\Gamma} \to 0$, the asymptotic stability of $\tilde{x} = 0$ is achieved.*

Proof 5 *Consider the positive function*

$$\mathcal{V}(\tilde{x}) = \frac{1}{2} \tilde{x}^T \mathcal{D} \tilde{x} \tag{4.14}$$

The time derivative of (4.14) along the trajectories of (4.13) is

$$\begin{aligned} \dot{\mathcal{V}}(\tilde{x}) &= -\tilde{x}^T \mathcal{R} \tilde{x} + \tilde{x}^T \tilde{\Gamma} \\ &\leq -\lambda_{\min}\{\mathcal{R}\} |\tilde{x}|^2 + |\tilde{x}||\tilde{\Gamma}| \\ &= -(1-\theta)\lambda_{\min}\{\mathcal{R}\} |\tilde{x}|^2 - \theta \lambda_{\min}\{\mathcal{R}\} |\tilde{x}|^2 + |\tilde{x}||\tilde{\Gamma}| \end{aligned}$$

with $0 < \theta < 1$, while $\lambda_{\min}\{\mathcal{R}\}$ is the minimum eigenvalue of $\mathcal{R}$ and $|\cdot|$ denotes the norm. So, it can be concluded that

$$\dot{\mathcal{V}}(\tilde{x}) \leq -(1-\theta)\lambda_{\min}\{\mathcal{R}\} |\tilde{x}|^2 \tag{4.15}$$

for all

$$|\tilde{x}| \geq \frac{|\tilde{\Gamma}|}{\theta \lambda_{\min}\{\mathcal{R}\}} > 0 \tag{4.16}$$

Since $(1-\theta)\lambda_{\min}\{\mathcal{R}\}|\tilde{x}|^2$ is a continuous positive definite function of $\tilde{x}$, inequality (4.15) shows that the solutions $\tilde{x}(t)$ are ultimately bounded. Moreover, note that if it is assumed that the control of the power converters guarantees that $\Gamma \to \Gamma^\star$, then the ball defined in (4.16) becomes the origin and $\tilde{x} = 0$ is asymptotically stable, which concludes the proof.

Remark 4 *As long as $\tilde{\Gamma} \neq 0$, the trajectories of the error tend to a ball of radius determined by the norm of $\tilde{\Gamma}$.*

Remark 5 *Note that the components of f_l, which are the loads, will tend to $f_l^\star$. Each $f_l^\star$ must be admissible, which means that it must satisfy the power flow equations that results from solving (4.9) in the sinusoidal regime.*

4.2.2 Three-phase microgrid dynamical model

A TP-μGrid can be modeled with three different reference frames, referred to as abc, $\alpha\beta$, and dq, as presented for three-phase power electronic converters in Chapter 3. In this section, the abc and $\alpha\beta$ models will be discussed, while dq will left for future analysis, since special assumptions on the TP-μGrid are required to develop this model.

A general dynamical model for a three-phase power system operating with a master-slave strategy requires the following definitions:

Definition 10 (Three-phase node) *A three phase node is a set of three nodes corresponding to each phase. For example, when we refer to the node* 5 *we are referring to the set of single phase nodes* $\{5a, 5b, 5c\}$*. The set of all three phase nodes is denoted by* $\mathcal{N}$*:*

$$\mathcal{N} = \{(1a, 1b, 1c), (2a, 2b, 2c), ..., (na, nb, nc)\}$$

where n *is the number of slave nodes. On the other hand, the master or slack node is represented by the three-phase node* 0*, that is,* $(0a, 0b, 0c)$*.*

Definition 11 (Three-phase branch) *A three-phase branch is a set of three branches that connect two adjacent three-phase nodes. For example, the branch* $7 - 5$ *is the set of three branches* $\{7a - 5a, 7b - 5b, 7c - 5c\}$*. The set of all three-phase branches is denoted by* $\mathcal{E}$ *and has dimension* $(3(n + 1)) \times (3n)$*.*

Definition 12 (Branch-to-node incidence matrix) *The branch-to-node incidence matrix* A *is an* $N \times E$ *matrix of which the entries* a_{ij} *are* $+1$ *if there is a three-phase branch between the tree-phase nodes* k *and* m *and the current flows in the direction* $i \to j$*,* -1 *if the current is in the direction* $j \to i$*, and zero if there is no direct connection between the nodes. Note that the branch-to-node incidence matrix is made with the three-phase nodes as individual nodes and branches in the graph.*

Definition 13 (Three-phase branch-to-node incidence matrix) *The three-phase incidence matrix corresponds to an extension of the branch-to-node incidence matrix previously defined considering each phase, as follows*

$$\mathcal{A} = \mathbf{1}_3 \otimes A$$

where $\otimes$ *denotes the Kronecker product and* $\mathbf{1}_3$ *is the* 3×3 *identity matrix.*

4.2.2.1 General assumptions

The formulation of the dynamical model is based on the following assumptions:

Assumption 5 *The graph that represents the grid is connected.*

Assumption 6 *The TP-μGrid operates under master-slave control. There exists a master controller (the slack in the grid) which imposes the electrical frequency and the voltage reference for all nodes in the grid.*

Assumption 7 *All elements on the TP-μGrid have a three-phase structure.*

Assumption 8 *The power electronic converters are three-phase without neutral access.*

4.2.2.2 Three-phase line segment

Each three-phase line segment is represented by a generalized π model as depicted in Fig. 4.3, where $[L_{\mathcal{E}_k}]$ and $[R_{\mathcal{E}_k}]$ are 3×3 matrices that represent the inductive and resistive effects respectively, while $[C_{\mathcal{E}_k}]$ corresponds to the line to ground capacitive effects. The general structure of these matrices is defined below:

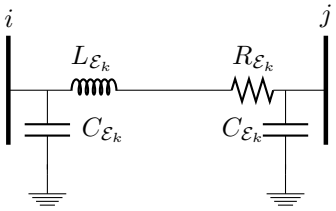

Figure 4.3: π model of an electrical three-phase branch $\mathcal{E}_k$ connected between i and j three-phase nodes

$$L_{\mathcal{E}_k} = \begin{bmatrix} l_{aa} & l_{ab} & l_{ac} \\ l_{ba} & l_{bb} & l_{bc} \\ l_{ca} & l_{cb} & l_{cc} \end{bmatrix} \quad R_{\mathcal{E}_k} = \begin{bmatrix} r_{aa} & r_{ab} & r_{ac} \\ r_{ba} & r_{bb} & r_{bc} \\ r_{ca} & r_{cb} & r_{cc} \end{bmatrix} \quad C_{\mathcal{E}_k} = \begin{bmatrix} c_{aa} & c_{ab} & c_{ac} \\ c_{ba} & c_{bb} & c_{bc} \\ c_{ca} & c_{cb} & c_{cc} \end{bmatrix} \tag{4.17}$$

The conventional representation of a TP-μGrid neglects the mutual effects between phases. In the present formulation, mutual resistances/inductances are possible and hence these matrices are not diagonal. Both $[L_{\mathcal{E}_k}]$ and $[R_{\mathcal{E}_k}]$ in (4.17) correspond to the reduced matrices obtained after applying Carson's ground return corrections. For more details, refers to [130].

In case of underground electrical lines or lines with cables as conductors, the $[C_{\mathcal{E}_k}]$ matrix has a diagonal structure. Nevertheless, $[R_{\mathcal{E}_k}]$ and $[L_{\mathcal{E}_k}]$ preserve the structure above defined.

Now, the resistance matrix of the entire microgrid is defined by block matrices as follows

$$R = \begin{bmatrix} [R_{\mathcal{E}_1}]_{3\times3} & [0]_{3\times3} & \cdots & [0]_{3\times3} \\ [0]_{3\times3} & [R_{(\mathcal{E}_2)}]_{3\times3} & \cdots & [0]_{3\times3} \\ \vdots & \vdots & \ddots & \vdots \\ [0]_{3\times3} & [0]_{3\times3} & \cdots & [R_{\mathcal{E}_m}]_{3\times3} \end{bmatrix} \tag{4.18}$$

where m corresponds to the total number of line segments. The capacitance and inductance matrices for the entire micro-grid (C and L) can also be defined in the same way. Note that all these matrices are non-singular.

4.2.2.3 Dynamical model in the *abc* reference frame

By using these definitions, the following current and voltage relations can be obtained for the whole of the TP-μGrid:

$$V_{\mathcal{E}} = \mathcal{A}V_{\mathcal{N}} + \mathcal{A}_0 V_0, \quad I_{\mathcal{N}} = \mathcal{A}^T I_{\mathcal{E}} \tag{4.19}$$

where $I_{\mathcal{E}}$ is a real vector that represents the current in the three-phase branches, $V_{\mathcal{E}}$ is the voltage drop in the three-phase branches, $I_{\mathcal{N}}$ and $V_{\mathcal{N}}$ are the total injected current and nodal voltage three-phase node, $\mathcal{A}_0$ is the three-phase incidence matrix for the master node, and V_0 is its three-phase voltage.

For any line segment (see Fig. 4.3), the following relation is fulfilled

$$V_{\mathcal{E}} = L\frac{d}{dt}I_{\mathcal{E}} + RI_{\mathcal{E}} = \mathcal{A}V_{\mathcal{N}} + \mathcal{A}_0 V_0 \tag{4.20}$$

Each node in $\mathcal{N}$ is represented by a constant resistive load R plus a power electronic converter (this converter controls a constant power load consumption) as depicted in Fig. 4.4. In case there is no resistive load, the admittance g is zero.

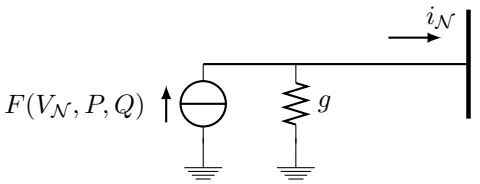

Figure 4.4: Interconnection of constant power terminals in a generic three-phase node

The current injection in each power electronic converter is represented by a non-linear function F. Consequently, the dynamic model of the nodes is given by

$$F(V_{\mathcal{N}}, P, Q) = GV_{\mathcal{N}} + C\frac{d}{dt}V_{\mathcal{N}} + \mathcal{A}^T I_{\mathcal{E}} \tag{4.21}$$

Note that C contains all the capacitive effects of the line segments, as well as the physical capacitors connected to the nodes, and G is a load admittance matrix (possibly singular).

Finally, the three-phase unbalanced micro-grid can be represented by the following dynamical system

$$\begin{bmatrix} L & 0 \\ 0 & C \end{bmatrix} \frac{d}{dt} \begin{bmatrix} I_{\mathcal{E}} \\ V_{\mathcal{N}} \end{bmatrix} = \begin{bmatrix} -R & \mathcal{A} \\ -\mathcal{A}^T & -G \end{bmatrix} \begin{bmatrix} I_{\mathcal{E}} \\ V_{\mathcal{N}} \end{bmatrix} + \begin{bmatrix} \mathcal{A}_0 V_0 \\ F\left(V_{\mathcal{N}}, P, Q\right) \end{bmatrix} \tag{4.22}$$

Note that model (4.22) is non-autonomous since V_0 and F are time dependent.

4.2.2.4 Dynamical system in the $\alpha\beta$ reference frame

To obtain an equivalent $\alpha\beta$ model for TP-μGrids, Clarke's transformation as given in (3.18) is employed, and in addition, a power conservation characteristic between the *abc* and $\alpha\beta$ model is taken into consideration. Moreover, Clarke's transformation satisies $T^T = T^{-1}$

$$T_{\mathcal{N}} = T \otimes 1_{\mathcal{N}} \quad , \quad T_{\mathcal{E}} = T \otimes 1_{\mathcal{E}} \tag{4.23}$$

These definitions are applied to (4.20) and (4.21) to obtain the following

$$\begin{aligned} LT_{\mathcal{E}}^{-1}\tfrac{d}{dt}\mathbb{I}_{\mathcal{E}} &= -RT_{\mathcal{E}}^{-1}\mathbb{I}_{\mathcal{E}} + \mathcal{A}T_{\mathcal{N}}^{-1}\mathbb{V}_{\mathcal{N}} + \mathcal{A}_0 T_c^{-1}\mathbb{V}_0 \\ CT_{\mathcal{N}}^{-1}\tfrac{d}{dt}\mathbb{V}_{\mathcal{N}} &= \mathbb{F}\left(\mathbb{V}_{\mathcal{N}}, P, Q\right) - GT_{\mathcal{N}}^{-1}\mathbb{V}_{\mathcal{N}} - \mathcal{A}^T T_{\mathcal{E}}^{-1}\mathbb{I}_{\mathcal{E}} \end{aligned} \tag{4.24}$$

where $\mathbb{I}_{\mathcal{E}} = T_{\mathcal{E}} I_{\mathcal{E}}$ and $\mathbb{V}_{\mathcal{N}} = T_{\mathcal{N}} V_{\mathcal{N}}$ are the three-phase line segment currents and three-phase node voltages in the $\alpha\beta 0$ reference frame, while $\mathbb{V}_0$ and $\mathbb{F}$ are the master voltage and the nonlinear power function in the $\alpha\beta$ reference frame.

To simplify the dynamical model defined by (4.24), the first equation is premultiplied by $T_{\mathcal{E}}$, while the second equation is premultiplied by $T_{\mathcal{N}}$

$$\begin{aligned} \mathbb{L}\tfrac{d}{dt}\mathbb{I}_E &= -\mathbb{R}\mathbb{I}_E + T_{\mathcal{E}}\mathcal{A}T_{\mathcal{N}}^{-1}\mathbb{V}_{\mathcal{N}} + \mathbb{T}_0\mathbb{V}_0 \\ \mathbb{C}\tfrac{d}{dt}\mathbb{V}_N &= \mathbb{F}\left(\mathbb{V}_{\mathcal{N}}, P, Q\right) - \mathbb{G}\mathbb{U}_N - T_{\mathcal{N}}\mathcal{A}^T T_{\mathcal{E}}^{-1}\mathbb{I}_{\mathcal{E}} \end{aligned} \tag{4.25}$$

where the following definitions have been used in (4.25) to complete the representation

$$\mathbb{L} = T_{\mathcal{E}} L T_{\mathcal{E}}^{-1}; \quad \mathbb{C} = T_{\mathcal{N}} C T_{\mathcal{N}}^{-1}; \quad \mathbb{G} = T_{\mathcal{N}} G T_{\mathcal{N}}^{-1}$$

$$\mathbb{T}_0 = T_{\mathcal{E}}\mathcal{A}_0 T_c^{-1}; \quad \mathbb{R} = T_{\mathcal{E}} R T_{\mathcal{E}}^{-1}$$

4.2.2.5 A compact representation

Proposition 2 (Hamiltonian model of the TP-μGrid) *The dynamical system of the TP-μGrid defined by (4.25) can be written as*

$$\mathbb{M}\dot{x} - \mathbb{J}x + \mathbb{D}x = \mathbb{S}(x,t) \tag{4.26}$$

where $\mathbb{M}$ is a positive definite matrix, $\mathbb{J}$ is a skew-symmetric matrix called the interconnection matrix, $\mathbb{D}$ is a positive semi-definite matrix called the dissipation matrix, and $\mathbb{S}(x,t)$ is an external time-varying perturbation.

Proof 6 *Define the following state variables and matrices to complete the proof.*

$$x = \begin{bmatrix} \mathbb{I}_{\mathcal{E}} \\ \mathbb{V}_{\mathcal{N}} \end{bmatrix},\ \mathbb{M} = \begin{bmatrix} \mathbb{L} & 0 \\ 0 & \mathbb{C} \end{bmatrix},\ \mathbb{D} = \begin{bmatrix} \mathbb{R} & 0 \\ 0 & \mathbb{G} \end{bmatrix}$$

$$\mathbb{J} = \begin{bmatrix} 0 & T_E \mathcal{A} T_{\mathcal{N}}^{-1} \\ -T_{\mathcal{N}} \mathcal{A}^T T_{\mathcal{E}}^{-1} & 0 \end{bmatrix} \tag{4.27}$$

$$\mathbb{S}(x,t) = \begin{bmatrix} \mathbb{T}_0 \mathbb{V}_0 \\ \mathbb{F}\left(\mathbb{V}_{\mathcal{N}}, P, Q\right) \end{bmatrix}$$

Definition 14 (Matrix $\mathbb{A}$ (Three-phase interconnection matrix)) *By using the definitions for $T_{\mathcal{E}}$ and $T_{\mathcal{N}}$ given by (4.23), and using the properties of the Kronecker product, it is easy to prove the next relation:*

$$\left[T_{\mathcal{N}} \mathcal{A}^T T_{\mathcal{E}}^{-1}\right]^T = T_{\mathcal{E}} \mathcal{A} T_{\mathcal{N}}^{-1} = \mathbb{A}$$

By employing this definition, $\mathbb{J}$ takes the following form, which proves that it is skew-symmetric definite.

$$\mathbb{J} = \begin{bmatrix} 0 & \mathbb{A} \\ -\mathbb{A}^T & 0 \end{bmatrix}$$

Note that (4.26) preserves the same Hamiltonian structural properties analyzed for the SP-μGrid model shown in (4.9). This implies that its stability analysis is the same as that presented for the SP-μGrid model, *mutatis mutandis*.

4.3 General comments

Next, the main characteristics of both single-phase and three-phase microgrids are given:

- The derivation of the dynamical models for single-phase or three-phase μGrids is based on the classical Kirchhoff's laws, together with incidence matrix modeling, and they do not evidence any structural difference in terms of Hamiltonian modeling, since both models are nonlinear non-autonomous dynamical systems.

- Single-phase or three-phase power electronic converters based on voltage or current source technologies can be integrated with SP-μGrids and TP-μGrids preserving passivity structural properties via interconnection and damping assignments of proportional integral passivity-based control approaches.

- Constant power terminals must be integrated via power electronic converters to guarantee their nominal consumption under power grid variations.

- The steady state behavior of single-phase and three-phase μGrids can be determined via a power flow analysis via numerical methods, e.g., Newton–Raphson [15], by assuming sinusoidal operation with constant frequency. These conditions must be provided by the master node of the μGrid.

4.4 Summary of the chapter

This chapter addressed the dynamical formulation of models for three-phase and single-phase μGrids from the point of view of circuit theory based on the incidence matrix as well as Kirchhoff's laws by considering the power electronic converters as ideal controlled current sources.

The three-phase and single-phase μGrid models showed exactly the same mathematical passive structure, since those μGrids are composed by passive components such as capacitors, inductors and resistors with external controlled and well-defined inputs.

Finally, the main conceptualizations about the operation of AC μGrids in grid-connected or isolated modes were briefly discussed and analyzed from the point of view of the master–slave control approach, which allows operating distributed energy resources in active and reactive power mode independently of the voltage and frequency supplier.

Chapter 5

Numerical validation and discussion

Simulation results for single-phase and three-phase alternating current μGrids will be analyzed in this chapter. The dynamical behavior of quadrature signals and single-phase converters for power compensation in an SP-μGrid as well as different reference frames for three-phase converter control will also be discussed. Test system configurations available in the specialized literature, which are derived from this thesis, will be used to validate the passivity-based proposed controllers.

5.1 Single-phase microgrids

The integration of DERs in SP-μGrids is studied in this section. The integration of supercapacitors and superconducting coil energy storage systems are analyzed considering an equivalent SP-μGrid to independently compensate for active and reactive power; additionally, an isolated operation is tested via a large-scale battery system which is controlled to support the voltage and frequency in the four-node small test feeder reported in [15].

5.1.1 Supercapacitor integration

The integration of a supercapacitor energy storage system is made as depicted in Fig. 5.1. The parameters of this test system are presented in Table 5.1.

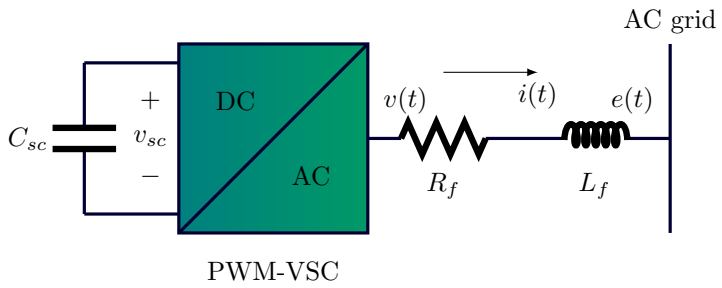

Figure 5.1: Supercapacitor integration in SP-μGrid via PWM-VSC

Parameter	Value	Unit	Parameter	Value	Unit
L_f	2.50	mH	R_f	1.25	mΩ
C_{sc}	2.50	F	v_{sc}	600	V
V_{rms}	220	V	f	50	Hz

Table 5.1: Parameters of the lateral branch presented in Fig. 5.1 for integrating supercapacitors

Note that this supercapacitor allows storing 450 kJ of electrical energy. Its operating voltages are from 350 V to 600 V. The PWM-VSC was designed with nominal power rate of 12 kVA.

Fig. 5.2 shows the charging process for the supercapacitor when the voltage begins from 350 V and the desired operating charges are 600 V. For this simulation test, the PI-PBC approach was employed, assuming that the PWM-VSC is operated under unity power factor with varied power transference capabilities: 50%, 75%, and 100% of its nominal capacity.

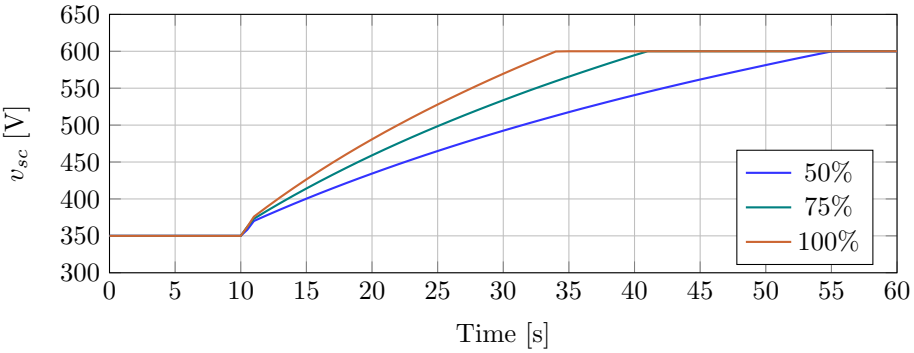

Figure 5.2: Charging process for supercapacitor with different power rates

Note that the required charging time for the supercapacitor system depends on the active power interchange between the AC grid and the converter. For this reason, when the active power transference is 6 kW, the charging time is around 45 s (from 10 s to 55 s, approximately, as shown in Fig. 5.2); when the rate of charging is 9 kW, the required time is reduced to approximately 30 s. When the active power transference corresponds to the nominal capacity of the PWM-VSC (12 kW), the needed time is around 23 s. Additionally, observe that the charging curve is not exactly a ramp curve since there is a quadratic relation between the active power and the voltage profile in the supercapacitor, as discussed in [72], which is solved by a root-square curve such as the one presented in Fig. 5.2.

Fig. 5.3 presents the active and reactive power behavior for the supercapacitor energy storage system, when an arbitrary set of reference has been selected for proving its ability to control active and reactive power independently.

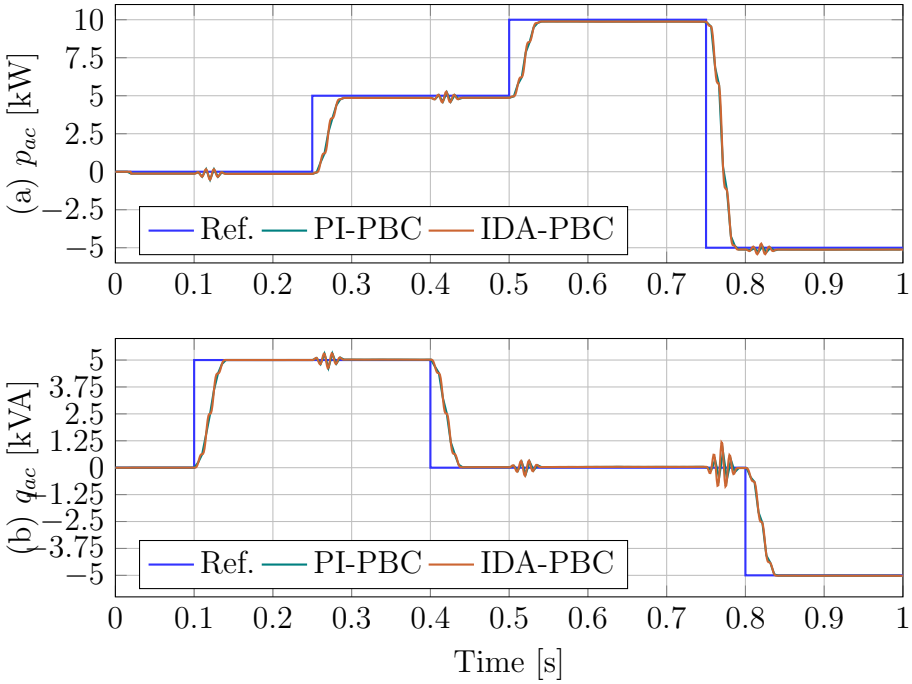

Figure 5.3: Active and reactive power for the supercapacitor energy storage system

Fig. 5.3 presents the active and reactive power behavior for a supercapacitor energy storage system in SP-μGrids. Observe that both proposed passivity-based controllers, IDA-PBC and PI-PBC, have the same dynamical performance. This behavior is expected in these controllers, since they have the same analytic derivation and the only difference is in the signal control associated to the error $\tilde{u}$, as presented in Chapter 2. Besides, both

control inputs directly actuate on the variable of interest (the filter current i), making it possible to design a direct control strategy, which simplifies the PWM-VSC when compared to PWM-CSC, where an indirect control design is required. Nevertheless, from Figs. 5.3(a) and 5.3(b) it is possible to conclude that both passive controllers allow satisfying the control objective in terms of active and reactive power control independently for SP-μGrid applications. Note that the selection of any one of those controllers (i.e., IDA-PBC and PI-PBC) depends on the requirements of the plant as well as the capabilities of signal processing of the hardware where the controller is implemented. Notwithstanding, when possible, the PI-PBC approach should be selected over the IDA-PBC approach, since the actions of the PI allow reducing the parametric uncertainties present in the filter parameters.

Fig. 5.4 shows the dynamical performance of the energy storage variable for both proposed passivity-based controllers. Observe that the voltage behavior is directly related to the active power behavior (see Fig. 5.3): when the active power is positive (5 kW from 0.25 s to 0.5 s and 10 kW from 0.5 s to 0.75 s) the voltage profile at the supercapacitor begins decreasing, which implies that energy is flowing from the supercapacitor to the main AC grid. When the active power is negative, the voltage profile starts to increase: see the period of time between 0.75 s to 1 s. Otherwise, the voltage remains constant, as observed from 0 s to 0.25 s in Figs. 5.3 and 5.4.

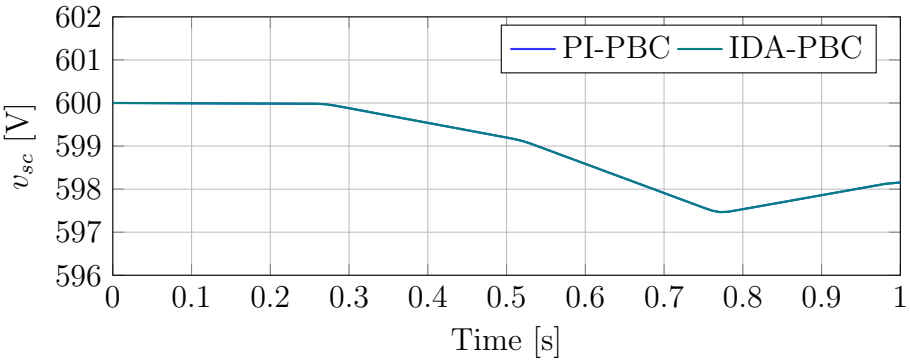

Figure 5.4: Voltage at the terminals of the supercapacitor when the active and reactive power references vary

It is important to stress that the reactive power behavior does not have any effect on the supercapacitor voltage, since it is directly interchanged between the commuted devices present in the PWM-VSC and the main grid.

5.1.2 Superconducting coil integration

The integration of superconducting coils in AC SP-μGrids is made as presented in Fig. 5.5. The parameters of the series filter and AC voltage and frequency operation are contained in Table 5.1. Additionally, the shunt capacitor filter C_f was taken to be 150 μF, while the superconducting coil was designed with the same energy storage capability used in the case of the supercapacitor, which implies that its nominal current rate i_{sc} is 300 A and its inductance value L_{sc} corresponds to 10 H.

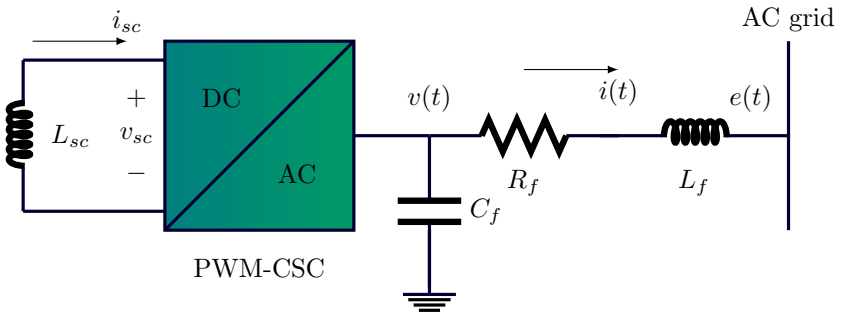

Figure 5.5: Interconnection of superconducting coils in AC SP-μGrids via PWM-CSC

The charging process of the superconducting coil is presented in Fig. 5.6. An IDA-PBC controller is employed in this case to validate the ability of passivity-based control theory to manage the energy stored in a superconducting coil system by controlling the PWM-CSC. For this test, it is supposed that the superconducting coil has an initial current of 175 A. When the simulation time has reached 5 s, different power rates are used to take its current to its nominal value. Recall that the PWM-CSC was designed and operated in this test with the same properties as the PWM-VSC.

From Fig. 5.6 it is possible to see that the rate of active power used to charge the superconducting coil (increase its current) is directly related to the required charging time. For example, when the active power rate is 6 kW, the charging time is approximately 50 s (from 5 s to 55 s); when the active power rate is 9 kW, the charging time is around 32 s. When the nominal power rate of the converter is used, the charging time is approximately 25 s.

Note that the form of the curve exhibit by the charging process of the superconducting coil (see Fig. 5.6) evidence a root-square form as as presented in [83] for the three-phase superconducting coil case. This behavior is expected for energy storage devices since, the energy function is quadratic in terms of the time, with implies that its inverse is a root-square function.

Fig. 5.7 shows the active and reactive power behavior for a superconducting coil energy

storage system when active and reactive power are controlled independently.

From Fig. 5.7 that both passivity-based controllers in general terms fulfill the control objectives; notwithstanding, IDA-PBC has a better tracking performance than the PI-PBC, since when the active (reactive) power changes its reference, the reactive (active) power has

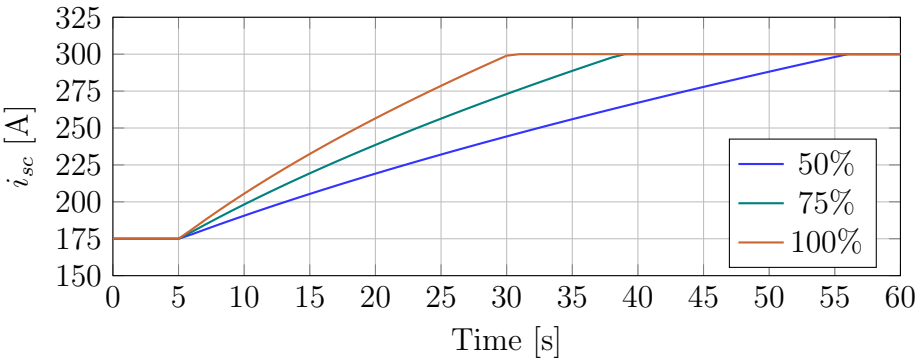

Figure 5.6: Charging process for the superconducting coil with different power rates

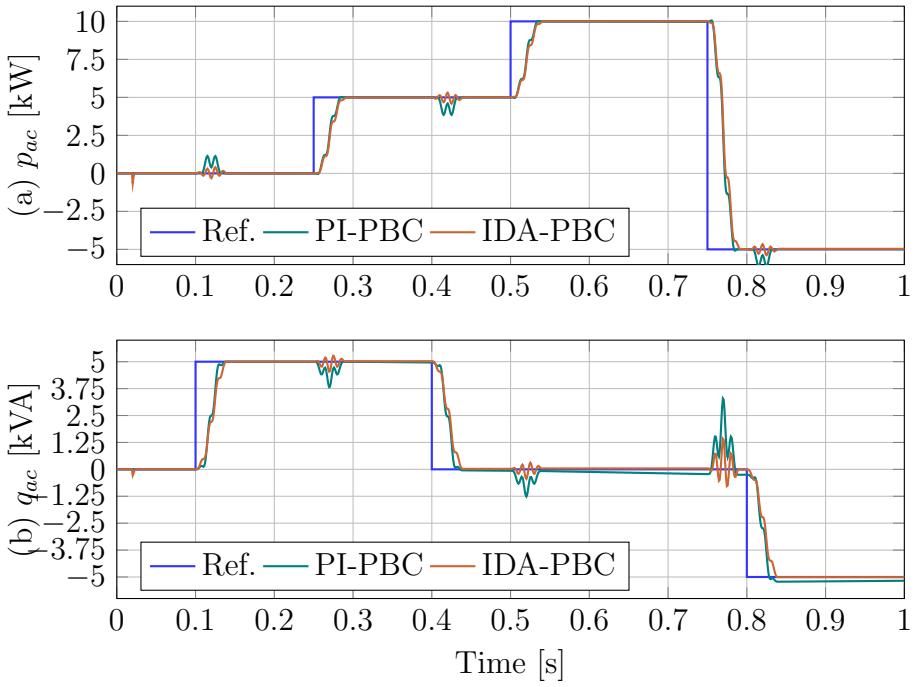

Figure 5.7: Active and reactive power for the superconducting magnetic energy storage system

lesser oscillations. Also observe that in the interval of time between 0.4 s and 0.8 s, the reactive power has an important deviation of its reference value for the PI-PBC approach, while IDA-PBC remains closer to its reference, as can be seen in Fig. 5.3b. This is a consequence of the greater oscillations produced by any change in the reference value of the active power, which moves the reactive power away from its desired value, as well as the oscillations present in the voltage signal of the capacitive filter C_f, which may be amplified by the integral action of the PI-PBC approach, and that it does not suffer in the IDA-PBC approach.

Finally, Fig. 5.8 presents the dynamical performance of the energy storage variable for the superconducting coil as a function of the active power variations shown in Fig. 5.7. Note that the same interpretation used to understand the dynamical behavior of the supercapacitor can be applied in this case.

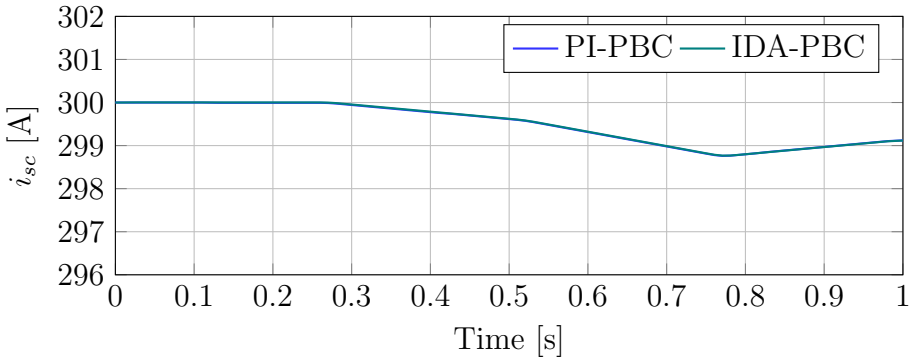

Figure 5.8: Current through the superconducting coil when active and reactive power references are varied

5.1.3 Integration of batteries and renewable generation

This section presents the possibility of using a passivity-based control for operating an SP-μGrid under a master–slave scheme. Nevertheless, this configuration corresponds to a large-scale of batteries integrated via PWM-VSC to control the voltage profile as well as the frequency in the whole microgrid. A photovoltaic system is also integrated via PWM-VSC, being operated as a constant power module with unity power factor. Additionally, a non-controlled constant power load is directly connected to the SP-MG. The configuration of the test system is presented in Fig. 5.9, while all data are listed in Table 5.2.

In the case of the photovoltaic system, its behavior is emulated as a variable current source i_s, such that $i_s \geq 0 \; \forall t \geq 0$. The current profile selected for emulating the photovoltaic

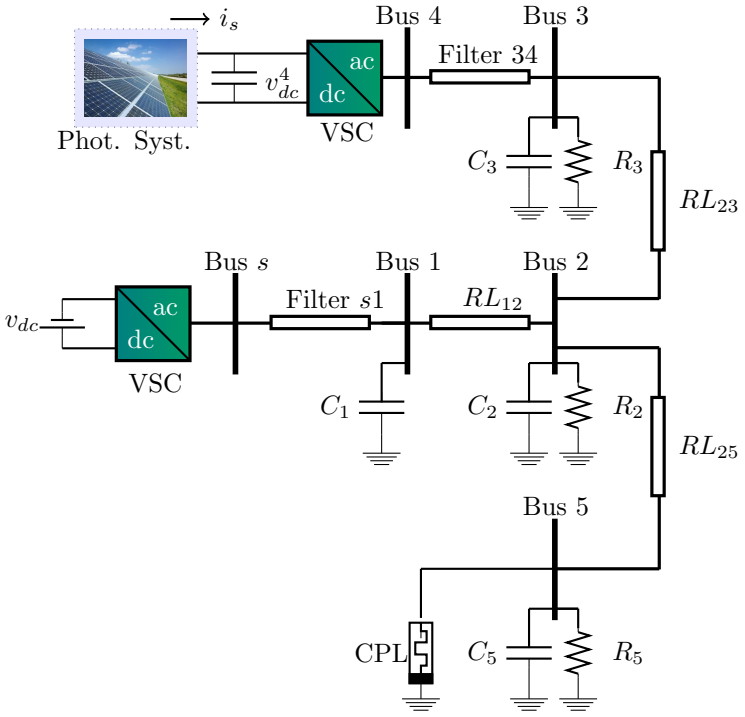

Figure 5.9: Electrical configuration of the test system [15]

Element	Value	Unit	Element	Value	Unit
C_1	50	μF	C_2	120	μF
C_3	100	μF	C_5	160	μF
C_{dc}^4	4700	μF	R_2	5	Ω
R_3	3	Ω	R_5	4	Ω
L_{s1}	1.25	mH	L_{34}	2.5	mH
L_{12}	1.5	mH	R_{12}	10	$m\Omega$
L_{23}	2.5	mH	R_{23}	10	$m\Omega$
L_{25}	1.25	mH	R_{25}	50	$m\Omega$
V_{rms}	127	V	f	60	Hz
v_{dc}	300	V	$\bar{v}_{dc}^4$	400	V

Table 5.2: Electrical parameters of the test system

system during a typical sunny day is presented in Fig. 5.10[1].

[1]This current curve was adapted from real values reported in [131]

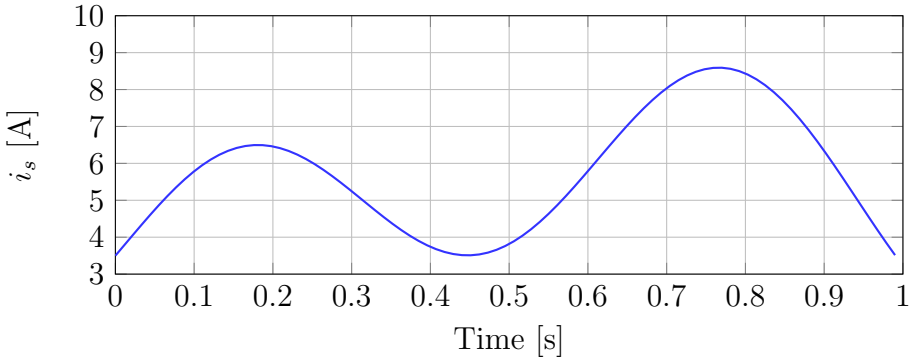

Figure 5.10: Current provided for the photovoltaic system

For simulation purposes, due to the fact that both proposed passivity-based controllers exhibit a similar dynamical performance, as was observed in the above sections, in this case, only the results obtained with the IDA-PBC approach will be presented in this section.

In the case of isolated μGrids operating under a master–slave control scheme, the main idea is to emulate the behavior of an ideal AC sinusoidal AC source. In this context, the battery system connected at node s is operated under voltage–frequency to support these variables at node 1, which implies that the objective of control for the battery system is

$$v_{C1}^{\star}(t) = \sqrt{2}V_{rms}\sin(2\pi f t); \tag{5.1}$$

where V_{rms} and f were listed in Table 5.2.

On the other hand, the photovoltaic system is operated with a unity power factor, in order to extract all active power available in the primary energy resource (see the current i_s in Fig. 5.9). Finally, the non-controlled constant power terminal located at node k consumes 3 kW and 2 kVA until 0.5 s of simulation time; after this period, this load operates under unity power factor, consuming 5 kW.

Fig. 5.11 presents the root mean square performance of voltage at the main nodes of the network as well as the frequency profile at node 1.

From Fig. 5.11(a) it is possible to observe that node 1 (the slack node) preserves its desired rms value with deviations lower than 1.5% independently of the photovoltaic generation or load consumptions. On the other hand, the other voltage profiles fulfill the conventional regulation voltage deviation estimated around 10% for AC low-voltage power grids [8]. Additionally, observe that their rms behavior is highly correlated to the active power generation by the photovoltaic system, since these voltages follow a similar curve to that presented by i_s (see Fig. 5.10). It is also important to point out that the commutation of the controlled constant power load at 0.5 s produces a transient behavior in the voltage profile of the network, since the currents through the lines change instantaneously, producing

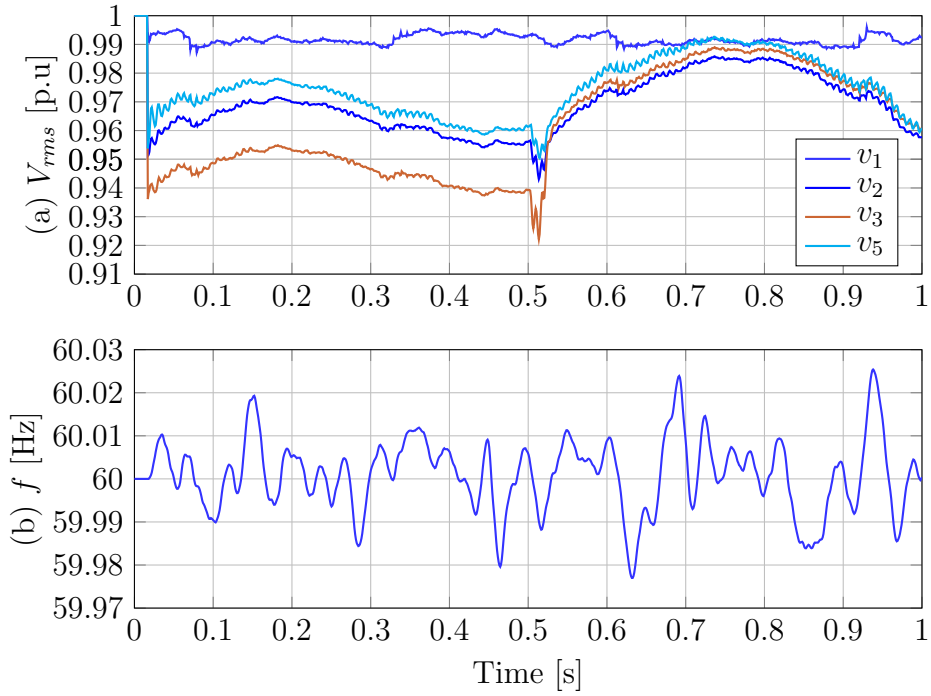

Figure 5.11: Voltage and frequency at the main nodes of the network

drastic variations in their terminal voltages. Note that the averaging frequency in the slack node is depicted in Fig. 5.11(b), which clearly evidences small oscillations around 60 Hz. These oscillations are lower than 0.05%. Note that these variations in the frequency are mainly cased by the commutation strategy applied to the PWM-VSC.

From the results depicted in Fig. 5.11 it is possible to conclude that the proposed IDA-PBC allows fulfilling the control objective for the voltage profile defined by (5.1) in terms of voltage amplitude and frequency.

Fig. 5.12 shows the active power performance in both sides of the PWM-VSC that interconnects the photovoltaic system to the AC grid as well as its DC voltage.

Note in Fig. 5.12(a) that the active prower transference from the DC side of the PWM-VSC to the AC main grid (node 3) follows the same behavior shown by i_s (see Fig. 5.10), since the power in the DC side corresponds to the product of this current and their DC link voltage (v_{dc}^4 in Fig. 5.9(a)), which implies that if the DC link voltage is constant (see Fig. 5.12(b)), then the DC power follows the same pattern exhibited by the current. Moreover, from 5.12(a) it is possible to see that the AC power p_{ac} wraps the DC power P_{dc}, which implies that the AC current follows its reference with minimal error. Finally, Fig. 5.12(b) shows a quite constant performance in the voltage on the DC link of the photovoltaic

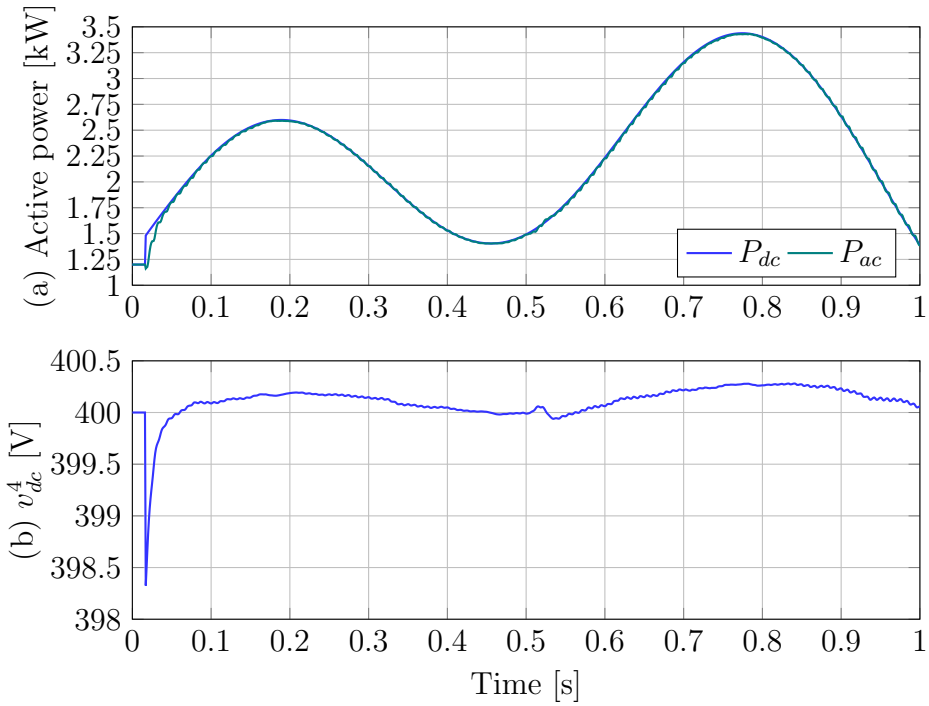

Figure 5.12: Active power and DC voltage in the photovoltaic system

system, which implies that the amplitude of the AC current through the filter only depends on the value of the current coming from the primary energy resource, i.e., i_s.

5.1.4 Additional comments

The performance of any PWM-CSC or PWM-VCS depends on the quadrature generator as presented by the differential first-order Hamiltonian system given in (3.13), since this quadrature generator allows controlling the current through the AC filter in order to control the active and reactive power in constant power operation mode. Fig. 5.13 shows the performance of the quadrature generator for different proportional gains, considering as normalized input a sinusoidal function.

Note that in Fig. 5.13 the parallel $e_{\parallel}$ and the quadrature $e_{\perp}$ signals associated to the input signal e have a rate of convergence related to the proportional gain k_{sync}, e.g., when $k_{sync} = 50$ the required time to reach the desired behavior is greater than five cycles of the reference signal; nevertheless, when $k_{sync} = 200$ only two cycles of the reference signal are required to obtain a perfect parallel-quadrature signal generator. Additionally, note that the simulations presented in Fig. 5.13(b) show a quadrature signal leading the parallel signal,

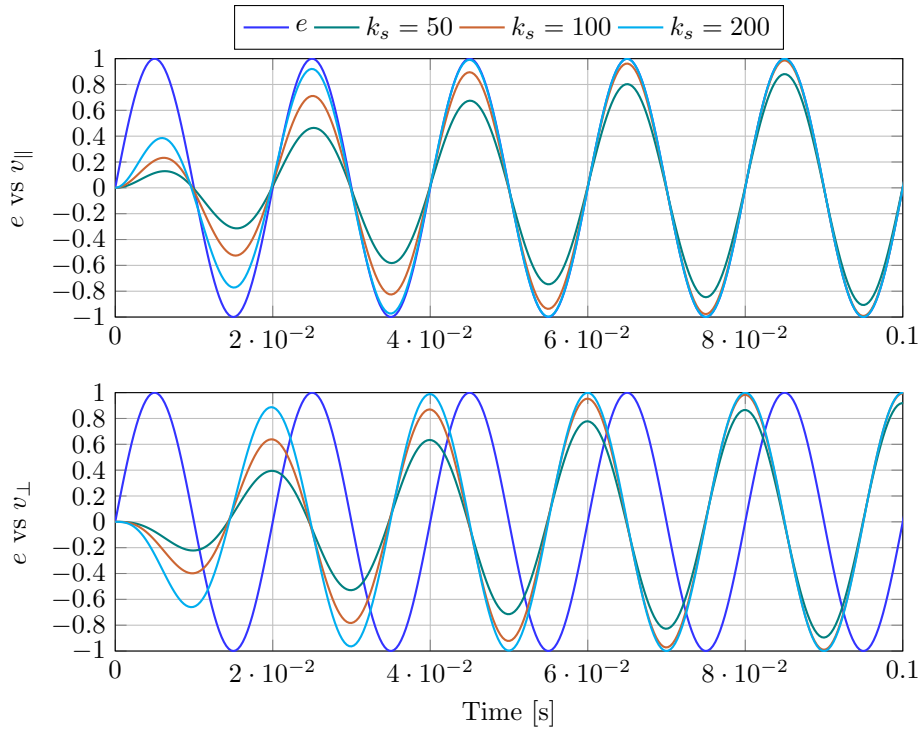

Figure 5.13: Dynamical behavior of the quadrature generator

which is related to the power factor in the operation of the converters.

It is important to mention that the comparison between the proposed PBC approaches with classical methods such as the PI control or feedback linearization methods can be found in the papers contained in the list of publications presented in Section 1.8.

5.2 Three-phase microgrids

The integration of DERs in TP-μGrids is studied in this section.

5.2.1 Battery/PV system for voltage and frequency support

Consider a reduced topology presented in Fig. 5.14, which corresponds to an interconnection between a battery energy storage system and a photovoltaic system to support the voltage and frequency of an isolated power grid modeled as a current source. The electrical parameters of this network are presented in Table 5.3.

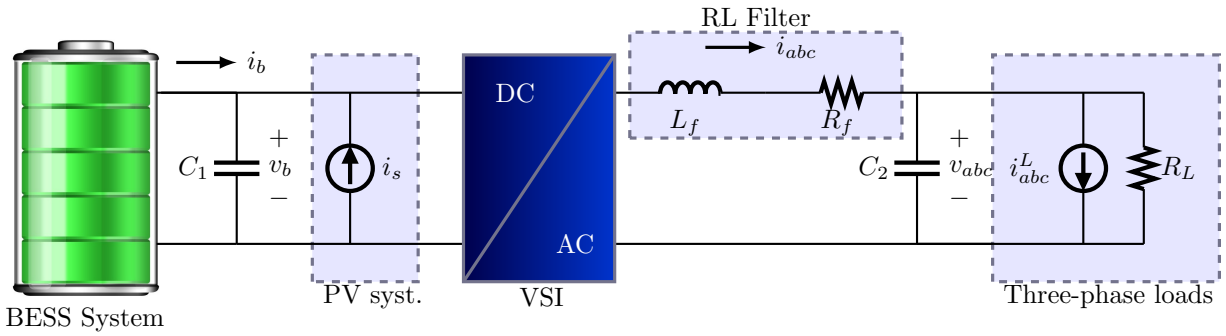

Figure 5.14: Proposed circuit configuration for voltage and frequency support in TP-μGrids in isolated operating mode

Parameter	Value	Unit	Parameter	Value	Unit
C_1	10	mF	C_2	250	μF
L_f	2.25	μF	R_f	1.25	mΩ
R_L	20	Ω	—	—	—

Table 5.3: Parameters of the test system presented in Fig. 5.14

The battery considered for this study is based on Lithium-Ion technology with 800 V and 30 Ah of voltage and current nominal values, respectively. We assume that the battery contains an initial charge of 70% and its time response is 30 s. The desired output voltage profile at the point of the three-phase load coupling is to $V_{rms} = 220$ V with an electrical frequency of 50 Hz. In addition, the current model i_s which is generated for the distributed energy resource is depicted in Fig. 5.15.

For simulation purposes, a constant power load is considered, as follows. If $t \in [0, 0.5)$ s, then $p_{ac} = 15$ kW and $q_{ac} = 5$ kVAr. If $t \in [0.5, 1]$ s, then $p_{ac} = 20$ kW and $q_{ac} = 10$ kVAr.

Fig. 5.16(a) shows the dynamical behavior of the frequency at the point of common coupling for the proposed PI-PBC as well as PI-PBC. Note the transient behavior in the interval of time from 0 s to 0.2 s; this behavior is produced by the single-phase system used to observe the frequency behavior, since it is composed by a proportional-integral action and it has a transient reaction when the AC signals have not reached a steady state behavior. It is possible to observe that both control approaches have a similar dynamical performance. Nevertheless, the PI-PBC approach has small oscillations around the desired value, while the IDA-PBC presents a quite constant behavior (see Fig. 5.16(b)).

Fig. 5.17 presents the root-mean-square performance of the voltage profile at the load coupling point for both proposed control approaches. Note that the percentage deviations are less than 1% for both controllers; notwithstanding, the PI-PBC method shows a smaller

steady state error than the IDA-PBC method. This can be explained by the active and reactive power behaviors presented in Fig. 5.18.

In Fig. 5.18 the dynamical behavior of the active and reactive power in the point of load coupling is presented. Note that the IDA-PBC and PI-PBC approaches have a similar behavior during the transient periods; nevertheless, under steady state conditions, the PI-PBC method tracks its reference with less error than does the IDA-PBC method. The active power in the case of PI-PBC has a 0.12% tracking error, while IDA-PBC exhibits 0.35% tracking error (see Fig. 5.18(a)). This difference in the active power tracking produces deviations in the rms voltage profile, as was shown in Fig. 5.17. On the other hand, Fig. 5.18(b) shows the reactive power performance. In this case, both controllers present tracking errors lower than 0.08%, which fulfills the control objective for both approaches.

Finally, Fig. 5.19 shows the dynamical performance of the current in the DC side of the converter, i.e., distributed energy resource current i_s as well as the battery current i_b for both proposed PBC approaches. Note that both behaviors have the same dynamical performance in terms of wave form. During the starting period, a transient phenomena is seen for $t < 0.1$ s, which is caused by the initial conditions of the simulation. During the period of time when i_s has enough energy to support all loads, the current through the battery is negative, as seen from 0.2 s to 0.5 s. This implies that the battery is storing energy during this period of time. Finally, the power consumption increase in the AC load for simulation times greater than 0.5 s: the current through the battery changes its sign, which implies that the battery starts to support the difference between the power provide by the distributed energy resource in the DC side of the converter and the AC power consumption.

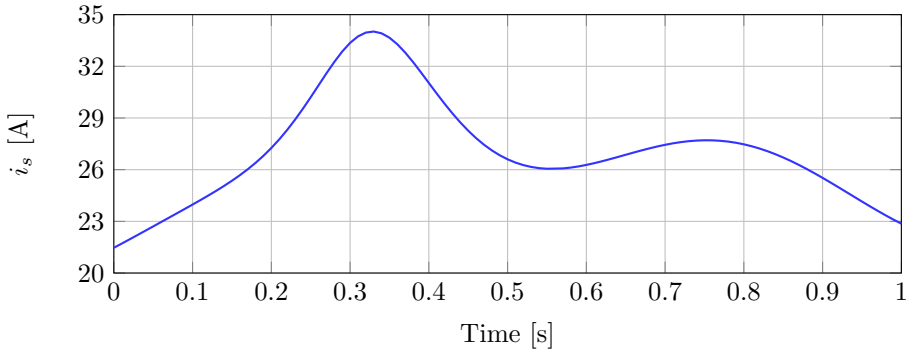

Figure 5.15: Behavior of the DC current present in the DC side of the PWM-VSC in Fig. 5.14

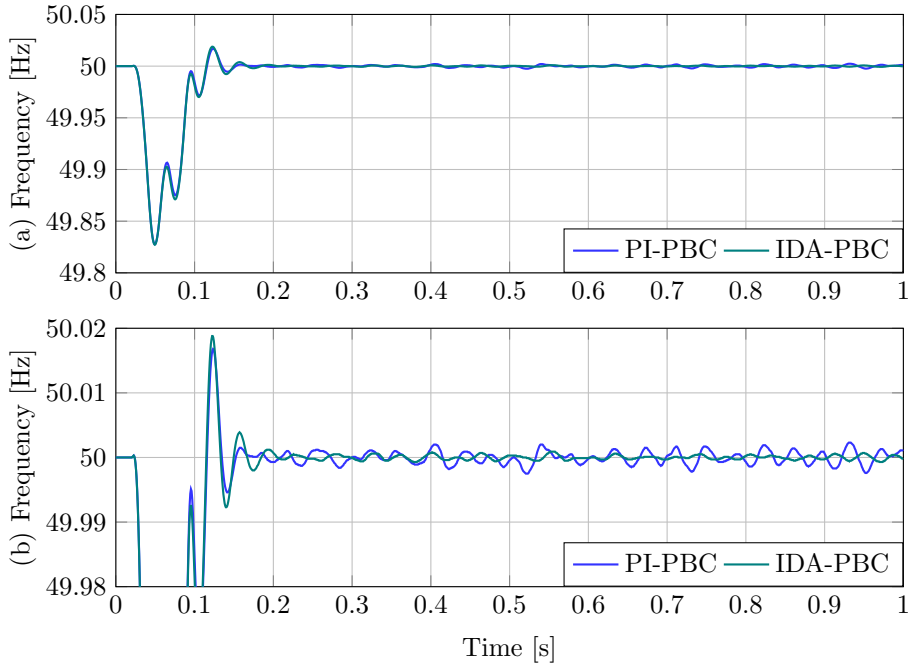

Figure 5.16: Dynamical behavior of the electrical frequency of the AC power grid for the IDA-PBC and PI-PBC approaches

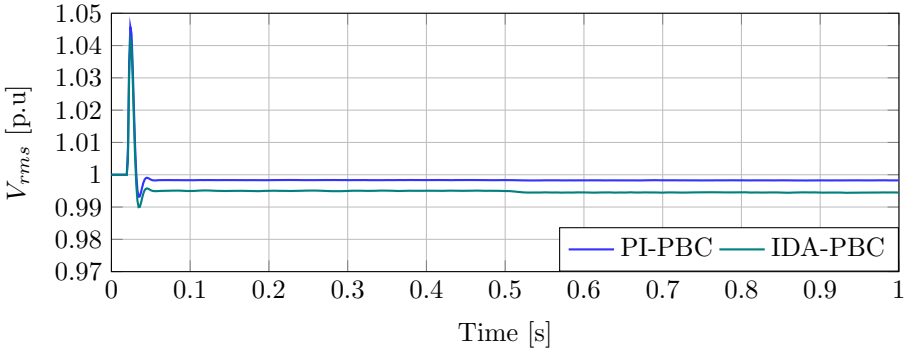

Figure 5.17: Dynamical behavior of the root-mean-square values in the point of load connection with IDA-PBC and PI-PBC approaches

5.2.2 Integration of superconducting coils

In this section the possibility of integrating superconducting coils in TP-μGrids via PWM-CSC is presented. The electrical parameters are presented in Table 5.4 and Fig.

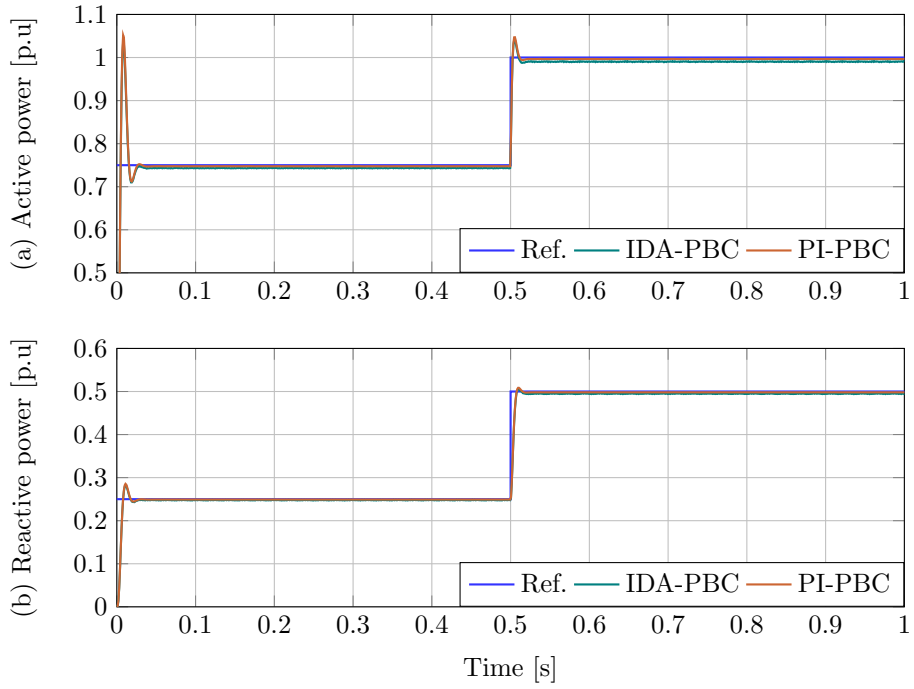

Figure 5.18: Active and reactive power supported at the point of three-phase load connection

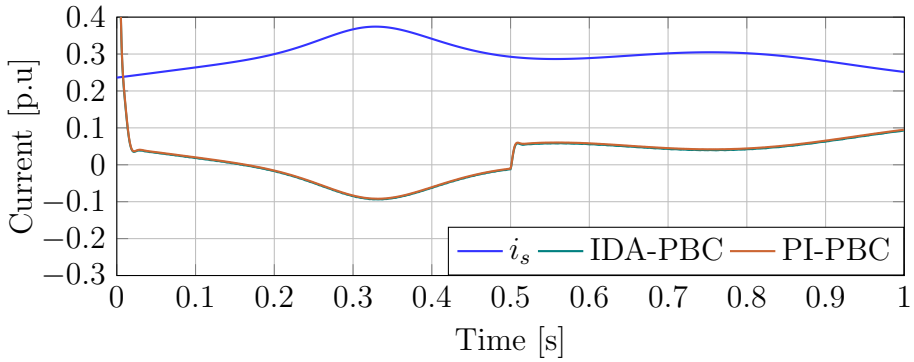

Figure 5.19: Current in the DC side of the converter

5.20 shows the interconnection of this device to the TP-MG.

To study the possibility of controlling the active and reactive power in three-phase superconducting coil applications via IDA-PBC theory, an arbitrary set of active and reactive power references have been selected. Park's reference frame as well as Clarke's reference frame are used to validate the possibility of controlling autonomous and non-autonomous dynamical

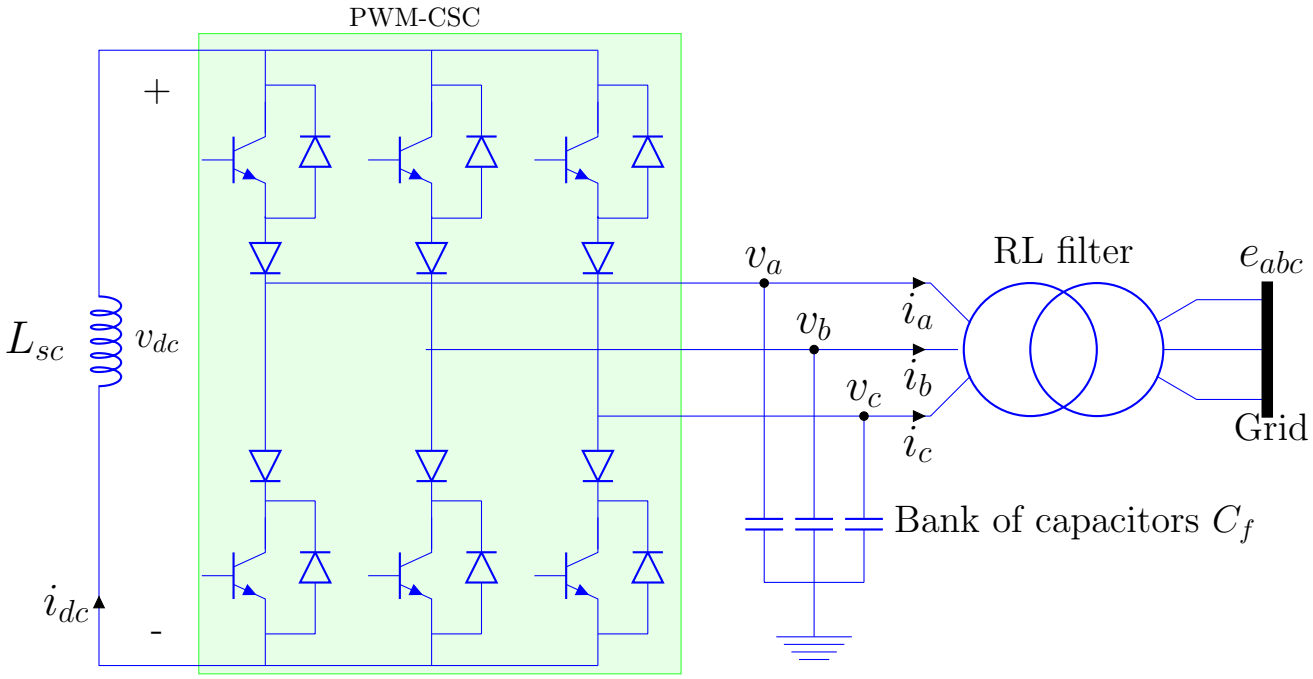

Figure 5.20: Connection of an SMES system using PWM-CSC to TP-μGrids

Parameter	Value	Unit	Parameter	Value	Unit
L_f	2.5	mH	R_f	1.25	mΩ
L_{SC}	7.5	H	C_f	160	μF
i_{dc}^{max}	100	A	i_{dc}^{min}	20	A
v_{LL}^{rms}	440	V	f	60	Hz

Table 5.4: Parameters for the simulation of the superconducting coil connection to a TP-MG

systems via passivity-based control theory.

Fig. 5.21 shows the active and reactive power output of the superconducting coil system when IDA-PBC control is applied with the dq and $\alpha\beta$ reference frames.

For both reference frames, the active and reactive power effectively follow their references; nevertheless, the dq reference frame has less tracking error when compared to the $\alpha\beta$ reference frame. This is since in the dq reference frame, a three-phase PLL is employed to estimate the electrical frequency of the grid. If this frequency is adequately estimated, then the dq reference frame has constant input signals and references, which implies that the control problem is easier than for the time varying signals present in the $\alpha\beta$ reference frame.

It is important to mention that the charging process as well as the dynamical behavior

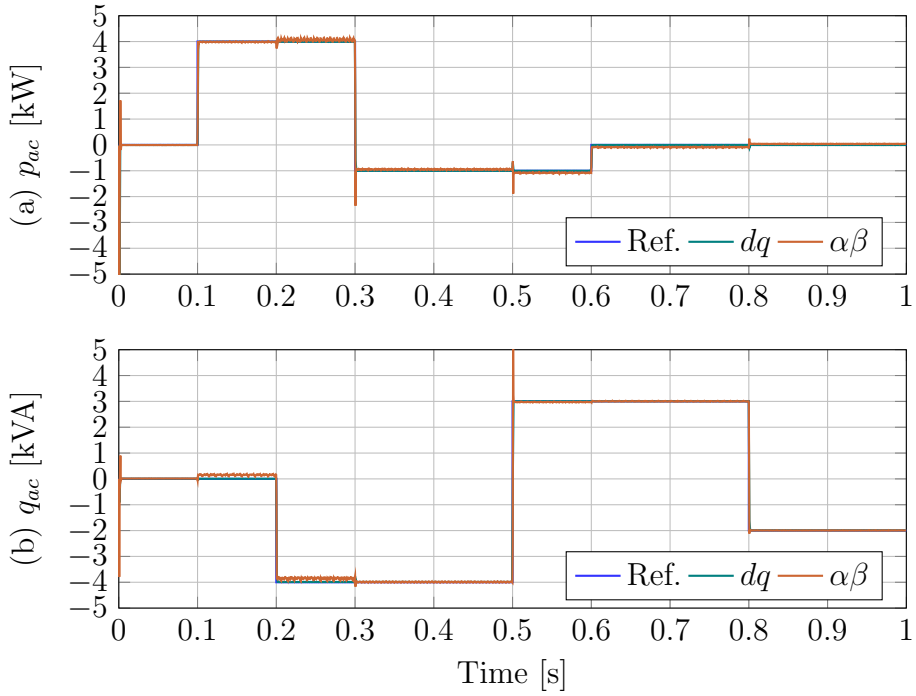

Figure 5.21: Active and reactive power in Clarke's and Park's reference frames

of the energy storage variable remain the same as in the single-phase case. For this reason, these simulations are not included in this section.

5.2.3 Unbalanced operation

As test system, a low voltage TP-μGrid is employed. Its configuration is depicted in Fig. 5.22. All parameters of this system are presented in Table 5.5. These values have been taken from [63].

The information related to the total active power available in the photovoltaic system is presented in Fig. 5.23(a). The active and reactive power of dynamic loads are depicted in Figs. 5.23(b) and 5.23(c), respectively.

Note that for DL3 there are balanced and unbalanced loads, which produces oscillations in the normal operation of the TP-MG.

As simulation cases, two scenarios are considered here:

> **Case 1:** In the photovoltaic system, the generic converter is controlled to transfer all active power available in the DC side at the same time that it supports all reactive power required by the dynamic load 1.

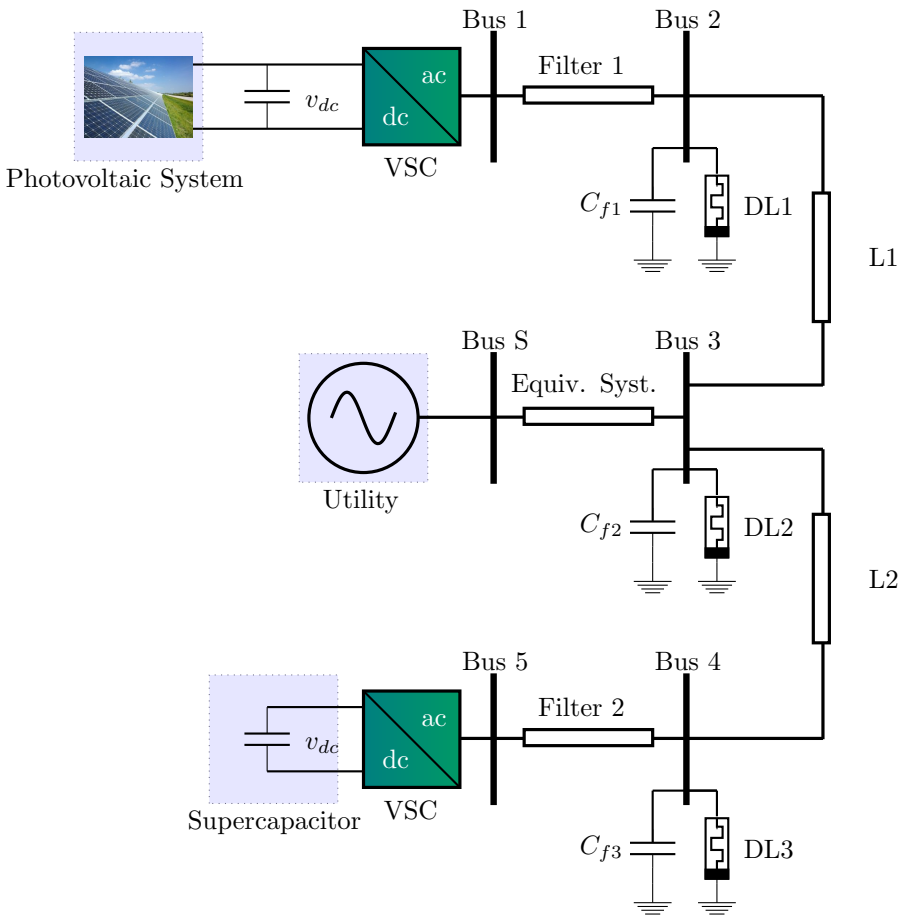

Figure 5.22: TP-μGrid configuration for unbalanced operation

Parameter	Value	Unit	Parameter	Value	Unit
DC voltage at the Phot. Syst.	800	V	Filter 2 resistance	50	mΩ
DC voltage at the SCES Syst.	1500	V	Grid voltage, line to line, rms	380	V
Capacitance at the Phot. Syst.	0.5	F	Grid fundamental frequency	50	Hz
Capacitance at the SCES Syst.	1	F	Line 1 inductance	100	μH
Capacitance at the bus 1	200	μF	Line 2 inductance	120	μH
Capacitance at the bus 2	150	μF	Line 1 resistance	50	mΩ
Capacitance at the bus 3	200	μF	Line 2 resistance	60	mΩ
Filter 1 inductance	800	μH	Equiv. Syst. inductance	200	μH
Filter 2 inductance	800	μH	Equiv. Syst. resistance	20	mΩ
Filter 1 resistance	50	mΩ	—	—	—

Table 5.5: Electrical parameters of the TP-MG

Case 2: The SCES system is employed to support all reactive power requirements in the dynamic load 3. This SCES is also used to reduce active power oscillations caused by unbalanced load conditions in this load.

Case 1 This simulation scenario evaluates the possibility of the VSC's holding the DC voltage in the capacitor at a constant value, in order to transfer all active power available in the photovoltaic system to the AC grid. The converter is used to support all reactive power demanded by DL1. In Fig. 5.24 are presented the active power transfered from the photovoltaic system to the AC side as well as the steady state error, the dc-link voltage and the power factor in the dynamic load before and after the compensation. **Case 2** In this simulation scenario there is evaluated the possibility of using a SCES system to compensate for the power oscillations caused by the unbalanced behavior in the DL3. The possibility of compensating all reactive power demanded by DL3 is also evaluated. Fig. 5.25 shows the active and reactive power in DL3 after compensation as well as the voltage behavior in the supercapacitor. The SCES system guarantees a power factor of unity in dynamic load 3 at the same time that its active power oscillations are reduced, considering an average consumption in this load of around 30 kW.

After evaluating the dynamic performance of the proposed IDA-PBC controller, it is possible to conclude that:

- The tracking error, between the total active power available in the photovoltaic system (DC link) and the active power in the AC side of the converter, is 2% of the average value, with oscillations of 2%, caused mainly by the unbalanced loads, as can be seen in Fig. 5.24(b). Additionally, there appear commutation losses in the converter and the resistance of the filter, which are not quantified. These power losses affect the tracking reference process, reducing the electrical efficiency of the system.

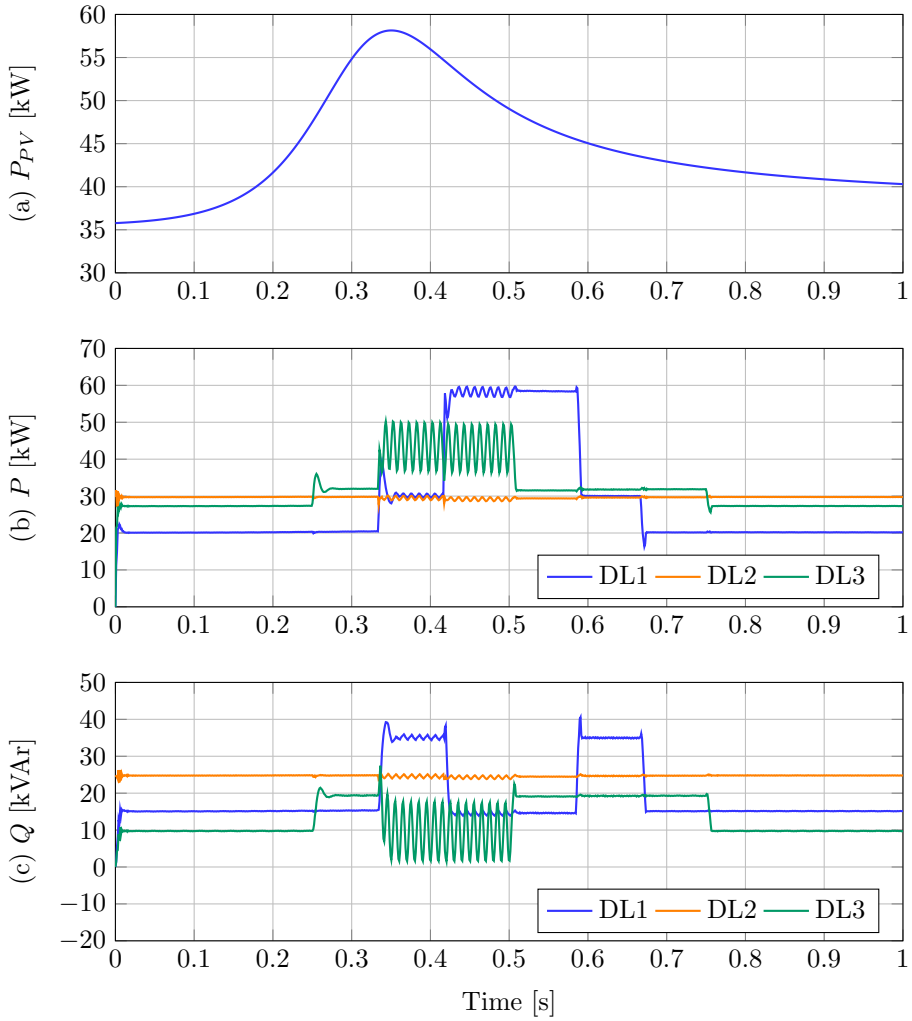

Figure 5.23: Active and reactive power consumed/generated in the dynamic loads and photovoltaic generation: (a) available power generation in the photovoltaic generation system, (b) active power consumption in the dynamic loads and (c) reactive power consumption in the dynamic loads

- The DC link voltage during the simulation time always remains at its nominal value, as shown in Fig. 5.24(c), which implies that the controller fulfills the control task, delivering all active power available in the photovoltaic system while holding the DC voltage as constant as possible.
- It is possible to use the VSC to support the reactive power consumed by the dynamic

load as presented in Fig. 5.24(d). Note that for all the period of simulation, the active power factor observed by the electric grid in the point of connection of DL1 is unitary as well as in DL3.

- Figure 5.25(c) shows that the dynamical behavior of the voltage profile in the supercapacitor device depends only on the active power delivered (consumed) to (from) the AC grid. When the active power is positive, the supercapacitor behaves as a power generator, which implies that it is discharging (reduction in this voltage value). In contrast, if the active power is negative, the supercapacitor behaves as a load (increasing the voltage magnitude). This behavior is easy to observe by comparing Figs. 5.25(b) and 5.25(c).

5.3 Summary of the chapter

This chapter summarized the application of the passivity-based controllers for the integration of multiple distributed energy resources in AC μGrids with single-phase and three-phase topologies, including grid-connected and isolated operation modes. Note that electrical energy storage systems based on supercapacitor and superconducting coil technologies and their integration with PWM-VSCs and PWM-CSCs exhibited the same applicability and dynamical performance, which clearly evidenced that the proposed pH-bilinear modeling and control allowed the generalization of these devices for single-phase and three-phase applications without structural changes in their mathematical conceptualizations.

Renewable energy as well as battery banks were included for long term operation in isolated μGrids, confirming that the master–slave control strategy can always be used for voltage and frequency support. The power electronic converters can also control the active and reactive power in four-quadrant operation, which allowed maximizing operating conditions on those networks without recurring to conventional power flow analysis under steady state conditions.

Finally, a complete analysis for three-phase μGrids showed the possibility of controlling the active and reactive power independently under different reference frames, even if the AC μGrid has uncontrolled and unbalanced loads, which implies that passivity-based control approaches based on interconnection and damping assignment or proportional-integral actions allowed satisfactory performance even under adverse operating conditions.

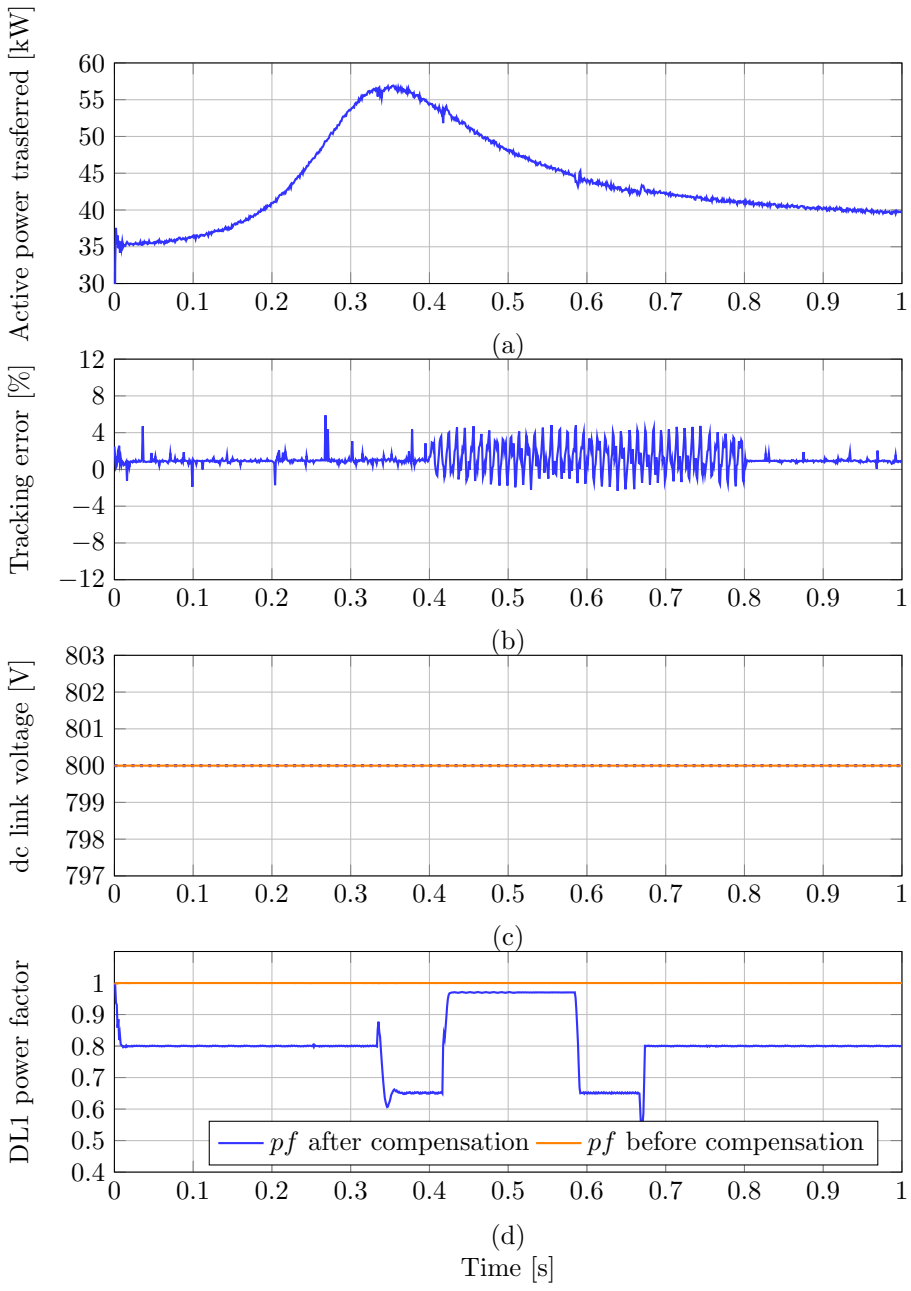

Figure 5.24: Dynamical behavior in the photovoltaic and DL1 systems (a) active power transfered from the photovoltaic system to AC system through VSC1 (b) steady state error between DC and AC power in the VSC1, (c) DC link voltage and (d) power factor in DL1 before and after compensation

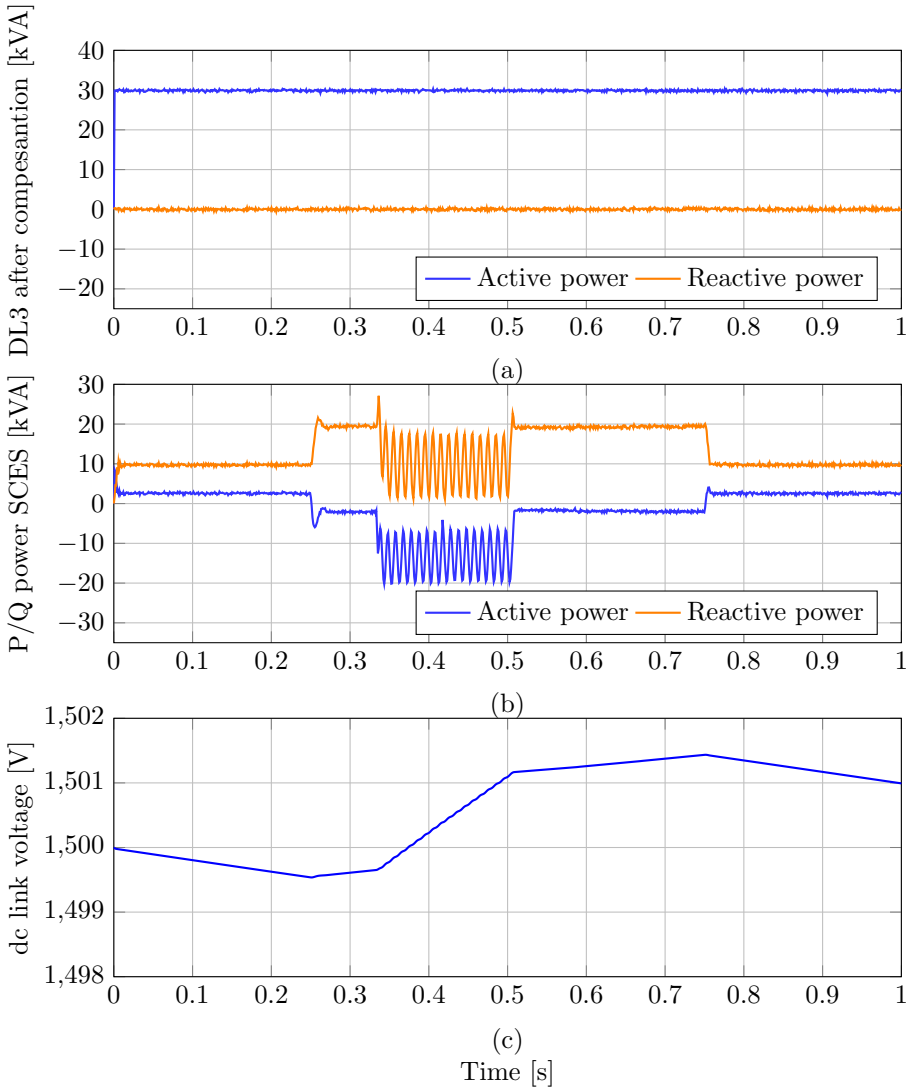

Figure 5.25: Dynamical behavior in the SCES system: (a) active and reactive power consumed in DL3 after compensation, (b) active and reactive power behavior in the SCES system and (c) DC voltage in the supercapacitor device

Chapter 6

Conclusions

This chapter recapitulates the main results of this thesis and gives some recommendations for future investigations.

6.1 Main results

The following conclusions can be made regarding the principal topics addressed in this thesis.

- This thesis reviewed passivity-based control theory in the Hamiltonian formulation for power electronic converters based on voltage and current source technologies with single-phase or three-phase topologies. The integration of distributed energy resources, such as renewable generation as well as energy storage systems based on electrical and chemical technologies, was studied from the point of view of the control of the active and reactive power transference between these devices and the main alternating-current power grid.

- General mathematical models for the integration of supercapacitors and superconducting coils in three-phase and single-phase microgrids were developed within the Hamiltonian paradigm. These models were obtained by using energy modeling methods, which permit directly observing the strong relation between power electronic converters for energy storage applications and Lyapunov's stability theory for control design. In addition, these Hamiltonian models allow developing general controllers based on passivity-based control theory for managing the power interchange between energy storage devices and AC electrical networks guaranteeing stability conditions in closed-loop operation for each energy storage device.

- Supercapacitors and battery energy storage systems were integrated with the AC grids via PWM-VSCs, since these devices allow controlling the voltage profile in the DC side

of the converters. PWM-VSCs exhibit a natural port-Hamiltonian formulation that was exploited via the PI-PBC and IDA-PBC approaches to manage the total energy stored in both energy storage systems, guaranteeing stable operation in the AC power grid. Battery energy storage systems allow controlling the active and reactive power flow in grid-connected operating mode or providing voltage and frequency regulation for isolated AC microgrids. Supercapacitors were used to control the active and reactive power in fourth-quadrants operation as dynamic compensators. The integration of renewable generation was made via PWM-VSCs, since they allow extracting the maximum power available in the generators while achieving a dynamic power factor. On the other hand, PWM-CSCs were studied for the integration of superconducting magnetic energy storage systems, since these power electronic converters allow directly controlling the current flow in the DC side without using an additional converter, which is the case of the energy stored in superconductors.

- Conventional circuit theory based on Kirchhoff's laws and Tellegen's theorems in conjunction with incidence branch-to-node matrices under single-phase and three-phase representation were used to formulate general grid models in Hamiltonian form giving information about the structural properties of AC power grids. In addition, these models showed that power electronic converters represented as Hamiltonian systems can be perfectly integrated with the grid, preserving their passivity properties and making a stability analysis by energy function representations easier.

- A Hamiltonian structure of classical phase-looked loops for three-phase power grids was also proposed in order to develop controllers in Clarke's reference frame for three-phase PWM-CSCs and PWM-VSCs. Additionally, a quadrature signal generator was proposed to control the active and reactive power in single-phase converters; this system also has a Hamiltonian structure with passive properties.

- Numerical validation of the proposed passivity-based controllers for single-phase and three-phase microgrids allowed demonstrating the dynamical properties and times required for achieving the desired references in isolated and grid connected scenarios. All the simulations were carried out in MATLAB by using the SimPowerSystems toolbox. The switching characteristics were included in the converter's simulation, showing the possibility of real applications of the proposed controllers for operating distributed energy resources on AC microgrids.

6.2 Future research

Next, some research topics about the stability and control of power grids are suggested for future research projects.

- Propose general passivity-based control models for controlling power electronic converters in direct-current power grids considering renewable generation and energy storage technologies. Power electronic converters for DC power grids exhibit a Hamiltonian structure that can be exploited via the IDA-PBC and PI-PBC approaches.
- The structural properties of DC power grids as well as AC power grids with constant power terminals could be analyzed with Hamiltonian modeling in order to provide sufficient conditions for stable operation. Such an investigation would allow understanding the borders of the stability region in terms of the voltage profiles when the power consumption increases as well as the impact of parametric variations on the dynamical performance of the power grids.
- Develop passivity based controllers for Quasi-Z and Z converters, since they allow integrating multiple distributed energy resources with AC or DC power grids, and they can be configured for controlling voltage or current variables with minimal topological variations. These control advantages will allow unifying voltage and current source converters in a unique converter, which will permit simplifying multiple control tasks in power grids.

Bibliography

[1] J. Campillo, "From Passive to Active Electric Distribution Networks," Ph.D. dissertation, Malardalen University, Future Energy Center, 2016.

[2] Y. Xu and X. Shen, "Optimal Control Based Energy Management of Multiple Energy Storage Systems in a Microgrid," *IEEE Access*, vol. 6, pp. 32 925–32 934, 2018.

[3] J. Kim, J. Jeon, S. Kim, C. Cho, J. H. Park, H. Kim, and K. Nam, "Cooperative Control Strategy of Energy Storage System and Microsources for Stabilizing the Microgrid during Islanded Operation," *IEEE Trans. Power Electron.*, vol. 25, no. 12, pp. 3037–3048, Dec 2010.

[4] S. Parhizi, H. Lotfi, A. Khodaei, and S. Bahramirad, "State of the art in research on microgrids: A review," *IEEE Access*, vol. 3, pp. 890–925, 2015.

[5] H. Bitaraf and S. Rahman, "Reducing curtailed wind energy through energy storage and demand response," *IEEE Trans. Sustain. Energy*, vol. 9, no. 1, pp. 228–236, Jan 2018.

[6] Z. Wang, C. Gu, F. Li, P. Bale, and H. Sun, "Active Demand Response Using Shared Energy Storage for Household Energy Management," *IEEE Trans. Smart Grid*, vol. 4, no. 4, pp. 1888–1897, Dec 2013.

[7] S. Kwon, L. Ntaimo, and N. Gautam, "Optimal Day-Ahead Power Procurement With Renewable Energy and Demand Response," *IEEE Trans. Power Syst.*, vol. 32, no. 5, pp. 3924–3933, Sep. 2017.

[8] L. F. Grisales, A. Grajales, O. D. Montoya, R. A. Hincapie, M. Granada, and C. A. Castro, "Optimal location, sizing and operation of energy storage in distribution systems using multi-objective approach," *IEEE Latin America Transactions*, vol. 15, no. 6, pp. 1084–1090, June 2017.

[9] T. Zhao and Z. Ding, "Cooperative Optimal Control of Battery Energy Storage System Under Wind Uncertainties in a Microgrid," *IEEE Trans. Power Syst.*, vol. 33, no. 2, pp. 2292–2300, March 2018.

[10] A. Ortega and F. Milano, "Generalized Model of VSC-Based Energy Storage Systems for Transient Stability Analysis," *IEEE Trans. Power Syst.*, vol. 31, no. 5, pp. 3369–3380, Sept 2016.

[11] J. Shi, Y. Tang, L. Ren, J. Li, and S. Cheng, "Discretization-based decoupled state-feedback control for current source power conditioning system of SMES," *IEEE Trans. Power Delivery*, vol. 23, no. 4, pp. 2097–2104, 2008.

[12] M. H. Ali, M. Park, I. K. Yu, T. Murata, and J. Tamura, "Improvement of Wind-Generator Stability by Fuzzy-Logic-Controlled SMES," *IEEE Trans. Ind. Appl.*, vol. 45, no. 3, pp. 1045–1051, May 2009.

[13] T. Morstyn, A. V. Savkin, B. Hredzak, and H. D. Tuan, "Scalable Energy Management for Low Voltage Microgrids Using Multi-Agent Storage System Aggregation," *IEEE Trans. Power Syst.*, vol. 33, no. 2, pp. 1614–1623, March 2018.

[14] K. P. Kumar and B. Saravanan, "Day ahead scheduling of generation and storage in a microgrid considering demand Side management," *Journal of Energy Storage*, vol. 21, pp. 78 – 86, 2019.

[15] S. Avila-Becerril, O. D. Montoya, G. Espinosa-Pérez, and A. Garcés, "Control of a Detailed Model of Microgrids from a Hamiltonian Approach," *IFAC-PapersOnLine*, vol. 51, no. 3, pp. 187 – 192, 2018, 6th IFAC Workshop on Lagrangian and Hamiltonian Methods for Nonlinear Control LHMNC 2018.

[16] D. Karimipour and F. R. Salmasi, "Stability Analysis of AC Microgrids With Constant Power Loads Based on Popov's Absolute Stability Criterion," *IEEE Trans. Circuits Syst. II*, vol. 62, no. 7, pp. 696–700, July 2015.

[17] J. Shi, L. Zhang, K. Gong, Y. Liu, A. Zhou, X. Zhou, Y. Tang, L. Ren, and J. Li, "Improved Discretization-Based Decoupled Feedback Control for a Series-Connected Converter of SCC," *IEEE Trans. Appl. Supercond.*, vol. 26, no. 7, pp. 1–6, Oct 2016.

[18] W. Gil-González, A. Garces, and A. Escobar, "Passivity-based control and stability analysis for hydro-turbine governing systems," *Appl. Math. Modell.*, vol. 68, pp. 471 – 486, 2019.

[19] S. Avila-Becerril, G. Espinosa-Pérez, and P. Fernandez, "Dynamic Characterization of Typical Electrical Circuits via Structural Properties," *Mathematical Problems in Engineering*, vol. 2016, pp. 1–13, 2016.

[20] L. Guo, X. Zhang, S. Yang, Z. Xie, L. Wang, and R. Cao, "Simplified model predictive direct torque control method without weighting factors for permanent magnet synchronous generator-based wind power system," *IET Electr. Power Appl.*, vol. 11, no. 5, pp. 793–804, 2017.

[21] P. Sreedharan, J. Farbes, E. Cutter, C. K. Woo, and J. Wang, "Microgrid and renewable generation integration: University of California, San Diego," *Appl. Energy*, vol. 169, pp. 709–720, 2016. [Online]. Available: http://dx.doi.org/10.1016/j.apenergy.2016.02.053

[22] S. C. Smith, P. K. Sen, and B. Kroposki, "Advancement of energy storage devices and applications in electrical power system," in *2008 IEEE Power and Energy Society General Meeting - Conversion and Delivery of Electrical Energy in the 21st Century*, July 2008, pp. 1–8.

[23] N. Amaro, J. M. Pina, J. Martins, and J. M. Ceballos, "Integration of SMES devices in power systems - Opportunities and challenges," *Proceedings - 2015 9th International Conference on Compatibility and Power Electronics, CPE 2015*, pp. 482–487, 2015.

[24] T. Wang, D. OŃeill, and H. Kamath, "Dynamic Control and Optimization of Distributed Energy Resources in a Microgrid," *IEEE Trans. Smart Grid*, vol. 6, no. 6, pp. 2884–2894, Nov 2015.

[25] D. Li and Z. Q. Zhu, "A Novel Integrated Power Quality Controller for Microgrid," *IEEE Trans. Ind. Electron.*, vol. 62, no. 5, pp. 2848–2858, 2015.

[26] L. Guo, S. Zhang, X. Li, Y. W. Li, C. Wang, and Y. Feng, "Stability Analysis and Damping Enhancement Based on Frequency-Dependent Virtual Impedance for DC Microgrids," *IEEE Journal of Emerging and Selected Topics in Power Electronics*, vol. 5, no. 1, pp. 338–350, March 2017.

[27] Y. Gu, W. Li, and X. He, "Passivity-Based Control of DC Microgrid for Self-Disciplined Stabilization," *IEEE Trans. Power Syst.*, vol. 30, no. 5, pp. 2623–2632, 2015.

[28] S. P. Nageshrao, G. A. D. Lopes, D. Jeltsema, and R. Babuska, "Port-Hamiltonian Systems in Adaptive and Learning Control: A Survey," *IEEE Trans. Autom. Control*, vol. 61, no. 5, pp. 1223–1238, May 2016.

[29] R. Cisneros, F. Mancilla-David, and R. Ortega, "Passivity-Based Control of a Grid-Connected Small-Scale Windmill With Limited Control Authority," *IEEE Journal of Emerging and Selected Topics in Power Electronics*, vol. 1, no. 4, pp. 247–259, Dec 2013.

[30] W. Haddad and V. Chellaboina, *Nonlinear Dynamical Systems and Control: A Lyapunov-Based Approach*. Princeton University Press, 2011. [Online]. Available: https://books.google.com.co/books?id=bUQN6Ph7YEIC

[31] F. Serra, C. D. Angelo, and D. Forchetti, "Passivity Based Control of a Three-Phase Front End Converter," *IEEE Latin America Transactions*, vol. 11, no. 1, pp. 293–299, Feb 2013.

[32] R. Ortega, A. van der Schaft, B. Maschke, and G. Escobar, "Interconnection and damping assignment passivity-based control of port-controlled Hamiltonian systems," *Automatica*, vol. 38, no. 4, pp. 585 – 596, 2002.

[33] J. Slotine and W. Li, *Applied Nonlinear Control*, ser. Prentice-Hall International Editions. Prentice-Hall, 1991. [Online]. Available: https://books.google.com.co/books?id=HddxQgAACAAJ

[34] Q. Fu, A. Hamidi, A. Nasiri, V. Bhavaraju, S. B. Krstic, and P. Theisen, "The Role of Energy Storage in a Microgrid Concept: Examining the opportunities and promise of microgrids," *IEEE Electrific. Mag.*, vol. 1, no. 2, pp. 21–29, Dec 2013.

[35] J. Quesada, R. Sebastían, M. Castro, and J. A. Sainz, "Control of inverters in a low-voltage microgrid with distributed battery energy storage. Part II: Secondary control," *Electr. Power Syst. Res.*, vol. 114, pp. 136–145, 2014. [Online]. Available: http://dx.doi.org/10.1016/j.epsr.2014.03.033

[36] I. Serban and C. Marinescu, "Control strategy of three-phase battery energy storage systems for frequency support in microgrids and with uninterrupted supply of local loads," *IEEE Trans. Power Electron.*, vol. 29, no. 9, pp. 5010–5020, 2014.

[37] G. Kyriakarakos, D. D. Piromalis, A. I. Dounis, K. G. Arvanitis, and G. Papadakis, "Intelligent demand side energy management system for autonomous polygeneration microgrids," *Appl. Energy*, vol. 103, pp. 39–51, 2013. [Online]. Available: http://dx.doi.org/10.1016/j.apenergy.2012.10.011

[38] N. Kinhekar, N. P. Padhy, F. Li, and H. O. Gupta, "Utility Oriented Demand Side Management Using Smart AC and Micro DC Grid Cooperative," *IEEE Trans. Power Syst.*, vol. 31, no. 2, pp. 1151–1160, 2016.

[39] S. Huang, D. C. Pham, K. Huang, and S. Cheng, "Space vector PWM techniques for current and voltage source converters: A short review," in *2012 15th International Conference on Electrical Machines and Systems (ICEMS)*, Oct 2012, pp. 1–6.

[40] A. Marzouki, M. Hamouda, and F. Fnaiech, "A review of PWM voltage source converters based industrial applications," in *2015 International Conference on Electrical Systems for Aircraft, Railway, Ship Propulsion and Road Vehicles (ESARS)*, March 2015, pp. 1–6.

[41] E. Planas, A. Gil-De-Muro, J. Andreu, I. Kortabarria, and I. Martínez De Alegría, "General aspects, hierarchical controls and droop methods in microgrids: A review," *Renewable Sustainable Energy Rev.*, vol. 17, pp. 147–159, 2013.

[42] E. Giraldo and A. Garces, "An adaptive control strategy for a wind energy conversion system based on PWM-CSC and PMSG," *IEEE Trans. Power Syst.*, vol. 29, no. 3, pp. 1446–1453, 2014.

[43] D. E. Olivares, A. Mehrizi-Sani, A. H. Etemadi, C. A. Canizares, R. Iravani, M. Kazerani, A. H. Hajimiragha, O. Gomis-Bellmunt, M. Saeedifard, R. Palma-Behnke, G. A. Jimenez-Estevez, and N. D. Hatziargyriou, "Trends in microgrid control," *IEEE Trans. Smart Grid*, vol. 5, no. 4, pp. 1905–1919, 2014.

[44] J. Shi, Y. Tang, K. Yang, L. Chen, L. Ren, J. Li, and S. Cheng, "SMES based dynamic voltage restorer for voltage fluctuations compensation," *IEEE Trans. Appl. Supercond.*, vol. 20, no. 3, pp. 1360–1364, 2010.

[45] M. H. Ali, B. Wu, and R. A. Dougal, "An overview of SMES applications in power and energy systems," *IEEE Trans. Sustainable Energy*, vol. 1, no. 1, pp. 38–47, 2010.

[46] S. Wang and J. Jin, "Design and Analysis of a Fuzzy Logic Controlled SMES System," *IEEE Trans. Appl. Supercond.*, vol. 24, no. 5, pp. 1–5, Oct 2014.

[47] M. Mohammedi, O. Kraa, M. Becherif, A. Aboubou, M. Ayad, and M. Bahri, "Fuzzy Logic and Passivity-based Controller Applied to Electric Vehicle Using Fuel Cell and Supercapacitors Hybrid Source," *Energy Procedia*, vol. 50, pp. 619 – 626, 2014, technologies and Materials for Renewable Energy, Environment and Sustainability (TMREES14 EUMISD).

[48] T. Govindaraj and D. Hemalatha, "Dynamic Reactive Power Control of Islanded Microgrid Using IPFC," *IEEE Trans. on Power Systems*, vol. 2, no. 4, pp. 3649–3657, 2014.

[49] F. M. Serra and C. H. D. Angelo, "IDA-PBC controller design for grid connected Front End Converters under non-ideal grid conditions," *Electr. Power Syst. Res.*, vol. 142, pp. 12 – 19, 2017.

[50] T.-S. Lee, "Lagrangian modeling and passivity-based control of three-phase AC/DC voltage-source converters," *IEEE Trans. Ind. Electron.*, vol. 51, no. 4, pp. 892–902, Aug 2004.

[51] M. Perez, R. Ortega, and J. R. Espinoza, "Passivity-based PI control of switched power converters," *IEEE Trans. Control Syst. Technol.*, vol. 12, no. 6, pp. 881–890, Nov 2004.

[52] I. Martínez-Pérez, G. Espinosa-Perez, G. Sandoval-Rodríguez, and A. Dòria-Cerezo, "IDA Passivity-Based Control of single phase back-to-back converters," *IEEE International Symposium on Industrial Electronics*, no. 2, pp. 74–79, 2008.

[53] M. Hilairet, O. Bthoux, M. Ghanes, V. Tanasa, J. P. Barbot, and M. D. Normand-Cyrot, "Experimental Validation of a Sampled-Data Passivity-Based Controller for Coordination of Converters in a Fuel Cell System," *IEEE Trans. Ind. Electron.*, vol. 62, no. 8, pp. 5187–5194, Aug 2015.

[54] A. Rahim and E. Nowicki, "Supercapacitor energy storage system for fault ride-through of a {DFIG} wind generation system," *Energy Convers. Manage.*, vol. 59, pp. 96 – 102, 2012.

[55] S. J. Ahn, J. W. Park, I. Y. Chung, S. I. Moon, S. H. Kang, and S. R. Nam, "Power-Sharing Method of Multiple Distributed Generators Considering Control Modes and Configurations of a Microgrid," *IEEE Trans. Power Del.*, vol. 25, no. 3, pp. 2007–2016, July 2010.

[56] N. L. Díaz, A. C. Luna, J. C. Vasquez, and J. M. Guerrero, "Centralized Control Architecture for Coordination of Distributed Renewable Generation and Energy Storage in Islanded AC Microgrids," *IEEE Trans. Power Electron.*, vol. 32, no. 7, pp. 5202–5213, July 2017.

[57] Q. Xu, J. Xiao, P. Wang, and C. Wen, "A Decentralized Control Strategy for Economic Operation of Autonomous AC, DC and Hybrid AC/DC Microgrids," *IEEE Trans. Energy Convers.*, vol. PP, no. 99, pp. 1–1, 2017.

[58] W. Gu, G. Lou, W. Tan, and X. Yuan, "A Nonlinear State Estimator-Based Decentralized Secondary Voltage Control Scheme for Autonomous Microgrids," *IEEE Trans. Power Syst.*, vol. PP, no. 99, pp. 1–1, 2017.

[59] W. Feng, M. Jin, X. Liu, Y. Bao, C. Marnay, C. Yao, and J. Yu, "A review of microgrid development in the United States - A decade of progress on policies, demonstrations, controls, and software tools," *Appl. Energy*, vol. 228, pp. 1656 – 1668, 2018.

[60] N. N. A. Bakar, M. Y. Hassan, M. F. Sulaima, M. N. M. Nasir, and A. Khamis, "Microgrid and load shedding scheme during islanded mode: A review," *Renewable Sustainable Energy Rev.*, vol. 71, pp. 161 – 169, 2017.

[61] F. Meng, B. Chowdhury, and M. S. Hossan, "Optimal integration of DER and SST in active distribution networks," *Int. J. Electr. Power Energy Syst.*, vol. 104, pp. 626 – 634, 2019.

[62] M. Usman, M. Coppo, F. Bignucolo, and R. Turri, "Losses management strategies in active distribution networks: A review," *Electr. Power Syst. Res.*, vol. 163, pp. 116 – 132, 2018.

[63] O. D. Montoya, A. Garcés, and F. M. Serra, "DERs integration in microgrids using VSCs via proportional feedback linearization control: Supercapacitors and distributed generators," *Journal of Energy Storage*, vol. 16, pp. 250–258, 2018. [Online]. Available: http://www.sciencedirect.com/science/article/pii/S2352152X17303912

[64] N. Hatziargyriou, *Microgrids: Architectures and Control*, ser. Wiley - IEEE. Wiley, 2014. [Online]. Available: https://books.google.com.co/books?id=ywxzAgAAQBAJ

[65] A. H. Fathima and K. Palanisamy, "Optimization in microgrids with hybrid energy systems - A review," *Renewable Sustainable Energy Rev.*, vol. 45, pp. 431–446, 2015. [Online]. Available: http://dx.doi.org/10.1016/j.rser.2015.01.059

[66] E. Alegria, A. Ma, and O. Idrees, "CERTS MICROGRID DEMONSTRATION WITH LARGE-SCALE ENERGY STORAGE AND RENEWABLES AT SANTA RITA JAIL," Chevron Energy Solutions Company, techreport, Mar. 2014.

[67] SDG&E. (2009, Sep.) Beach Cities MicroGrid Project. online. Southera California Gas Company. [Online]. Available: http://microgrid-symposiums.org/wp-content/uploads/2014/12/sandiego_bialek.pdf

[68] U. of Hawaii. MAUI SMART GRID PROJECT. online. University of Hawaii. [Online]. Available: https://www.hnei.hawaii.edu/sites/www.hnei.hawaii.edu/files/Final%20Report%20Presentation%20of%20MSGP.pdf

[69] M. Power, "West Virginia Super Circuit Project," U.S. Department of Energy, techreport, 2014. [Online]. Available: https://www.smartgrid.gov/files/USDOE_WVSC_Project_Final_Report_5-30-2014_R1.pdf

[70] R. Pena-Alzola, R. Sebastián, J. Quesada, and A. Colmenar, "Review of Flywheel based Energy Storage Systems," *International Conference on Power Engineering, Energy and Electrical Drives*, no. May, pp. 1–6, 2011.

[71] R. Elliman, C. Gould, and M. Al-Tai, "Review of current and future electrical energy storage devices," in *2015 50th International Universities Power Engineering Conference (UPEC)*, Sept 2015, pp. 1–5.

[72] O. D. Montoya, A. Garcés, and G. Espinosa-Pérez, "A generalized passivity-based control approach for power compensation in distribution systems using electrical energy storage systems," *Journal of Energy Storage*, vol. 16, pp. 259–268, 2018.

[73] O. D. Montoya, W. Gil-González, A. Garcés, and G. Espinosa-Pérez, "Indirect IDA-PBC for active and reactive power support in distribution networks using SMES systems with PWM-CSC," *Journal of Energy Storage*, vol. 17, pp. 261–271, 2018.

[74] X. Quan, X. Dou, Z. Wu, M. Hu, and J. Yuan, "Harmonic voltage resonant compensation control of a three-phase inverter for battery energy storage systems applied in isolated microgrid," *Electr. Power Syst. Res.*, vol. 131, pp. 205–217, 2016. [Online]. Available: http://dx.doi.org/10.1016/j.epsr.2015.10.010

[75] M. Farhadi and O. Mohammed, "Energy Storage Technologies for High-Power Applications," *IEEE Trans. Ind. Appl.*, vol. 52, no. 3, pp. 1953–1961, May 2016.

[76] O. D. Montoya, A. Garces, F. M. Serra, and G. Magaldi, "Apparent power control in single-phase grids using SCES devices: An IDA-PBC approach," in *2018 IEEE 9th Latin American Symposium on Circuits Systems (LASCAS)*, Feb 2018, pp. 1–4.

[77] W. Gil-González and O. D. Montoya, "Passivity-based PI control of a SMES system to support power in electrical grids: A bilinear approach," *Journal of Energy Storage*, vol. 18, pp. 459 – 466, 2018. [Online]. Available: http://www.sciencedirect.com/science/article/pii/S2352152X18300483

[78] W. J. Gil-González, A. Garcés, and A. Escobar, "A Generalized Model and Control for Supermagnetic and Supercapacitor Energy Storage," *Ingeniería y Ciencia*, vol. 13, no. 26, pp. 147–171, dec 2017.

[79] O. D. Montoya, A. Garcés, I. Ortega, and G. R. Espinosa-Pérez, "Passivity-Based Control for Battery Charging/Discharging Applications by Using a Buck-Boost DC-DC Converter," in *2018 IEEE Green Technologies Conference (GreenTech)*, April 2018, pp. 89–94.

[80] O. D. Montoya, W. J. Gil-González, A. Garcés, A. Escobar-Mejía, and L. F. Grisales-Noreña, "Nonlinear Control for Battery Energy Storage Systems in Power Grids," in *2018 IEEE Green Technologies Conference (GreenTech)*, April 2018, pp. 65–70.

[81] F. Castaños and D. Gromov, "Passivity-based control of implicit port-Hamiltonian systems with holonomic constraints," *Systems and Control Letters*, vol. 94, pp. 11–18, 2016.

[82] H. Khalil, *Nonlinear Systems*, ser. Always learning. Pearson Education, Limited, 2013. [Online]. Available: https://books.google.com.co/books?id=VZ72nQEACAAJ

[83] W. Gil-González, O. D. Montoya, A. Garcés, and G. Espinosa-Pérez, "IDA-Passivity-Based Control for Superconducting Magnetic Energy Storage with PWM-CSC," in *2017 Ninth Annual IEEE Green Technologies Conference (GreenTech)*, March 2017, pp. 89–95.

[84] W. Gil-González, O. D. Montoya, A. Garcés, and A. Escobar-Mejía, "Supervisory LMI-Based State-Feedback Control for Current Source Power Conditioning of SMES," in *2017 Ninth Annual IEEE Green Technologies Conference (GreenTech)*, March 2017, pp. 145–150.

[85] R. Hou, H. Song, T. Nguyen, Y. Qu, and H. Kim, "Robustness Improvement of Superconducting Magnetic Energy Storage System in Microgrids Using an Energy Shaping Passivity-Based Control Strategy," *Energies*, vol. 10, no. 5, pp. 1–23, May 2017. [Online]. Available: http://www.mdpi.com/1996-1073/10/5/671

[86] T. T. Nguyen, H. J. Yoo, and H. M. Kim, "Applying Model Predictive Control to SMES System in Microgrids for Eddy Current Losses Reduction," *IEEE Trans. Appl. Supercond.*, vol. 26, no. 4, pp. 1–5, June 2016.

[87] W. Kreeumporn and I. Ngamroo, "Optimal Superconducting Coil Integrated Into PV Generators for Smoothing Power and Regulating Voltage in Distribution System With PHEVs," *IEEE Trans. Appl. Supercond.*, vol. 26, no. 7, pp. 1–5, Oct 2016.

[88] S. Mane, M. Mejari, F. Kazi, and N. Singh, "Improving Lifetime of Fuel Cell in Hybrid Energy Management System by Lure: Lyapunov-Based Control Formulation," *IEEE Trans. Ind. Electron.*, vol. 64, no. 8, pp. 6671–6679, Aug 2017.

[89] M. D. Mufti, S. J. Iqbal, S. A. Lone, and Q. u. Ain, "Supervisory Adaptive Predictive Control Scheme for Supercapacitor Energy Storage System," *IEEE Syst. J.*, vol. 9, no. 3, pp. 1020–1030, Sept 2015.

[90] N. Jabbour and C. Mademlis, "Improved Control Strategy of a Supercapacitor-Based Energy Recovery System for Elevator Applications," *IEEE Trans. Power Electron.*, vol. 31, no. 12, pp. 8398–8408, Dec 2016.

[91] M. R. Mojallizadeh and M. A. Badamchizadeh, "Adaptive Passivity-Based Control of a Photovoltaic/Battery Hybrid Power Source via Algebraic Parameter Identification," *IEEE J. Photovolt.*, vol. 6, no. 2, pp. 532–539, March 2016.

[92] T. I. Bo and T. A. Johansen, "Battery Power Smoothing Control in a Marine Electric Power Plant Using Nonlinear Model Predictive Control," *IEEE Trans. Control Syst. Technol.*, vol. 25, no. 4, pp. 1449–1456, July 2017.

[93] P. Golchoubian and N. L. Azad, "Real-Time Nonlinear Model Predictive Control of a Battery-Supercapacitor Hybrid Energy Storage System in Electric Vehicles," *IEEE Trans. Veh. Technol.*, vol. PP, no. 99, pp. 1–1, 2017.

[94] M. I. Ghiasi, M. A. Golkar, and A. Hajizadeh, "Lyapunov Based-Distributed Fuzzy-Sliding Mode Control for Building Integrated-DC Microgrid With Plug-In Electric Vehicle," *IEEE Access*, vol. 5, pp. 7746–7752, 2017.

[95] F. Mancilla-David and R. Ortega, "Adaptive passivity-based control for maximum power extraction of stand-alone windmill systems," *Control Eng. Pract.*, vol. 20, no. 2, pp. 173 – 181, 2012. [Online]. Available: http://www.sciencedirect.com/science/article/pii/S0967066111002139

[96] R. P. na, R. Fernández, and R. Mantz, "Passivity control via Power Shaping of a wind turbine in a dispersed network," *Int. J. Hydrogen Energy*, vol. 39, no. 16, pp. 8846 – 8851, 2014. [Online]. Available: http://www.sciencedirect.com/science/article/pii/S036031991302956X

[97] E. Rezaei, M. Ebrahimi, and A. Tabesh, "Control of DFIG Wind Power Generators in Unbalanced Microgrids Based on Instantaneous Power Theory," *IEEE Transactions on Smart Grid*, vol. 8, no. 5, pp. 2278–2286, Sept 2017.

[98] W. Dai, Y. Yu, M. Hua, and C. Cai, "Voltage Regulation System of Doubly Salient Electromagnetic Generator Based on Indirect Adaptive Fuzzy Control," *IEEE Access*, vol. 5, pp. 14 187–14 194, 2017.

[99] L. Y. Lu and C. C. Chu, "Consensus-Based Secondary Frequency and Voltage Droop Control of Virtual Synchronous Generators for Isolated AC Micro-Grids," *IEEE Journal on Emerging and Selected Topics in Circuits and Systems*, vol. 5, no. 3, pp. 443–455, Sept 2015.

[100] A. Nemmour, F. Mehazzem, A. Khezzar, M. Hacil, L. Louze, and R. Abdessemed, "Advanced Backstepping controller for induction generator using multi-scalar machine model for wind power purposes," *Renewable Energy*, vol. 35, no. 10, pp. 2375 – 2380, 2010. [Online]. Available: http://www.sciencedirect.com/science/article/pii/S0960148110000868

[101] C. Meza, D. Jeltsema, J. Scherpen, and D. Biel, "Passive P-Control of a Grid-Connected Photovoltaic Inverter," *IFAC Proceedings Volumes*, vol. 41, no. 2, pp. 5575 – 5580, 2008, 17th IFAC World Congress. [Online]. Available: http://www.sciencedirect.com/science/article/pii/S1474667016398330

[102] W. Qi, J. Liu, and P. D. Christofides, "Supervisory Predictive Control of an Integrated Wind/Solar Energy Generation and Water Desalination System," *IFAC Proceedings Volumes*, vol. 43, no. 5, pp. 829 – 834, 2010, 9th IFAC Symposium on Dynamics and Control of Process Systems. [Online]. Available: http://www.sciencedirect.com/science/article/pii/S1474667016301380

[103] S. Adhikari, F. Li, and H. Li, "P-Q and P-V Control of Photovoltaic Generators in Distribution Systems," *IEEE Trans. Smart Grid*, vol. 6, no. 6, pp. 2929–2941, Nov 2015.

[104] J. Schiffer, R. Ortega, A. Astolfi, J. Raisch, and T. Sezi, "Conditions for stability of droop-controlled inverter-based microgrids," *Automatica*, vol. 50, no. 10, pp. 2457 – 2469, 2014. [Online]. Available: http://www.sciencedirect.com/science/article/pii/S0005109814003100

[105] J. Liu, W. Zhang, and G. Rizzoni, "Robust Stability Analysis of DC Microgrids with Constant Power Loads," *IEEE Trans. Power Syst.*, vol. PP, no. 99, pp. 1–1, 2017.

[106] L. Herrera, W. Zhang, and J. Wang, "Stability Analysis and Controller Design of DC Microgrids With Constant Power Loads," *IEEE Trans. Smart Grid*, vol. 8, no. 2, pp. 881–888, March 2017.

[107] J. Xiang, Y. Wang, Y. Li, and W. Wei, "Stability and steady-state analysis of distributed cooperative droop controlled DC microgrids," *IET Control Theory Applications*, vol. 10, no. 18, pp. 2490–2496, 2016.

[108] A. P. N. Tahim, D. J. Pagano, E. Lenz, and V. Stramosk, "Modeling and Stability Analysis of Islanded DC Microgrids Under Droop Control," *IEEE Trans. Power Electron.*, vol. 30, no. 8, pp. 4597–4607, Aug 2015.

[109] J. L. WILLEMS, "A system theory approach to unified electrical machine analysis," *Int. J. Control*, vol. 15, no. 3, pp. 401–418, 1972. [Online]. Available: https://doi.org/10.1080/00207177208932158

[110] J. C. Willems, "Dissipative dynamical systems part I: General theory," *Arch. Ration. Mech. Anal.*, vol. 45, no. 5, pp. 321–351, 1972.

[111] ——, "Dissipative dynamical systems Part II: Linear systems with quadratic supply rates," *Arch. Ration. Mech. Anal.*, vol. 45, no. 5, pp. 352–393, Jan. 1972.

[112] R. Ortega, J. Perez, P. Nicklasson, and H. Sira-Ramirez, *Passivity-based Control of Euler-Lagrange Systems: Mechanical, Electrical and Electromechanical Applications*, ser. Communications and Control Engineering. Springer London, 1998. [Online]. Available: https://books.google.com.co/books?id=GCVn0oRqP9YC

[113] S. M. Ávila-Becerril, "Caracterización y control de microrredes viá propiedades estructurales," Ph.D. dissertation, Facultad de Ingeniería, Universidad Nacional Autónoma de México, 2016. [Online]. Available: http://132.248.9.195/ptd2016/junio/098003280/Index.html

[114] L. Perko, *Differential Equations and Dynamical Systems*, ser. Texts in Applied Mathematics. Springer New York, 2013. [Online]. Available: https://books.google.com.co/books?id=VFnSBwAAQBAJ

[115] R. Cisneros, M. Pirro, G. Bergna, R. Ortega, G. Ippoliti, and M. Molinas, "Global Tracking Passivity-based PI Control of Bilinear Systems and its Application to the Boost and Modular Multilevel Converters," *IFAC-PapersOnLine*, vol. 48, no. 11, pp. 420 – 425, 2015, 1st IFAC Conference on Modelling, Identification and Control of Nonlinear Systems MICNON 2015.

[116] H. Ramírez, Y. Le Gorrec, B. Maschke, and F. Couenne, "On the passivity based control of irreversible processes: A port-Hamiltonian approach," *Automatica*, vol. 64, pp. 105–111, 2016.

[117] O. D. Montoya, W. Gil-Gonzlez, and F. M. Serra, "PBC Approach for SMES Devices in Electric Distribution Networks," *IEEE Trans. Circuits Syst. II Express Briefs*, pp. 1–6, 2018.

[118] E. Planas, J. Andreu, J. I. Gárate, I. Martínez De Alegría, and E. Ibarra, "AC and DC technology in microgrids: A review," *Renewable Sustainable Energy Rev.*, vol. 43, pp. 726–749, 2015.

[119] C. Natesan, A. Devendiran, S. Chozhavendhan, D. Thaniga, and R. Revathi, "IGBT and MOSFET: A comparative study of power electronics inverter topology in distributed generation," in *2015 International Conference on Circuits, Power and Computing Technologies [ICCPCT-2015]*, March 2015, pp. 1–5.

[120] M. Rashid, *Power Electronics Handbook*, ser. ElSevier. Pearson Education, Limited, 2013. [Online]. Available: https://www.sciencedirect.com/book/9780123820365/power-electronics-handbook

[121] X. Zong, "A Single Phase Grid Connected DC/AC Inverter with Reactive Power Control for Residential PV Application," Master's thesis, Department of Electrical and Computer Engineering, University of Toronto, 2011. [Online]. Available: https://tspace.library.utoronto.ca/handle/1807/31665

[122] M. M. Canteli, A. O. Fernandez, L. I. Eguiluz, and C. R. Estebanez, "Three-phase adaptive frequency measurement based on Clarke's transformation," *IEEE Trans. Power Del.*, vol. 21, no. 3, pp. 1101–1105, July 2006.

[123] S. Golestan, J. M. Guerrero, and J. C. Vasquez, "Three-Phase PLLs: A Review of Recent Advances," *IEEE Trans. Power Electron.*, vol. 32, no. 3, pp. 1894–1907, March 2017.

[124] E. Adzic, V. Porobic, B. Dumnic, N. Celanovic, and V. Katic, "PLL Synchronization in Grid-Connected Converters," in *The 6th PSU-UNS International Conference on Engineering and Technology (ICET-2013)*, 2013, pp. 1–5.

[125] Y. Han, M. Luo, X. Zhao, J. M. Guerrero, and L. Xu, "Comparative Performance Evaluation of Orthogonal-Signal-Generators-Based Single-Phase PLL Algorithm - A Survey," *IEEE Trans. Power Electron.*, vol. 31, no. 5, pp. 3932–3944, May 2016.

[126] S. Hwang, L. Liu, H. Li, and J. Kim, "DC Offset Error Compensation for Synchronous Reference Frame PLL in Single-Phase Grid-Connected Converters," *IEEE Trans. Power Electron.*, vol. 27, no. 8, pp. 3467–3471, Aug 2012.

[127] A. Micallef, M. Apap, C. Spiteri-Staines, and J. M. Guerrero, "Single-Phase Microgrid with Seamless Transition Capabilities between Modes of Operation," *IEEE Trans. Smart Grid*, vol. 6, no. 6, pp. 2736–2745, 2015.

[128] A. R. Kim, G. H. Kim, S. Heo, M. Park, I. K. Yu, and H. M. Kim, "SMES application for frequency control during islanded microgrid operation," *Physica C: Superconductivity and its Applications*, vol. 484, pp. 282–286, 2013.

[129] T. Caldognetto and P. Tenti, "Microgrids Operation Based on MasterSlave Cooperative Control," *IEEE Journal of Emerging and Selected Topics in Power Electronics*, vol. 2, no. 4, pp. 1081–1088, Dec 2014.

[130] N. D. Tleis, "3 - Modelling of multi-conductor overhead lines and cables," in *Power Systems Modelling and Fault Analysis*, ser. Newnes Power Engineering Series, N. D. Tleis, Ed. Oxford: Newnes, 2008, pp. 74 – 199.

[131] I. Ortega-Velázquez, G. R. Espinosa-Pérez, O. D. Montoya-Giraldo, A. Garcés-Ruiz, and L. F. Grisales-Noreña, "Current Control Mode in PV Systems Integrated with DC-DC Converters for MPPT: An IDA-PBC Approach," in *2018 IEEE Green Technologies Conference (GreenTech)*, April 2018, pp. 1–6.